ANL-7358

Argonne National Laboratory

ENERGY LEVELS AND INTENSITIES IN THE SOLUTION ABSORPTION SPECTRA OF THE TRIVALENT LANTHANIDES

by

W. T. Carnall, P. R. Fields,
and K. Rajnak

DISCLAIMER

The facilities of Argonne National Laboratory are owned by the United States Government. Under the terms of a contract (W-31-109-Eng-38) between the U. S. Atomic Energy Commission, Argonne Universities Association and The University of Chicago, the University employs the staff and operates the Laboratory in accordance with policies and programs formulated, approved and reviewed by the Association.

MEMBERS OF ARGONNE UNIVERSITIES ASSOCIATION

The University of Arizona
Carnegie-Mellon University
Case Western Reserve University
The University of Chicago
University of Cincinnati
Illinois Institute of Technology
University of Illinois
Indiana University
Iowa State University
The University of Iowa
Kansas State University
The University of Kansas
Loyola University
Marquette University
Michigan State University
The University of Michigan
University of Minnesota
University of Missouri
Northwestern University
University of Notre Dame
The Ohio State University
Ohio University
The Pennsylvania State University
Purdue University
Saint Louis University
Southern Illinois University
University of Texas
Washington University
Wayne State University
The University of Wisconsin

Printed in the United States of America
Available from
Clearinghouse for Federal Scientific and Technical Information
National Bureau of Standards, U. S. Department of Commerce
Springfield, Virginia 22151
Price: Printed Copy $3.00; Microfiche $0.65

ANL-7358
Chemistry (TID-4500)
AEC Research and
Development Report

ARGONNE NATIONAL LABORATORY
9700 South Cass Avenue
Argonne, Illinois 60439

ENERGY LEVELS AND INTENSITIES IN THE SOLUTION ABSORPTION SPECTRA OF THE TRIVALENT LANTHANIDES

by

W. T. Carnall, P. R. Fields,
and K. Rajnak

Chemistry Division

March 1968

THIS PAGE
WAS INTENTIONALLY
LEFT BLANK

TABLE OF CONTENTS

TABLE OF CONTENTS

LIST OF FIGURES

LIST OF FIGURES

LIST OF TABLES

LIST OF TABLES

ENERGY LEVELS AND INTENSITIES IN THE SOLUTION ABSORPTION SPECTRA OF THE TRIVALENT LANTHANIDES

by

W. T. Carnall, P. R. Fields,
and K. Rajnak

I. INTRODUCTION

The solution absorption spectra of the trivalent lanthanides characteristically exhibit distinctive sharp, rather weak absorption bands which have been observed primarily in the visible-near-ultraviolet region of the spectrum. Most of these bands result from transitions within the $4f^N$-electron configurations.[67;73] It is also characteristic of lanthanide spectra that the absorption bands are relatively insensitive to the influence of the solvent medium. This is to be expected since the 4f-electrons are interior to, and are well shielded by, the filled 5s and 5p shells. Such behavior may be contrasted to the pronounced influence of the medium on the spectra of the d-transition elements. However, weak environmental effects are observed in the absorption spectra of the lanthanides,[15,42,72] and certain transitions show a particular sensitivity to the host medium. These are frequently referred to as the hypersensitive transitions.[7,8,9,37]

Since extensive measurements in solution have already been reported in the literature,[2,28,52,62] the characteristics of lanthanide absorption spectra are relatively well known. This report is primarily concerned with the theoretical interpretation of the spectra. We will examine the extent to which experimentally measured energies and intensities of the bands can be correlated with those computed from theory.

The attempt to fit calculated energy-level schemes to experimentally observed transitions in the lanthanides has occupied the efforts of many investigators over a number of years. Most of this work has been directed to the studies of lanthanides incorporated in crystal media where the symmetry of the lanthanide sites is known. Although a number of such investigations were published before 1940, it was only after the advent of the tensor operator methods of Racah[21,53] that it became practical to carry out the calculations for complex spectra. Considerable progress has been made in the last 20 years, but our understanding of the energy-level structures of Sm^{3+}, Eu^{3+}, Gd^{3+}, Tb^{3+}, and Dy^{3+} in crystal media is still rudimentary.

In 1962, Judd[40] and Ofelt[51] published theoretical treatments of the intensities of intra f-electron transitions. The experimental data necessary to examine all the ramifications of these theories were not available. However, on the basis of the intensities reported for certain bands in the solution

absorption spectra of Nd^{3+} and Er^{3+} (Refs. 2 and 62), Judd was able to establish a good correlation with the theory. The computations required were formidable, and thus only the simplest configurations, f^2 and f^3, could reasonably be undertaken with hand calculations. It was clear that a detailed examination of the degree to which the theory correlated experimental data throughout the lanthanide series would require high-speed computers and considerable additional experimental data. As of 1962, the published lanthanide solution absorption spectra had already been considerably extended by unpublished work done at the Argonne National Laboratory.

In addition to the intensity correlation, the Judd-Ofelt theory held out at least the possibility of testing different models of the structure of the ion in solution. In this sense, a given lanthanide ion could be considered a probe; we would expect that the characteristics of its environment, particularly its site symmetry with respect to nearest neighbor ligands, would be reflected in measurable effects on its absorption spectrum. We therefore undertook the project of carrying out the requisite calculations and extending the experimental work as required. This report summarizes the results we have obtained with the trivalent lanthanides. A separate report will cover similar studies of actinide spectra.

There were several prerequisites to performing the intensity calculations. It was first necessary to establish the identity of the transitions involved in a given absorption band. The techniques for doing this, Zeeman and polarization studies, are applicable to crystal spectra but not to solutions. However, the center of gravity of levels identified in crystals often occurs at very nearly the same energy in solution; so by comparison of results in the two media, a number of bands in solution have been identified.[7,8,9,39] After the comparison technique was used to identify as many levels as possible in the solution spectrum of a given lanthanide, the next step was to determine values for the interelectronic repulsion and spin-orbit coupling parameters which would generate a set of calculated energy levels in good agreement with the observed data. The description of states implicit in these parameters was then used directly in the intensity calculations.

We were able to show that Judd's theory provided a basis for calculating intensities that were in good agreement with those observed experimentally, not only for Nd^{3+} and Er^{3+}, but over the entire lanthanide series.[6,11] At this point, it became clear that the intensity calculations could be viewed in a new perspective. The correlations that had been observed between theory and experiment were for the most part limited to bands in the near-infrared-visible region of the spectrum. This was because of a lack of energy-level assignments at higher energies. We therefore used the intensity calculations as a basis for making numerous new assignments to bands observed in the ultraviolet region. Sets of electrostatic and spin-orbit parameters were then derived by a least-squares analysis of data which included the new assignments. Thus the intensity calculations became a tool for elucidating the energy-level structure of all of the hydrated lanthanide ions.

II. THEORY OF LANTHANIDE ABSORPTION SPECTRA

A. Energy-level Calculations

The theoretical treatment of lanthanide absorption spectra is discussed in considerable detail in numerous articles and books. We will follow the formalism used by Wybourne,[73] and only present a brief summary here.

The total energy of a system consisting of a point nucleus of infinite mass, surrounded by N electrons can be represented by the Hamiltonian

$$H = H_0 + H_e + H_{so} + \Delta$$

where H_0 represents the kinetic energy of all the electrons and the Coulomb interaction with the nucleus; H_e is the Coulomb interaction between pairs of electrons; H_{so} represents the coupling of spin and orbital angular momenta, which is the most important magnetic interaction for f-electrons; and Δ represents higher-order interactions.

Using a central field approximation which assumes that each electron moves independently in an average spherically symmetric potential, we can solve for the energies of the different configurations. Calculations of this type show that the f^N configuration is the lowest-energy configuration for the trivalent lanthanides, and this is confirmed experimentally.[19]

Since it can be demonstrated that the term H_0 does not affect the energy-level structure within a given configuration, and since the absorption spectra of the trivalent lanthanides at $< 50{,}000\ cm^{-1}$ involve, almost exclusively, transitions between states within the f^N configuration, we need not concern ourselves with H_0 any further. A substantial simplification is also possible in the formulation of H_e. Including the effect of electrons in closed shells in the calculation merely shifts the energy of a configuration; thus, for our purposes it is sufficient to consider only the electrostatic interaction between electrons in the incomplete 4f shell.

1. Electrostatic and Magnetic Interactions

The energy arising from the remaining first-order terms in the Hamiltonian, H_e and H_{so}, can be written in the form

$$E = E_e + E_{so},$$

where

$$E_e = \sum_{k=0}^{6} f^k F_k \quad (k \text{ even}),$$

and

$$E_{so} = A_{so}\zeta_{nf} \quad \text{(for the lanthanides, n = 4).}$$

Higher-order interactions will be discussed in Section A.2 below.

The electrostatic energy is expressed as a sum of radial integrals F_k and coefficients f^k, which represent the angular part of the interaction. Similarly, A_{so} represents the angular part of the spin-orbit interaction, and ζ_{4f} is a radial integral. The angular parts of both perturbation energies can be evaluated by using Racah's tensor operator formalism[53] and an intermediate coupling scheme with Russell-Saunders (SLJ) basis states. Since evaluation of the radial integrals must be approximate in the absence of reliable wave functions, these integrals are, in practice, treated as parameters to be determined from experimental data. Since $f^\circ = N(N - 1)$, the effect of F_0 is to shift the energies of all the levels in the f^N configuration equally. Thus F_0 does not play a role in the level assignments. There are, therefore, three parameters, F_2, F_4, and F_6, associated with electrostatic interactions, and one parameter, ζ_{4f}, associated with the spin-orbit interaction. All must be determined by a fit to observed energy levels for which J-assignments have been made.

For the more complex spectra, the data obtained using crystal media are incomplete. In most instances, assignments have been made only to rather low-lying levels: the ground-term multiplet and the first few excited multiplet levels. Even this limited information can, however, be used to obtain an initial set of values for F_2, F_4, F_6, and ζ_{4f}. If it assumed that the 4f radial-wave function is hydrogenic, values for the ratios F_4/F_2 and F_6/F_2 can be calculated, to give the following results:[21]

$$F_4/F_2 = 41/297,$$

and

$$F_6/F_2 = 175/11583.$$

Further, an initial estimate for F_2 can be obtained from the formula[21]

$$F_2 = 12.4(Z - 34)\ \text{cm}^{-1}.$$

Although these approximate parameters produce a satisfactory fit to the low-lying levels, it should be emphasized that they may give a completely invalid picture of the energy-level scheme at high energies.

In practice, the methods of Racah[53] are used in calculating the matrix elements of electrostatic interaction. It is therefore advantageous to construct operators that have simple transformation properties with

respect to the symmetry groups that are used to classify the states. In this system, the electrostatic energy becomes

$$E = \sum_{k=0}^{3} e_k E^k,$$

where the e_k are the angular parts of the new operators and E^k are linear combinations of the F_k, as follows:

$$E^1 = \tfrac{1}{9}(70F_2 + 231F_4 + 2002F_6);$$

$$E^2 = \tfrac{1}{9}(F_2 - 3F_4 + 7F_6);$$

$$E^3 = \tfrac{1}{3}(5F_2 + 6F_4 - 91F_6).$$

As with F_0, E^0 does not play a role in the level assignments. The initial sets of parameters E^k and F_k derived during the present investigation are given in Table I.

TABLE I. Values of Electrostatic and Spin-orbit Parameters Used in Preliminary Energy Level Calculations

	No. of f-electrons	E^1	E^2	E^3	ζ_{4f}	F_2	F_4	F_6
Pr^{3+}	2	4811.2	20.889	454.27	714.93	304.7	50.80	5.114
Nd^{3+}	3	5004.5	24.520	489.60	886.89	330.9	49.03	5.272
Pm^{3+}	4	4989.6	21.014	516.33	1019.1	325.6	56.14	4.569
Sm^{3+}	5	5596.4	29.850	545.88	1177.6	377.8	50.64	6.104
Eu^{3+}	6	6582.0	32.506	775.94	1297.4	470.6	70.91	4.953
Gd^{3+}	7	6353.9	43.670	715.78	1460.6	487.4	45.97	6.216
Tb^{3+}	8	6558.1	34.631	691.01	1707.0	455.0	62.60	6.349
Dy^{3+}	9	5962.1	23.833	580.81	1906.1	375.2	67.36	5.910
Ho^{3+}	10	6581.6	29.839	602.00	2123.4	416.0	66.37	7.385
Er^{3+}	11	6646.9	31.097	633.89	2390.2	430.2	66.75	7.139
Tm^{3+}	12	6835.6	33.062	657.63	2652.0	447.6	67.12	7.336

The energies of the low-lying levels are primarily a function of ζ_{4f}, so that the E^k parameters are only well defined if a number of levels belonging to different multiplets can be assigned. This usually requires making assignments at higher energies, and making such assignments is usually difficult. Many of the values of E^k and ζ_{4f} reported in the literature are not the result of a true least-squares fitting process where enough levels were assigned to adequately define each parameter. Frequently, the parameters quoted are closely related to those predicted assuming that the

4f wave functions are hydrogenic. All the parameters reported in the present study were determined as the result of a least-squares fitting process. The foregoing includes the parameters calculated from levels observed in crystal media.

2. Configuration Interaction

It has been shown[12,55,56,64] that the effects of configuration interaction must frequently be considered in order to obtain an adequate interpretation of the energy-level schemes of lanthanide ions. This can be accomplished in second-order perturbation theory by adding to the Hamiltonian certain model interactions acting wholly within the f^N configuration.[57] Such a procedure accounts for the part of the interaction that does not have the same angular form as the coefficients, e_k, of the electrostatic interaction parameters. The part that does have the same form as e_k is automatically absorbed in the E^k parameters. For f^N configurations, the additional interactions may be written as $H' = \alpha L(L+1) + \beta G(G_2) + \gamma G(R_7)$, where α, β, and γ are linear combinations of radial integrals and are treated as adjustable parameters. $G(G_2)$ and $G(R_7)$ are eigenvalues of Casimir's operator for the groups G_2 and R_7, respectively, and have been tabulated by Wybourne.[73] The parameters α and β have been determined previously for some ions, but crystal studies frequently do not allow assignment of a sufficient number of levels for a least-squares fit of six parameters (E^1, E^2, E^3, ζ_{4f}, α, and β). The γ used by Trees[66] is 1/12 of the β used here. The $\gamma G(R_7)$ is related to the correction βQ used by Racah[54] and Trees.[66] It is expected to be important only when large components in the eigenvectors of the observed levels have a seniority number different from that of the ground state. An attempt to determine γ has previously been possible only for the free-ion spectrum of Pr^{2+} (Ref. 58). In the present work, however, levels have been observed that have sufficient dependence on states of different seniority from that of the ground state to allow determination of γ for all of the trivalent lanthanides from Pr^{3+} through Er^{3+}. Note that γ and E^1 are not independent; they are related by a common term, $S(S+1)$, in their coefficients. Thus, changes in E^1 are expected when γ is added to the calculation.

In Fig. 1, the results of calculating the energy levels by diagonalizing the combined matrices of electrostatic and spin-orbit interaction are compared to the experimental data for the case of Pr^{3+} ($4f^2$). For two f-electrons, in the absence of any interaction with the environment (free-ion spectra), the spectrum should be composed of 13 levels, each $(2J+1)$ fold degenerate. Additional splitting does occur when the ion is incorporated in either a solid or liquid matrix. The crystal field levels for Pr^{3+} in LaF_3 (Ref. 13) are shown in Line A of Fig. 1. The centers of gravity of the crystal-field manifolds are shown in Line B. The latter is the type of spectrum that would be observed for the free ion. The levels calculated by fitting

the data of Line B with four parameters (E^1, E^2, E^3, and ζ_{4f}) are given in Line C. The spectrum of Pr^{3+} in dilute acid solution is shown at the bottom of Fig. 1. Thus, we characteristically find a band in solution corresponding to a given set of crystal levels in a solid matrix. The individual components that make up the band are not usually resolved. For our purposes, we identify the center of gravity of the band with the appropriate free-ion level.

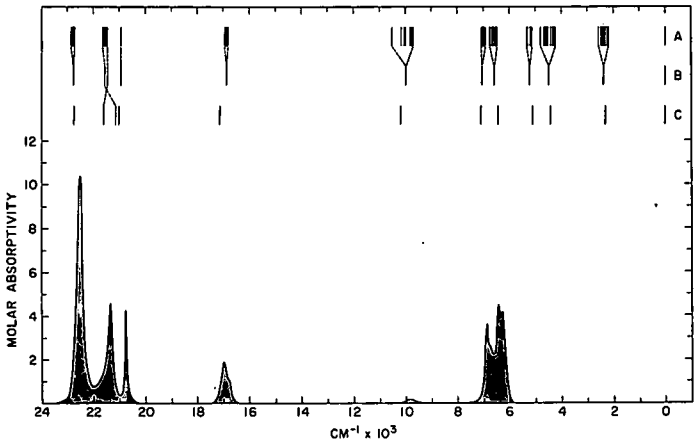

121-2513

Fig. 1
Comparison of (A) Observed Stark Components[13] and (B) Calculated Average Energies of Stark Components for Pr^{3+} in LaF_3 with (C) Calculated (Four-parameter) Free-ion Levels and Observed Absorption Spectrum of Pr^{3+} (AQ)

Detailed studies of lanthanide spectra in crystalline matrices require measurements taken at liquid-helium temperature. The ground level of a lanthanide ion is also split into Stark components by the crystal field, and only at very low temperatures is there assurance that all transitions arise from the lowest Stark level. Instead of placing the ground level at zero energy for parameter-fitting purposes, we have adopted the procedure of assigning it an energy corresponding to the center of gravity of the Stark components of the ground term in a suitable crystalline matrix.

3. Effect of Crystal-field Splitting on Energy-level Assignments

At room temperature, one can usually assume that a small percentage of the transitions may arise even from the highest Stark components of the ground level. One would, therefore, predict that a band observed at room temperature would be appreciably broadened by the presence of additional components on the low-energy side, compared to the band observed at low temperatures. Thus if an energy corresponding to the center of such a broadened band is assigned to the transition in question, an error (always in the direction of too low an energy) would result. Actually, the indicated effect is small.

Since the energies of the crystal-field components of many of the levels for Nd^{3+} in $LaCl_3$ (Ref. 5) and in LaF_3 (Ref. 14) have already been recorded in the literature, we examined the spectra of similar crystals at room temperature. The spectra were recorded with the same instrument that was used in all the other work reported here. Energies were assigned on the same basis as that used for the solution spectra. The results are given in Table II. In general, the satellites to a band arising from transitions

that originate in one of the higher Stark components of the ground level are relatively weak and do not appreciably affect the center of gravity observed at room temperature as compared to that established at liquid-helium temperature. In some cases, the satellites are well resolved from the principal band and can be clearly identified. For example, the incompletely resolved group of bands centered at 11,441 cm^{-1} for Nd^{3+} in $LaCl_3$ could be assigned to transitions arising from the lowest Stark component in the ground level and terminating in the $^4F_{3/2}$ level. Two isolated satellites, one centered at 11,322 cm^{-1} and a second weaker band at 11,198 cm^{-1}, were assigned to transitions from known Stark components of the ground level[5] at 115 and 244 cm^{-1}, respectively. We concluded that except in cases of resolved satellites, the process of assigning energies based on centers of gravity of bands observed at room temperature does not appear to be subject to any consistent error. Consequently, this procedure has been followed throughout the investigation.

TABLE II. Comparison between the Centers of Gravity of Levels for Nd^{3+} in $LaCl_3$ and in LaF_3 Crystals Observed at Liquid He Temperature and at Room Temperature

	Nd^{3+} in $LaCl_3$		Nd^{3+} in LaF_3	
S'L'J'	ν cm^{-1} (liquid He)[5]	ν cm^{-1}[(a)]	ν cm^{-1} (liquid He)[14]	ν cm^{-1}[(a)]
$^4I_{13/2}$	4010	3937	4089	4000
$^4I_{15/2}$	-	-	-	-
$^4F_{3/2}$	11439	11441	11613	11600
$^4F_{5/2}$	12466	12422	12610	12610
$^2H_{9/2}$	12618	-	12707	
$^4F_{7/2}$	13437	13386	13646	13586
$^4S_{3/2}$	13524			
$^4F_{9/2}$	14722	14577	14849	14792
$^2H_{11/2}$	15935	15847	16050	16025
$^4G_{5/2}$	17135	17094	17328[b]	17391
$^2G_{7/2}$	-	-	17551[b]	
$^2K_{13/2}$	-	-	-	-
$^4G_{7/2}$	19020	18939	19239	19230
$^4G_{9/2}$	19434	19379	19700[b]	19607
$^2K_{15/2}$	-	20876	-	-
$^2G_{9/2}$	21056	21141	-	-
$(^2D,^2F)_{3/2}$	21129	21459	-	-
$^4G_{11/2}$	21426		-	-
$^2P_{1/2}$	23214	23239	23468	23474
$^2D_{5/2}$	23780	23781	-	-

(a)Present measurement for center of band observed at room temperature.
(b)Approximate center of gravity calculated from incomplete data.

B. Calculation of Band Intensities

Any theoretical consideration of the intensities of the intra f^N-electron transitions observed in trivalent lanthanide spectra must begin with a determination of the possible mechanisms involved. This problem has been examined in detail.[2,6,40,67] The results show that there is some magnetic-dipole character in a few transitions, but only extremely weak contributions occur via an electric-quadrupole mechanism. An induced electric-dipole mechanism must be invoked to account for the intensities observed for most of the bands. The designation induced or forced electric dipole is used to acknowledge the fact that true electric-dipole transitions require the initial and final states to be of different parity, whereas for transitions occurring within the f^N configurations, the initial and final states have the same parity. In contrast to the foregoing, electric-quadrupole and magnetic-dipole transitions within the f^N configuration are (parity) allowed. Since the intensities of the intra f^N-electron transitions are extremely weak in comparison to true electric-dipole transitions, these intensities can be accounted for by assuming that a small amount of the character of higher-lying configurations of opposite parity is mixed into the f^N-electron states. It is postulated that this mixing is accomplished via the odd terms in the potential due to the ligand field experienced by the lanthanide ion. Note that in ligand fields with inversion symmetry there are no odd terms to induce such mixing.

1. Definition of Oscillator Strength

Experimentally determined band intensities are related to the probability for absorption of radiant energy P (oscillator strength) by the expression[33]

$$P = \frac{2303mc^2}{N\pi e^2} \int \epsilon_i(\sigma)\, d\sigma = 4.32 \times 10^{-9} \int \epsilon_i(\sigma)\, d\sigma, \qquad (1)$$

where ϵ is the molar absorptivity of the band at an energy σ (cm^{-1}), and the other symbols have their usual meaning. Notice that P is a dimensionless quanitity. The values of P reported here may be compared directly with those of Hoogschagen and co-workers,[32,33] although these workers calculated ϵ in terms of $\ln (I_0/I) = 2.303 \log (I_0/I)$ instead of the formula used here,

$$\epsilon = \frac{1}{c\ell} \log \frac{I_0}{I},$$

where

c = concentration of the lanthanide in moles/liter,

ℓ = light path in solution (cm),

and

$$\log (I_0/I) = \text{optical density measured at } \sigma \text{ cm}^{-1}.$$

The maximum molar absorptivities of lanthanide absorption bands in dilute aqueous solutions are seldom greater than 10 and average nearer to unity. Oscillator strengths of these bands are of the order of 1×10^{-6}.

2. Induced Electric-dipole Transitions

Judd[40] has shown that the oscillator strength of an induced electric-dipole transition may be related to the frequency of the transition (ν) expressed in sec^{-1}, and the square of the matrix elements of the unit tensor operators $\mathbf{U}^{(\lambda)}$ connecting the initial and final states (ψJ and $\psi' J'$) via three complex expressions T_λ ($\lambda = 2, 4$, and 6). These three quantities are related to the radial parts of the $4f^N$ wave functions, to the wave functions of perturbing configurations such as $4f^{N-1}5d$, the refractive index of the medium, and the ligand field parameters that characterize the environmental field. In principle, they can be calculated. In practice, as with the Slater integrals, they are treated as parameters to be determined from experimental data. Judd's result is given as

$$P = \sum_{\lambda=2,4,6} T_\lambda \nu \left(f^N \psi J || U^{(\lambda)} || f^N \psi' J' \right)^2 . \tag{2}$$

In the development of this expression, the relevant matrix elements were summed over the projection quantum numbers (m) and it was assumed that the crystal components of the ground level are equally populated.

The intermediate-coupling eigenvectors $|f^N \psi J>$ in the $|f^N \alpha SLJ>$ basis are of the form

$$|f^N \psi J> = \sum_{\alpha,S,L} C(\alpha,S,L) |f^N \alpha SLJ>, \tag{3}$$

where $C(\alpha,S,L)$ are the numerical coefficients resulting from the simultaneous diagonalization of the electrostatic and spin-orbit matrices. These eigenvectors were used to transform matrix elements, calculated in the LS-basis, into the intermediate-coupling scheme.

The matrix elements of Eq. 2 were calculated in the LS-basis by using the equation[41]

$$\left(f^N \alpha SLJ || U^{(\lambda)} || f^N \alpha' SL'J' \right) = (-1)^{S+L'+J+\lambda} [(2J+1)(2J'+1)]^{1/2} \begin{Bmatrix} J & J' & \lambda \\ L' & L & S \end{Bmatrix} \left(f^N \alpha SL || U^{(\lambda)} || f^N \alpha' SL' \right). \tag{4}$$

The reduced matrix elements on the right-hand side of Eq. 4 were taken from the tables of Nielson and Koster.[50] The matrix elements of Eq. 4 were then transformed from the LS-basis states to the intermediate-coupling scheme before being squared and substituted into Eq. 2.

The frequency of the transition ν, which appears in Eq. 2, can be expressed in terms of the measured energy in cm^{-1} (σ), using the identity $\nu = c\sigma$. In addition, the parameters T_λ contain the weighting factor $(2J+1)^{-1}$. To facilitate the comparison of the parameters for different ions, it is desirable to extract this factor. Thus we chose to rewrite Eq. 2 in the form

$$P = \sum_{\lambda=2,4,6} \frac{\mathcal{T}_\lambda \sigma \left(f^N \psi J \| U^{(\lambda)} \| f^N \psi' J' \right)^2}{2J+1}, \tag{5}$$

where

$$\mathcal{T}_\lambda = (2J+1)\, T_\lambda c \ (\text{cm}).$$

3. Magnetic-dipole Transitions

The oscillator strength for a magnetic-dipole transition is given by[2,73]

$$P_{M.D.} = \frac{8\pi^2 mc}{3he^2}\, \sigma\, \frac{\mathcal{S}(\psi J; \psi' J')}{2J+1}\, \eta = P' \eta \tag{6}$$

where $\mathcal{S}$ is the line strength whose square root is defined as

$$\mathcal{S}^{1/2}(\psi J; \psi' J') = \frac{-e}{2mc} (\psi J \| L + 2S \| \psi' J'). \tag{7}$$

The nonzero matrix elements will be those diagonal in the quantum numbers α, S, and L. Equation 7 was evaluated for all three cases permitted by the $\Delta J = 0, \pm 1$ selection rule using the following relationships:[2;73]

1) $J = J'$

$$(\alpha SLJ \| L + 2S \| \alpha SLJ) = g\hbar \sqrt{J(J+1)(2J+1)}, \tag{8}$$

where

$$g = 1 + \frac{J(J+1) + S(S+1) - L(L+1)}{2J(J+1)};$$

2) $J' = J - 1$

$$(\alpha SLJ \| L + 2S \| \alpha SLJ - 1) = \hbar \sqrt{\frac{(S+L+J+1)(S+L+1-J)(J+S-L)(J+L-S)}{4J}}; \tag{9}$$

3) $J' = J + 1$

$$(\alpha SLJ||L + 2S||\alpha SLJ+1) = \hbar\sqrt{\frac{(S+L+J+2)(S+J+1-L)(L+J+1-S)(S+L-J)}{4(J+1)}}. \quad (10)$$

The matrix elements calculated from Eqs. 8-10 were transformed into the intermediate coupling scheme and the magnetic-dipole oscillator strengths computed by using Eq. 6.

The magnetic-dipole oscillator strength is directly proportional to the refractive index, η. It was therefore necessary to include this factor in the calculation. A refractive index factor $\chi = (\eta^2+2)^2/9\eta$ also occurs in the parameter $\mathcal{T}_\lambda$. Since the solutions examined were dilute both in terms of lanthanide and acid concentration, η was taken as that of pure H_2O.[34] Calculation showed that χ changed less than 3% (from 1.179 to 1.208) in the spectral range 8000-32,500 cm^{-1}, and only 5% between 32,500 and 50,000 cm^{-1}. Since we are mainly concerned with the relative values of $\mathcal{T}_\lambda$ over the series, we treated χ as a constant equal to unity in the induced electric-dipole calculations.

To compare the results tabulated here with those published elsewhere, the following conversion factors are given:

(a) $\mathcal{T}_\lambda = (2J+1)\, cT_\lambda$ (Judd)

(b) Krupke[44] has applied Judd's expression to the spectra of Pr^{3+}, Nd^{3+}, Er^{3+}, Tm^{3+}, and Yb^{3+} in matrices of solid Y_2O_3 and LaF_3. The value of f (oscillator strength) is identical to P in the present report, and Krupke's $\overline{\Omega}_\lambda$ is related to $\mathcal{T}_\lambda$ by the expression

$$\mathcal{T}_\lambda = \frac{8\pi^2 mc}{3h}\,\chi\overline{\Omega}_\lambda$$

$$= 1.085 \times 10^{11}\,\chi\overline{\Omega}_\lambda.$$

We assume $\chi_{AVE}\,(Y_2O_3) \sim 1.9$ and $\chi_{AVE}\,(LaF_3) \sim 1.4$.

In the relatively few transitions where the calculated magnetic-dipole oscillator strength ($P_{M.D.}$) constituted an appreciable fraction of the total oscillator strength of the corresponding absorption band, P_{TOT}, a correction was made. The residual, $P_{TOT} - P_{M.D.}$, was used as the induced electric-dipole intensity. Calculated magnetic dipole oscillator strengths for all the 3+ lanthanides were obtained from Table III, where $P' \times 10^8$ (Eq. 6) is the quantity tabulated. For dilute acid solutions, $\eta = 1.33$ was used to obtain $P_{M.D.}$

TABLE III. Calculated Magnetic Dipole Oscillator Strengths for the 3+ Lanthanides[a]

	S'L'J'	E_{calc} (cm^{-1})[b]	P' x 10^{8} [c]		S'L'J'	E_{calc} (cm^{-1})[b]	P' x 10^{8} [c]
Pr^{3+}	$^3H_5$	2322	9.76	Tb^{3+}	$^7F_5$	2112	12.11
	$^3F_3$	6540	0.02		$^5G_6$	26425	5.03
	$^3F_4$	6973	0.49		$^5G_5$	27795	0.36
	$^1G_4$	9885	0.25		$^5L_6$	29550	0.14
Nd^{3+}	$^4I_{11/2}$	2007	14.11		$^5H_7$	31537	0.06
	$^2H_{9/2}$	12738	1.12		$^5H_6$	33027	0.46
	$^4F_{9/2}$	14854	0.20		$^5H_5$	33879	0.03
	$^2G_{7/2}$	17333	0.02		$^5F_5$	34927	1.87
	$^2I_{11/2}$	28624	0.05		$^5G_6$	41082	0.23
Pm^{3+}	$^5I_5$	1577	16.36	Dy^{3+}	$^6H_{13/2}$	3506	22.68
	$^5F_4$	14562	0.08		$^4I_{15/2}$	22293	5.95
	$^3H_4$	17327	1.30		$^4I_{13/2}$	25919	0.41
	$^5G_4$	20181	0.26		$^4K_{17/2}$	26365	0.09
	$^3G_4$	23897	0.11		$(^4M,^4I)_{15/2}$	29244	0.69
	$^3I_5$	27916	0.23		$^4M_{17/2}$	30892	0.03
	$^3H_4$	35473	0.04		$^4K_{15/2}$	31795	0.12
Sm^{3+}	$^6H_{7/2}$	1080	17.51		$^4H_{13/2}$	33471	0.60
	$^6F_{3/2}$	6641	0.02		$(^4K,^4L)_{13/2}$	33776	0.37
	$^6F_{5/2}$	7131	0.08		$(^2K,^2L)_{15/2}$	38811	0.09
	$^4G_{5/2}$	17924	1.76		$^4I_{15/2}$	41596	0.03
	$^4F_{3/2}$	18832	0.03	Ho^{3+}	$^5I_7$	5116	29.47
	$^4G_{7/2}$	20014	0.05		$^3K_8$	21308	6.39
	$^4F_{5/2}$	22098	0.45		$^3K_7$	26117	0.28
	$^4H_{7/2}$	28396	0.67		$^3L_9$	29020	0.12
	$^4G_{5/2}$	30232	0.03		$^3L_8$	34306	0.17
	$^4G_{5/2}$	42714	0.02		$^3L_7$	38022	0.04
	$^4G_{7/2}$	42965	0.06		$^3I_7$	38470	0.36
	$(^4H,^2G)_{7/2}$	44237	0.04	Er^{3+}	$^4I_{13/2}$	6610	30.82
Eu^{3+}	$^7F_1$	350	17.73		$^2K_{15/2}$	27801	3.69
	$^5D_1$	19026	1.62		$^2K_{13/2}$	33085	0.11
	$^5F_1$	33429	2.16		$^2L_{17/2}$	41686	0.03
Gd^{3+}	$^6P_{7/2}$	32224	4.13		$^2I_{13/2}$	43717	0.12
	$^6P_{5/2}$	32766	2.33	Tm^{3+}	$^3H_5$	8390	27.25
	$^6D_{9/2}$	39779	0.03		$^1I_6$	34886	1.40
	$^6D_{7/2}$	40712	0.39	Yb^{3+}	$^2F_{3/2}$	10400	17.76
	$^6D_{5/2}$	40977	0.20				

[a]Results are recorded only for transitions in which P' > 0.015 x 10^{-8}.

[b]The eigenvectors used in these calculations are those generated by the parameters recorded in Table XXX for aqueous solutions.

[c]For dilute acid solutions of the lanthanides, it was assumed that η = 1.33 in the expression $P_{M.D.} = P'\eta$.

4. Determination of the Intensity Parameters, $\mathcal{T}_\lambda$

The parameters $\mathcal{T}_\lambda$ are a function of the quantities that describe the immediate environment of the ion, the index of refraction of the medium, and the radial-wave functions of the states involved.[40] Since we are not at this time able to calculate $\mathcal{T}_\lambda$, although in principle this could be done, we adopted a semiempirical procedure for testing the validity of the theory. The quantities $\mathcal{T}_\lambda$ were evaluated by relating the experimentally determined oscillator strength, P, to the energy of the transition, σ, and the calculated matrix elements of the operator $\mathbf{U}^{(\lambda)}$.

Typical sets of experimental oscillator strengths and calculated matrix elements are shown for Pr^{3+} in Tables IV and V.* Where two or

TABLE IV. Oscillator Strengths for Pr^{3+} (AQ)

Spectral Region[a] cm^{-1}	S'L'J'	P x 10^6			
		$HClO_4$-$DClO_4$			$PrCl_3$[32]
		Expt	Calc[b]	Calc[c]	Expt
5800-7700	$^3F_3$, $^3F_4$	12.79	14.09	41.12	
9100-11000	$^1G_4$	0.32	0.67	1.32	0.34
16000-17500	$^1D_2$	3.08	2.18	4.45	3.12
20200-21000	$^3P_0$	2.54	6.88	2.99	2.52
21000-22100	$^3P_1$, $^1I_6$	7.63	4.14	7.27	6.66
22100-23500	$^3P_2$	15.06	12.49	14.64	14.6
RMS Deviation			3.7×10^{-6}	1.3×10^{-6}	

[a]Range encompassing observed band(s).
[b]This fit included the six indicated bands.
$\mathcal{T}_2 = -309.6 \pm 147.6 \times 10^{-9}$
$\mathcal{T}_4 = 17.28 \pm 6.66 \times 10^{-9}$
$\mathcal{T}_6 = 32.22 \pm 9.09 \times 10^{-9}$
[c]This fit included data for five bands; the band extending from 5800 to 7700 cm^{-1} was not included.
$\mathcal{T}_2 = 42.0 \pm 91.8 \times 10^{-9}$
$\mathcal{T}_4 = 7.4 \pm 3.2 \times 10^{-9}$
$\mathcal{T}_6 = 41.2 \pm 3.8 \times 10^{-9}$

*In Table V and other related tables, we have adopted the following convention respecting $U(\lambda) = (\psi J||U^{(\lambda)}||\psi'J')^2$. If $(\psi J||U^{(\lambda)}||\psi'J')^2 < 10^{-14}$, $U(\lambda) = 0$; if $5 \times 10^{-5} > (\psi J||U^{(\lambda)}||\psi'J')^2 > 10^{-14}$, $U(\lambda) = \sim 0$.

TABLE V. Energy Level Assignments and Matrix Elements of $U^{(\lambda)}$ for Pr^{3+} (AQ)

S'L'J'	E_{expt} (cm^{-1})	E_{calc}[a] (cm^{-1})	ΔE (cm^{-1})	U(2)[b]	U(4)[b]	U(6)[b]
$^3H_4$	200[c]	245	-45	-	-	-
$^3H_5$	2360[c]	2322	38	0.1095	0.2017	0.6109
$^3H_6$	4500	4496	4	0.0001	0.0330	0.1395
$^3F_2$	5200	5149	51	0.5089	0.4032	0.1177
$^3F_3$	6500	6540	-40	0.0654	0.3469	0.6983
$^3F_4$	6950	6973	-23	0.0187	0.0500	0.4849
$^1G_4$	9900	9885	15	0.0012	0.0072	0.0266
$^1D_2$	16840	16840	0	0.0026	0.0170	0.0520
$^3P_0$	20750	20706	44	0	0.1728	0
$^3P_1$	21300	21330	-30	0	0.1707	0
$^1I_6$	21500[c]	21500	0	0.0093	0.0517	0.0239
$^3P_2$	22520	22535	-15	~0	0.0362	0.1355
$^1S_0$	46900[c]	46900	0	0	0.0070	0
	RMS Deviation		48			

[a]The parameters used to generate this set of energies are given in Table XXX.

[b]$U(\lambda) = [\psi J||U^{(\lambda)}||\psi' J']^2$.

[c]Assumed energy based on data in Ref. 13 and 47.

more transitions gave rise to a band system that could not be clearly resolved into the requisite components, the total area was measured and equated to the combined matrix elements of the transitions involved. A least-squares analysis was used to obtain the optimum set of the parameters $\mathcal{T}_2$, $\mathcal{T}_4$, and $\mathcal{T}_6$. The statistical significance of the parameters was gauged by computing their standard errors in the usual manner. The root-mean-square (rms) deviation of the observed and calculated oscillator strengths was defined as

$$\text{RMS} = \left(\frac{\text{sum of squares of deviations}}{\text{number of observations--number of parameters}}\right)^{1/2}. \quad (11)$$

III. EXPERIMENTAL PROCEDURES AND CURVE FITTING

The absorption spectra reported here were observed by using a high-resolution, prism-grating recording spectrophotometer with a useful spectral range of 0.19-2.6 μ. The lanthanides used, except for Pm^{3+}, were supplied as oxides of >99.9% purity. Crystals of $LaCl_3$ and LaF_3 doped with Nd^{3+} were obtained through the courtesy of J. G. Conway, University of California. The techniques for purifying and obtaining the solution spectra of Pm^{3+} have already been described.[8] Both dilute $DClO_4$ and $HClO_4$ were used as solvent media. The former was useful in extending the region in which absorption bands could be measured in the near infrared.[11] No difference was observed in measurements in the two solvents in the visible-ultraviolet region.

The spectral data were recorded on punched cards via digital readout equipment connected directly to the spectrophotometer. The data for any single curve or set of curves were then read into a computer and resolved into a suitable number of components (m) to enable evaluation of the total area involved. Originally, we used a Gaussian function as the basis for resolution and curve fitting.[6] Subsequently it became clear that a function intermediate between a Gaussian, where the tailing is not as great as that observed experimentally, and a Lorentzian, where the tailing is excessive, would be useful.

The modified Gaussian-Lorentzian function adopted had the form

$$y = \sum_{i=1}^{m} \frac{a_i}{\left(\frac{x - b_i}{c_i}\right)^2 + 1} \exp\left[-\frac{1}{K}\left(\frac{x - b_i}{c_i}\right)^2\right], \qquad (12)$$

where

m is the number of components in the band,

a_i is the peak of height,

b_i is the energy at which a_i is observed,

c_i is related to the width of the peak,

and

$K \geq 1$ and integral.

After attempting to fit several different experimental absorption bands with the foregoing function, varying the value of K, we found that $K = 24$ gave the best agreement with the area obtained independently by integration over the observed data points. The attempt to "fit" the band due to the transition from the ground state to the $^1D_2$ level in Pr^{3+} is shown in Fig. 2 to illustrate the difference in results obtained with the pure Gaussian,

the pure Lorentzian, and the modified function finally adopted. Of course, in some other cases the data were fit almost equally well with pure Gaussian curves. It should be emphasized that the modified function was developed from an examination of the experimental data and was not derived from theoretical considerations.

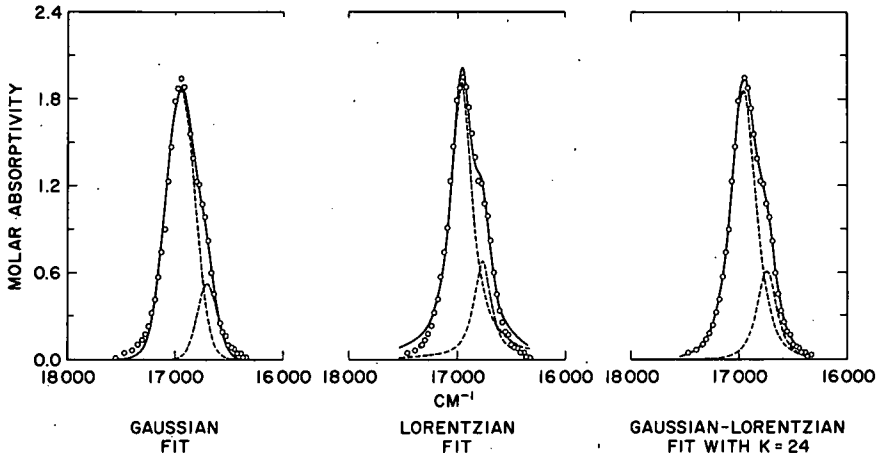

121-2510

Fig. 2. Comparison of Attempts to "Fit" the Shape of an Observed Absorption Band with the Three Different Functions: Gaussian, Lorentzian, and Modified Gaussian-Lorentzian. oooooo observed data points; ------- resultant two components based upon computer resolution using one of the functions; and ——— sum of the two component curves.

IV. RESULTS OF INTENSITY CORRELATIONS

A. Discussion of Experimental Results

1. Pr^{3+} (f^2)

In an earlier attempt to fit the experimental intensity data for Pr^{3+} using Gaussian curves as a basis for integrating observed absorption bands, we found that $\mathcal{T}_2$ was particularly poorly determined.[6] Subsequent recalculation of the data using matrix elements based on a better energy-level fit and resolution of the complex ^3P - ^1I structure based upon the Gaussian-Lorentzian function, has clarified some aspects of the problem (as shown in Table V).

We were not able to resolve the complex band due to transitions to the $^3F_3$ and $^3F_4$ levels near 6700 cm^{-1}, shown in Fig. 3, but we resolved the ^3P - ^1I group into components due to $^3P_0$, $^3P_2$, and the combined $^3P_1$ + $^1I_6$ transitions. Thus the parameters $\mathcal{T}_\lambda$ were determined by a fit to a maximum of six bands (as shown in Table IV).

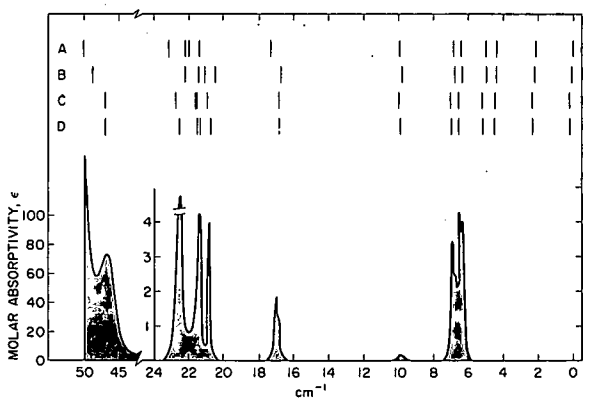

Fig. 3

Comparison of Experimental and Calculated Energy Levels with Observed Absorption Spectrum of Pr^{3+} (AQ)

A. Experimentally determined free-ion levels of Pr^{3+} (Ref. 64).
B. Average energies of Stark levels for Pr^{3+} in $LaCl_3$ (Ref. 59).
C. Average energies of Stark levels for Pr^{3+} in LaF_3 (Ref. 13).
D. Calculated (seven-parameter) free-ion levels for Pr^{3+} (AQ).

121-951 Rev. 3

The large matrix elements of $\mathbf{U}^{(4)}$ and $\mathbf{U}^{(6)}$ for the $^3F_3$ and $^3F_4$ transitions, together with values for $\mathcal{T}_4$ and $\mathcal{T}_6$ computed for the visible region of the spectrum, predicted much more intensity near 6700 cm^{-1} than was actually observed (as shown in Table IV). When the 6700-cm^{-1} band is included in the fitting process, a negative value is calculated for $\mathcal{T}_2$, since within the framework of the problem this is the only mechanism to compensate for the excessively large oscillator strength computed from $\mathcal{T}_4$ and $\mathcal{T}_6$. No additional weighting factors were used in obtaining the indicated fit.

In fitting the experimental data for Pr^{3+} in LaF_3, Krupke[44] obtained good agreement between observed and calculated intensities for the infrared portion of the spectrum and a poor fit (values of P_{calc} that were too small) to the observed intensities due to $^3P_1$ + $^1I_6$ and $^3P_2$. Thus, in effect the results were similar to those obtained in solution, and we conclude that Judd's theory cannot fully account for the intensity relationships in Pr^{3+}. Since we were able to fit the energy-level scheme quite satisfactorily, the

problem is not one of poorly determined electrostatic and spin-orbit parameters. Clearly we can force a good fit on the bands observed in solution in the visible-near-infrared region, and argue that the resulting poor fit to the ^3P - ^1I group is related to the proximity of the excited $f^{N-1}d$ configuration.[17,47] However, the resulting parameters involve a negative value for $\mathcal{T}_2$, and this is inconsistent with Judd's theory.

2. Nd^{3+} (f^3)

Recalculation of the intensity parameters for Nd^{3+} based on more extensive experimental data and on an improved energy-level fit to the bands observed in solution (as shown in Table VI), has only slightly modified the values we originally reported.[6] It is characteristic of trivalent lanthanide spectra that the intra-f-transitions in the ultraviolet region are superimposed upon the tail of a much more intense absorption. It is reasonable to assume that the absorption in this case is due to an f → d transition,[17] which has a maximum at >45,000 cm^{-1}. Thus, any intensity measurements involving f → f transitions in the ultraviolet region normally require that a background absorption be subtracted. The correction, particularly for weak bands such as are observed in the spectrum Nd^{3+} in the region 30,000-50,000 cm^{-1} (shown in Fig. 4), imparts a rather large

TABLE VI. Values of $\mathcal{T}_\lambda$ for the Lanthanides in Dilute Acid

	$\mathcal{T}_2 \times 10^9$ (cm)	$\mathcal{T}_4 \times 10^9$ (cm)	$\mathcal{T}_6 \times 10^9$ (cm)
Pr^{3+}	42.0 ± 91.8	7.4 ± 3.2	41.2 ± 3.8
Nd^{3+}	1.20 ± 0.41	6.44 ± 0.36	10.2 ± 0.54
Pm^{3+}	3.61 ± 0.31	3.25 ± 0.48	5.42 ± 0.27
Sm^{3+}	1.17 ± 1.12	5.32 ± 0.35	3.47 ± 0.33
Eu^{3+}	1.88	8.59	6.96 ± 0.46
Gd^{3+}	3.30 ± 0.62	6.06 ± 0.53	6.10 ± 0.10
Tb^{3+}	0.005 ± 0.04	9.26 ± 2.96	4.45 ± 0.29
Dy^{3+}	1.93 ± 5.23	4.44 ± 0.21	4.46 ± 0.28
Ho^{3+}	0.47 ± 0.18	4.05 ± 0.21	3.96 ± 0.21
Er^{3+}	2.05 ± 0.16	2.51 ± 0.24	2.45 ± 0.12
Tm^{3+}	1.03 ± 0.82	2.68 ± 0.38	2.40 ± 0.21
Yb^{3+}	-	2.13	2.13

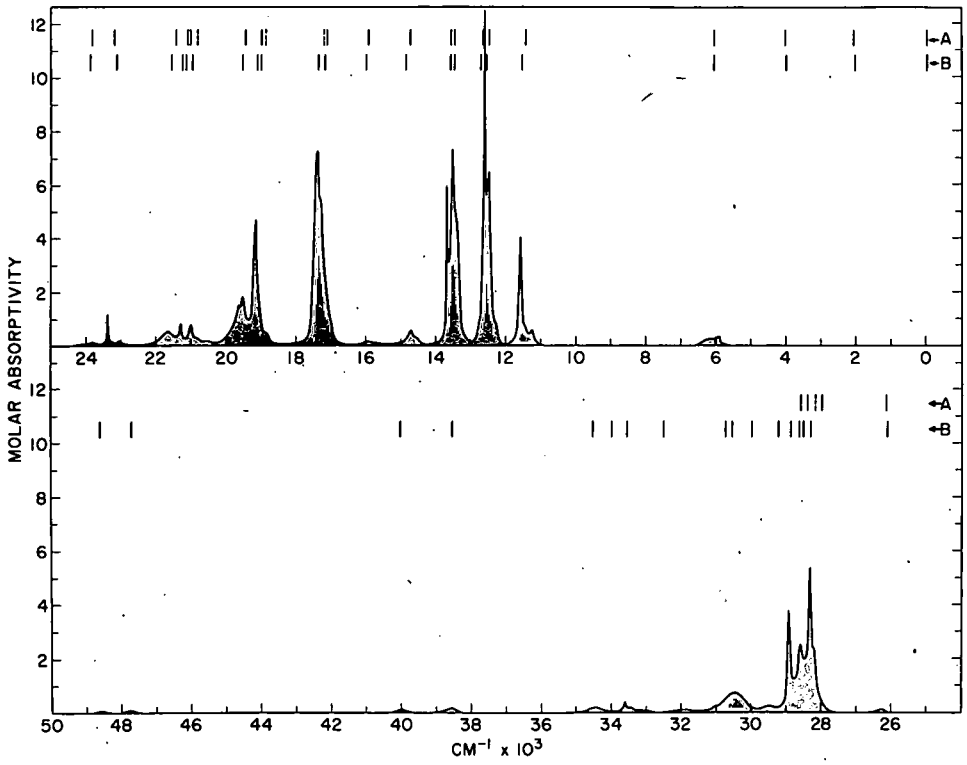

Fig. 4. Comparison of Experimental and Calculated Energy Levels with Observed Absorption Spectrum of Nd^{3+} (AQ). A. Centers of gravity of Stark components for Nd^{3+} in $LaCl_3$ (Ref. 5). B. Calculated free-ion levels for Nd^{3+} (AQ).

probable error to the experimental values obtained. Nevertheless, the correlation between observed and calculated oscillator strengths up to 40,000 cm^{-1} (listed in Table VII) is satisfactory in practically every instance. The notable exception is the band near 30,500 cm^{-1}, where the calculated matrix elements of $\mathbf{U}^{(\lambda)}$, shown in Table VIII, are much too small to account for the observed intensity.

3. Pm^{3+} (f^4)

We were only able to obtain reproducible intensity measurements for Pm^{3+} to ~21,000 cm^{-1} (as shown in Fig. 5), although weaker bands were observed between 21,000 and 25,000 cm^{-1}. Beyond 25,000 cm^{-1}, no bands were observed above the very large background absorption due primarily to products of radiation decomposition of the solutions.[8] The strong bands reported by Gruber and Conway[23] near 30,000 cm^{-1}, are consistent with the large matrix elements of $\mathbf{U}^{(4)}$ calculated for transitions to $^5D_{0,1,2}$ (as shown in Table IX).

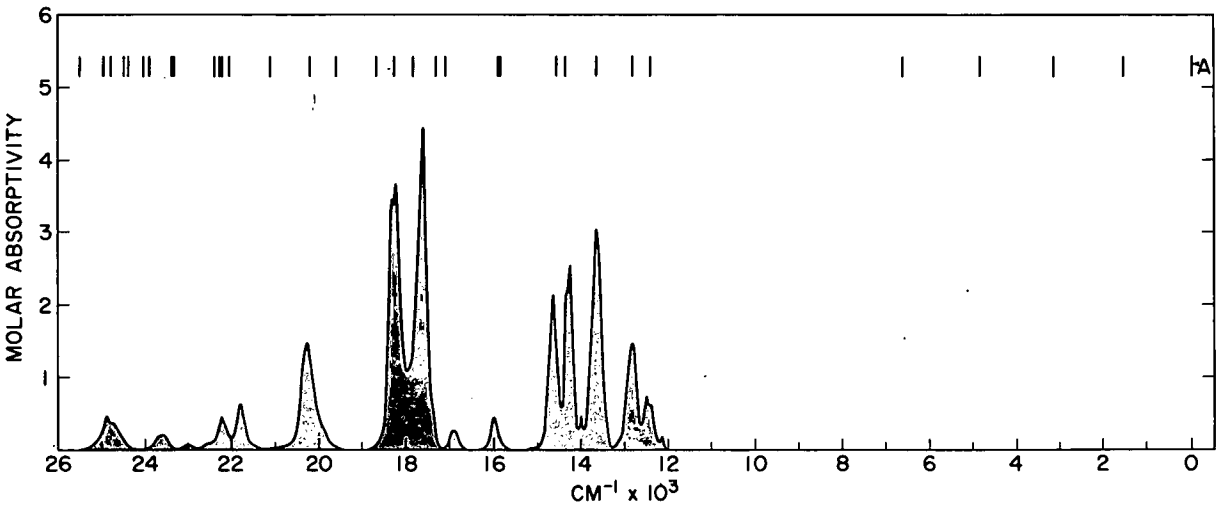

121-2511 Rev. 2

Fig. 5. Comparison of (A) Calculated Energy Levels with Observed Absorption Spectrum of Pm^{3+} (AQ)

Observed and calculated oscillator strengths are compared in Table X, using the parameters shown in Table VI. Over the limited region in which reproducible measurements could be made, the correlation was good.

4. Sm^{3+} (f^5)

Aside from the relatively intense bands in the near infrared region, most of the transitions in Sm^{3+} give rise to rather weak absorption maxima. The level density is very high in the visible-ultraviolet region (as shown in Fig. 6). However, on the basis of the assignments made, and the resolution of complex groups, it was possible to obtain the intensity correlation shown in Table XI. The parameters used to generate the calculated oscillator strengths are given in Table VI. At energies >30,000 cm^{-1}, as indicated by the very small matrix elements of $\mathbf{U}^{(\lambda)}$ (listed in Table XII), only very weak bands are observed.

TABLE VII. Oscillator Strengths for Nd^{3+} (AQ)

Spectral Region[a] (cm^{-1})	S'L'J'	P x 10^6			
		$HClO_4$-$DClO_4$		$NdCl_3$[32]	$Nd(ClO_4)_3$[62]
		Expt	Calc[b]	Expt	Expt
5600-6900	$^4I_{15/2}$	0.49	0.28		
11000-12000	$^4F_{3/2}$	2.56	2.34	3.02	2.3
12000-13000	$^4F_{5/2}$, $^2H_{9/2}$	8.84	8.62	9.22	7.7
13000-14200	$^4S_{3/2}$, $^4F_{7/2}$	8.90	9.50	8.88	7.6
14200-15200	$^4F_{9/2}$	0.65	0.72	0.83	0.51
15600-16200	$^2H_{11/2}$	0.15	0.19	0.39	0.14
16600-18200	$^4G_{5/2}$, $^2G_{7/2}$	9.76	9.88	10.5	8.3
18600-20200	$^2K_{13/2}$, $^4G_{7/2}$, $^4G_{9/2}$	7.01	5.35	6.58	5.8
20200-22400	$^2K_{15/2}$, $^2G_{9/2}$, $(^2D,^2F)_{3/2}$, $^4G_{11/2}$	2.33	1.39	2.31	1.9
23100-23500	$^2P_{1/2}$	0.41	0.55	0.38	0.30
23500-24200	$^2D_{5/2}$	0.09	0.05	0.08	0.06
26000-26500	$(^2P,^2D)_{3/2}$	0.03	0.04	0.05	0.02
27600-29800	$^4D_{3/2}$, $^4D_{5/2}$, $^2I_{11/2}$, $^4D_{1/2}$, $^2L_{15/2}$	9.42	10.29	9.52	9.8
29800-31300	$^2I_{13/2}$, $^4D_{7/2}$, $^2L_{17/2}$	2.70	0.15	2.36	1.7
31300-32300	$^2H_{9/2}$	0.13	0.17	-	0.76
33000-34000	$^2D_{3/2}$, $^2H_{11/2}$	0.33	0.48	-	0.60
34000-34900	$^2D_{5/2}$	0.28	0.13	-	0.76
38200-40000	$^2F_{5/2}$	0.18	0.09	-	1.9
	RMS Deviation		5.8×10^{-7}		

[a]Range encompassing observed band(s).
[b]The parameters used to obtain these values are given in Table VI.

TABLE VIII. Energy Level Assignments and Matrix Elements of $U^{(\lambda)}$ for Nd^{3+} (AQ)

	Nd^{3+} in $LaCl_3$ [5]			Nd^{3+} (AQ)					
S'L'J'	E_{expt} (cm^{-1})	E_{calc} [a] (cm^{-1})	ΔE (cm^{-1})	E_{expt} (cm^{-1})	E_{calc} [a] (cm^{-1})	ΔE (cm^{-1})	U(2) [b]	U(4) [b]	U(6) [b]
$^4I_{9/2}$	146	178	-32	146[c]	130	16	-	-	-
$^4I_{11/2}$	2028	2043	-15	2028[c]	2007	21	0.0194	0.1073	1.1652
$^4I_{13/2}$	4010	4029	-19	4050	4005	45	0.0001	0.0136	0.4557
$^4I_{15/2}$	6058	6092	-34	6050	6080	-30	0	0.0001	0.0452
$^4F_{3/2}$	11438	11475	-37	11460	11527	-67	0	0.2293	0.0549
$^4F_{5/2}$	12466	12517	-51	12480	12573	-93	0.0010	0.2371	0.3970
$^2H_{9/2}$	12618	12710	-92	12590	12738	-148	0.0092	0.0080	0.1151
$^4F_{7/2}$	13437	13504	-67	13500	13460	40	0	0.0027	0.2352
$^4S_{3/2}$	13524	13435	89	13500	13565	-65	0.0010	0.0422	0.4245
$^4F_{9/2}$	14722	14793	-71	14700	14854	-154	0.0009	0.0092	0.0417
$^2H_{11/2}$	15935	16001	-66	15870	16026	-156	0.0001	0.0027	0.0104
$^4G_{5/2}$	17135	16999	136	17300	17167	133	0.8979	0.4093	0.0359
$^2G_{7/2}$	-	17194	-	17460	17333	127	0.0757	0.1848	0.0314
$^2K_{13/2}$	-	18874	-	-	19018	-	0.0068	0.0002	0.0312
$^4G_{7/2}$	19020	18965	55	19160	19103	57	0.0550	0.1570	0.0553
$^4G_{9/2}$	19434	19369	64	19550	19544	6	0.0046	0.0608	0.0406
$^2K_{15/2}$	-	20858	-	21000	21016	-16	0	0.0052	0.0143
$^2G_{9/2}$	21056	21060	-4	21300	21171	129	0.0010	0.0148	0.0139
$(^2D, ^2P)_{3/2}$	21129	21191	-62	21300	21266	34	0	0.0188	0.0002
$^4G_{11/2}$	21426	21357	69	21650	21563	87	~0	0.0053	0.0080
$^2P_{1/2}$	23214	23050	164	23250	23140	110	0	0.0367	0
$^2D_{5/2}$	23780	23750	30	23900	23865	35	~0	0.0002	0.0021
$(^2P, ^2D)_{3/2}$	26160	26158	2	26300	26260	40	0	0.0014	0.0008
$^4D_{3/2}$	27981	27990	-9	28300	28312	-12	0	0.1960	0.0170
$^4D_{5/2}$	-	28187	-	28500	28477	23	0.0001	0.0567	0.0275
$^2I_{11/2}$	-	28388	-	-	28624	-	0.0049	0.0146	0.0034
$^4D_{1/2}$	28505	28563	-58	28850	28894	-44	0	0.2584	0
$^2L_{15/2}$				-	29260	-	0	0.0248	0.0097
$^2I_{13/2}$				-	29966	-	0.0001	0.0013	0.0017
$^4D_{7/2}$				30500	30554	-54	~0	0.0037	0.0080
$^2L_{17/2}$				-	30747	-	0	0.0010	0.0012
$^2H_{9/2}$				-	32567	-	0.0001	0.0085	~0
$^2D_{3/2}$				33400	33481	-81	0	0.0112	0.0012
$^2H_{11/2}$				-	33913	-	0.0001	0.0001	0.0002
$^2D_{5/2}$				34450	34474	-24	0.0007	0.0006	0.0034
$^2F_{5/2}$				38500	38504	-4	0.0021	0.0033	~0
$^2F_{7/2}$				39950	39926	24	~0	0.0004	0.0007
$^2G_{9/2}$				47700	47696	4	~0	0.0015	0.0001
$^2G_{7/2}$				48600	48586	14	0.0004	0.0024	0.0002
	RMS Deviation		84	RMS Deviation		88			

[a] The parameters used to generate this set of energies are given in Table XXX.

[b] $U(\lambda) = \left[\psi J \| U^{(\lambda)} \| \psi' J'\right]^2$.

[c] Assumed energy based on data in Ref. 5.

TABLE IX. Energy Level Assignments and Matrix Elements of $U^{(\lambda)}$ for Pm^{3+} (AQ)

S'L'J'	E_{expt} (cm^{-1})	E_{calc}[a] (cm^{-1})	ΔE (cm^{-1})	U(2)[b]	U(4)[b]	U(6)[b]
$^5I_4$	150[c]	99	51			
$^5I_5$	-	1577	-	0.0246	0.1172	0.9694
$^5I_6$	-	3186	-	0.0018	0.0301	0.6893
$^5I_7$	4850	4876	-26	0	0.0025	0.1581
$^5I_8$	6600	6611	-11	0	~0	0.0103
$^5F_1$	12400	12398	2	0	0.1404	0
$^5F_2$	12820	12811	9	0.0026	0.1992	0.1264
$^5F_3$	13600	13651	-51	~0	0.1041	0.4253
$^5S_2$	14300	14337	-37	~0	0.0011	0.2295
$^5F_4$	14650	14562	88	0.0005	0.0291	0.2403
$^5F_5$	15900	15863	37	~0	0.0021	0.0346
$^3K_6$	15900	15875	25	0.0024	0.0025	0.0104
$^3K_7$	-	17163	-	0	0.0020	0.0200
$^3H_4$	17300	17327	-27	0.0064	0.0210	0.0240
$^5G_2$	17700	17857	-157	0.7215	0.2433	0.0041
$^5G_3$	18300	18256	44	0.1444	0.2655	0.0454
$^3K_8$	-	18719	-	0	0.0003	0 0088
$^3H_5$	-	19617	-	0.0001	0.0057	0.0062
$^5G_4$	20250	20181	69	0.0093	0.0957	0.0787
$^3G_3$	-	21102	-	0.0228	0.0652	0.0075
$^5G_5$	21900	21998	-98	0.0003	0.0103	0.0365
$^3D_2$	-	22178	-	0.0072	0.0025	0.0028
$^5G_6$	22300	22262	38	~0	0.0002	0.0008
$^3L_7$	22300	22372	-72	0	0.0016	0.0099
$^3D_1$	-	23321	-	0	0.0001	0
$^3L_8$	23500	23444	56	0	0.0019	0.0133
$^3G_4$	-	23897	-	0.0013	0.0112	0.0044
$^3H_6$	-	23995	-	~0	0.0002	0.0041
$^3L_9$	-	24412	-	0	0	0.0019
$(^3M,^1L)_8$	-	24462	-	0	0.0045	0.0013
$^3D_3$	24800	24800	0	0.0007	0.0032	0.0095
$^3P_0$	-	25066	-	0	~0	0
$(^1D,^3P)_2$	-	25538	-	~0	0.0002	0.0003
$^3G_5$	-	26235	-	0.0002	0.0006	0.0007
$^3F_4$	-	26643	-	~0	0.0005	0.0008
$^3P_1$	-	27051	-	0	0.0003	0
$^3M_9$	-	27804	-	0	0	0.0007
$^3F_2$	-	27894	-	0.0091	0.0062	~0
$^3I_5$	-	27916	-	0.0042	0.0004	0.0006
$^3F_2$	-	28193	-	0.0048	0.0097	0.0025
$^3M_{10}$	-	28395	-	0	0	~0
$^3F_3$	-	28810	-	0.0002	0.0031	0.0013
$^3I_6$	-	29078	-	0.0003	0.0006	0.0011
$^1L_8$	-	29189	-	0	0.0015	0.0008
$^3I_7$	-	29587	-	0	0.0001	0.0002
$^5D_0$	30040	29979	61	0	0.1520	0
$^5D_1$	30480	30471	9	0	0.2361	0
$^3F_3$	-	30816	-	0.0012	0.0096	0.0046
$^5D_2$	31250	31266	-16	0	0.1013	0.0214
	RMS Deviation		78			

[a] The parameters used to generate this set of energy levels are given in Table XXX.

[b] $U(\lambda) = (\psi_J \| U^{(\lambda)} \| \psi' J')^2$.

[c] Assumed center of Stark components of the ground level.

TABLE X. Oscillator Strengths for Pm^{3+} (AQ)

Spectral Region[a] (cm^{-1})	S'L'J'	P x 10^6 $HClO_4$-$DClO_4$ Expt	P x 10^6 $HClO_4$-$DClO_4$ Calc[b]	P x 10^6 $Pm(ClO_4)_3$ (62) Expt
12000-12600	$^5F_1$	0.77	0.63	2.5
12600-13200	$^5F_2$	1.94	1.93	3.2
13200-14000	$^5F_3$	3.76	4.00	4.6
14000-14400	$^5S_2$	2.38	1.97	3.0
14400-15200	$^5F_4$	2.29	2.29	2.8
15700-16300	$^5F_5$, $^3K_6$	0.42	0.46	2.5
16600-18800	$^3K_7$, $^3H_4$, $^5G_2$, $^5G_3$, $^3K_8$	10.93	10.89	10.4
19400-21100	$^3H_5$, $^5G_4$, $^3G_3$	2.57	2.56	5.5
RMS Deviation			2.02×10^{-7}	

[a]Range encompassing observed band(s).
[b]The parameters used to obtain these values are given in Table VI.

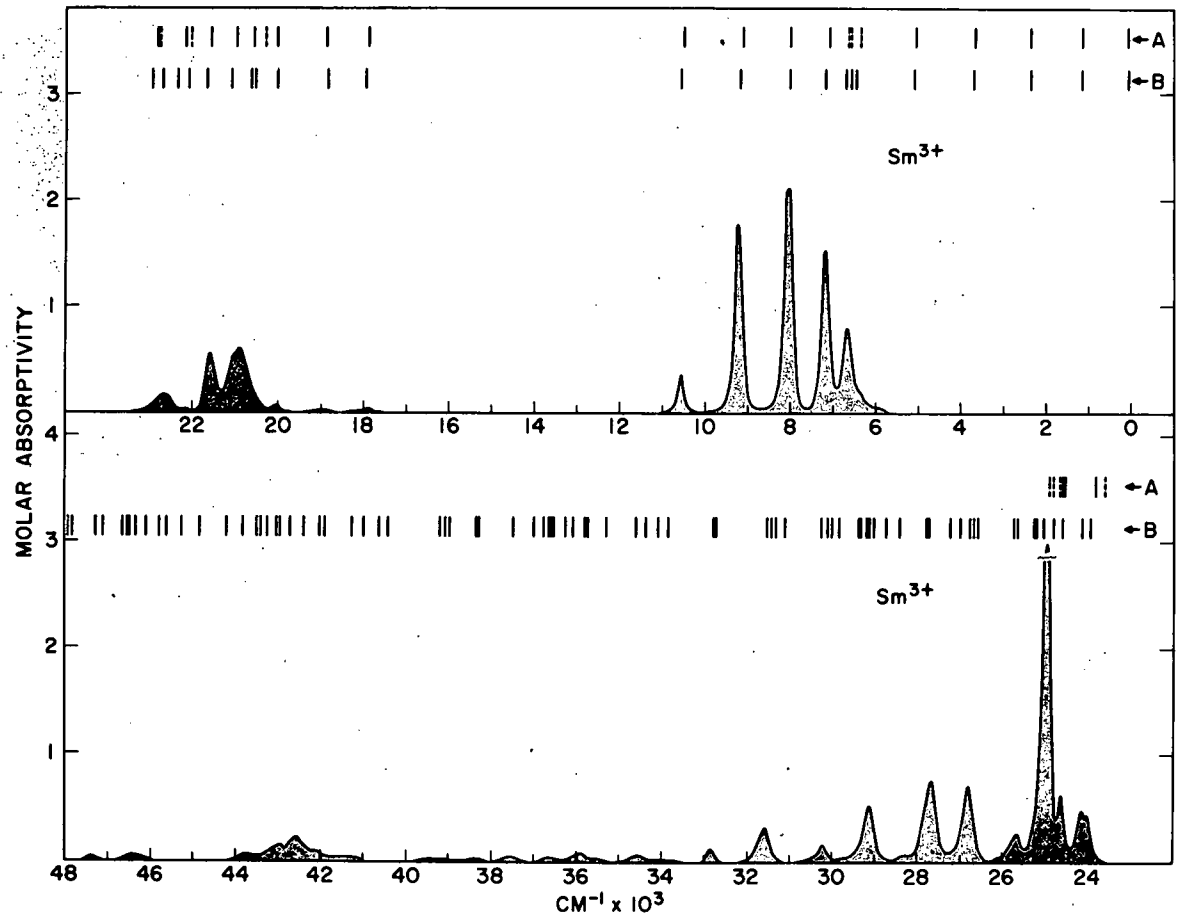

121-2520 Rev. 2

Fig. 6. Comparison of Experimental and Calculated Energy Levels with Observed Absorption Spectrum of Sm^{3+} (AQ)

A. Centers of gravity of Stark components for Sm^{3+} in $LaCl_3$ (Ref. 49).

B. Calculated free-ion levels for Sm^{3+} (AQ).

TABLE XI. Oscillator Strengths for Sm^{3+} (AQ)

Spectral Region[a] (cm^{-1})	S'L'J'	P x 10^6 $HClO_4$-$DClO_4$ Expt	$HClO_4$-$DClO_4$ Calc[b]	$Sm(NO_3)_3$ (32) Expt	$Sm(ClO_4)_3$ (62) Expt
5600-6500	$^6F_{1/2}$, $^6H_{15/2}$	0.26	0.26	-	-
6500-6800	$^6F_{3/2}$	0.97	0.99	-	-
6800-7600	$^6F_{5/2}$	1.70	1.84	-	-
7600-8600	$^6F_{7/2}$	2.74	3.00	-	-
8800-9800	$^6F_{9/2}$	1.97	1.98	1.70	1.99
10200-11000	$^6F_{11/2}$	0.31	0.32	0.33	0.30
17600-18200	$^4G_{5/2}$	0.030	0.023[c] 0.012[d]	0.036	0.057
18700-19300	$^4F_{3/2}$	0.009	0.001		
19800-20300	$^4G_{7/2}$	0.52	0.62	0.061	0.076
20300-21300	$^4I_{9/2}$, $^4M_{15/2}$, $^4I_{11/2}$	1.53	0.54	1.26	1.38
21300-22000	$^4I_{13/2}$	0.68	0.34	0.68	0.64
22000-22200	$^4F_{5/2}$	0.03	0.006[c] 0.010[d]	0.02	0.08
22200-23400	$^4M_{17/2}$, $^4G_{9/2}$, $^4I_{15/2}$	0.39	0.13	0.33	0.40
24400-24700	$^4L_{13/2}$	0.43	0.31		
24700-25500	$^4F_{7/2}$, $^6P_{3/2}$, $^4K_{11/2}$, $^4M_{21/2}$	3.84	3.80	4.90	4.15
25500-26200	$^4L_{15/2}$, $^4G_{11/2}$	0.42	0.11	0.30	0.31
26400-27200	$^4D_{1/2}$, $^6P_{7/2}$, $^4L_{17/2}$, $^4K_{13/2}$, $^4F_{9/2}$	1.06	1.26	1.05	1.02
27200-28100	$^4D_{3/2}$, $(^4D, ^6P)_{5/2}$	1.23	1.03	0.90	1.26
28100-28600	$^4H_{7/2}$	0.06	0.009[c] 0.020[d]		
28600-29800	$^4K_{15/2}$, $^4H_{9/2}$, $^4D_{7/2}$, $(^4K, ^4L)_{17/2}$, $^4L_{19/2}$, $^4H_{11/2}$	0.80	0.67		1.08
	RMS Deviation		2.91×10^{-7}		

[a]Range encompassing observed band(s).
[b]The parameters used to obtain these values are given in Table VI.
[c]Calculated magnetic dipole oscillator strength (Table III).
[d]Calculated electric dipole oscillator strength.

TABLE XII. Energy Level Assignments and Matrix Elements of $U^{(\lambda)}$ for Sm^{3+} (AQ)

	Sm^{3+} in $LaCl_3$[49]			Sm^{3+} (AQ)					
S'L'J'	E_{expt} (cm^{-1})	E_{calc}[a] (cm^{-1})	ΔE (cm^{-1})	E_{expt} (cm^{-1})	E_{calc}[a] (cm^{-1})	ΔE (cm^{-1})	U(2)[b]	U(4)[b]	U(6)[b]
$^6H_{5/2}$	36	12	24	36[c]	46	-10	-	-	-
$^6H_{7/2}$	1080	1067	13	1080[c]	1080	0	0.2062	0.1962	0.0952
$^6H_{9/2}$	2286	2279	7	2286[c]	2290	-4	0.0256	0.1395	0.3267
$^6H_{11/2}$	3608	3618	-10	3608[c]	3624	-16	0	0.0240	0.2649
$^6H_{13/2}$	5014	5044	-30	5000	5042	-42	0	0.0007	0.0659
$^6F_{1/2}$	-	6299	-	6400	6397	3	0.1939	0	0
$^6H_{15/2}$	-	6523	-	-	6508	-	0	0	0.0043
$^6F_{3/2}$	-	6544	-	6630	6641	-11	0.1444	0.1364	0
$^6F_{5/2}$	7033	7041	-8	7100	7131	-31	0.0332	0.2840	0
$^6F_{7/2}$	7900	7898	2	8000	7977	23	0.0020	0.1429	0.4301
$^6F_{9/2}$	9075	9069	6	9200	9136	64	~0	0.0206	0.3413
$^6F_{11/2}$	10460	10458	2	10500	10517	-17	0	0.0006	0.0515
$^4G_{5/2}$	17860	18053	-193	17900	17924	-24	0.0002	0.0007	0
$^4F_{3/2}$	18860	18632	228	18900	18832	68	0.0003	~0	0
$^4G_{7/2}$	20010	20100	-90	20050	20014	36	0.0004	0.0018	0.0025
$^4I_{9/2}$	20600	20556	44	-	20526	-	0.0022	0.0005	0.0014
$^4M_{15/2}$	-	20279	-	20800	20627	173	0	0	0.0307
$^4I_{11/2}$	20977	20996	-19	21100	21096	4	0	~0	0.0108
$^4I_{13/2}$	21562	21497	65	21600	21650	-50	0	0.0030	0.0228
$^4F_{5/2}$	22129	22172	-43	22200	22098	102	0.0004	0.0002	0
$^4M_{17/2}$	-	22006	-	-	22370	-	0	0	0.0053
$^4G_{9/2}$	22850	22749	101	22700	22706	-6	0.0001	0.0010	0.0028
$^4I_{15/2}$	-	22797	-	-	22966	-	0	0	0.0002
$^4M_{19/2}$	-	23543	-	-	23902	-	0	0	0
$(^6P, ^4P)_{5/2}$	23784	23776	8	24050	24101	-51	~0	0.0263	0
$^4L_{13/2}$	24560	24424	136	24570	24562	8	0	0.0081	0.0096
$^4F_{7/2}$	-	24783	-	-	24775	-	0.0002	0.0012	0.0003
$^6P_{3/2}$	-	24631	-	24950	24999	-49	~0	0.1684	0
$^4K_{11/2}$	24532	24752	-220	-	25177	-	0	0.0004	0.0027
$^4M_{21/2}$				-	25224	-	0	0	0
$^4L_{15/2}$				25650	25638	12	0	0	0.0060
$^4G_{11/2}$				-	25718	-	0	0.0001	0.0010
$^4D_{1/2}$				-	26573	-	0.0001	0	0
$^6P_{7/2}$				26750	26660	90	~0	0.0016	0.0751
$^4L_{17/2}$				-	26749	-	0	0	0.0002
$^4K_{13/2}$				-	26967	-	0	0.0005	0.0011
$^4F_{9/2}$				-	27207	-	~0	0.0004	~0
$^4D_{3/2}$				27700	27714	-14	0.0001	0.0251	0
$(^4D, ^6P)_{5/2}$				27700	27722	-22	~0	0.0170	0
$^4H_{7/2}$				28250	28396	-146	0.0013	0.0006	~0
$^4K_{15/2}$				-	28732	-	0	0	~0
$^4H_{9/2}$				29100	29012	88	0.0001	0.0002	0.0006
$^4D_{7/2}$				29100	29107	-7	~0	0.0005	0.0375
$(^4K, ^4L)_{17/2}$				-	29178	-	0	0	~0
$^4L_{19/2}$				-	29322	-	0	0	0
$^4H_{11/2}$				-	29381	-	0	0.0001	0.0005
$^4H_{13/2}$				-	29827	-	0	~0	0.0002
$^4G_{7/2}$				-	29980	-	~0	0.0006	0.0004
$^4G_{9/2}$				30200	30099	101	0.0001	0.0009	0.0013
$^4G_{5/2}$				-	30232	-	0.0002	0.0002	0
$^4P_{1/2}$				-	31093	-	~0	0	0
$^4G_{11/2}$				-	31349	-	0	~0	0.0003
$^2L_{15/2}$				-	31408	-	0	0	0.0002
$^4P_{3/2}$				31550	31508	42	~0	0.0136	0
$^4P_{5/2}$				32800	32706	94	~0	0.0021	0

TABLE XII. (Contd.)

S'L'J'	Sm^{3+} in $LaCl_3$[49] E_{expt} (cm^{-1})	E_{calc}[a] (cm^{-1})	ΔE (cm^{-1})	Sm^{3+} (AQ) E_{expt} (cm^{-1})	E_{calc}[a] (cm^{-1})	ΔE (cm^{-1})	U(2)[b]	U(4)[b]	U(6)[b]
$^2F_{5/2}$				33800	33767	33	~0	0.0005	0
$^2K_{13/2}$				33800	33825	-25	0	0.0002	0.0001
$^4F_{9/2}$				-	34061	-	~0	~0	~0
$^2L_{17/2}$				-	34357	-	0	0	~0
$(^4I, ^4F)_{9/2}$				34600	34591	9	~0	0.0004	0.0003
$^2N_{19/2}$				-	35385	-	0	0	0
$^2P_{1/2}$				-	35718	-	~0	0	0
$^4F_{7/2}$				-	35785	-	~0	0	~0
$^4I_{11/2}$				36000	36053	-53	0	0.0002	0.0003
$^2N_{21/2}$				-	36238	-	0	0	0
$^4F_{5/2}$				-	36520	-	~0	~0	0
$^4I_{15/2}$				-	36586	-	0	0	~0
$^4F_{3/2}$				36700	36586	114	~0	0.0002	0
$^4I_{13/2}$				36700	36757	-57	0	~0	0.0001
$^2M_{17/2}$				-	36982	-	0	0	~0
$(^2H, ^4I)_{9/2}$				37600	37487	113	~0	0.0005	0.0001
$(^2D, ^2F)_{3/2}$				38300	38270	30	~0	0.0003	0
$^2F_{7/2}$				-	38303	-	0	~0	~0
$^2K_{15/2}$				-	38949	-	0	0	~0
$^2G_{7/2}$				-	39057	-	0.0001	~0	~0
$^2H_{11/2}$				39250	39188	62	0	0.0002	~0
$^2M_{19/2}$				-	40417	-	0	0	0
$^2D_{5/2}$				-	40664	-	~0	~0	0
$^2I_{11/2}$				-	40990	-	0	0.0001	~0
$^2K_{13/2}$				-	41269	-	0	0.0001	~0
$^2D_{3/2}$				-	41369	-	~0	~0	0
$^2G_{9/2}$				42000	41941	49	~0	0.0002	0.0001
$^2O_{23/2}$				-	42022	-	0	0	0
$^2O_{21/2}$				-	42406	-	0	0	0
$^4G_{5/2}$				-	42714	-	0.0016	0.0010	0
$^4G_{7/2}$				42900	42965	-65	0.0013	0.0025	0.0006
$^2K_{15/2}$				-	43028	-	0	0	~0
$(^4H, ^4G)_{9/2}$				43100	43250	-150	0.0003	0.0008	0.0015
$(^2I, ^4H)_{11/2}$				-	43414	-	0	0.0006	0.0006
$(^2I, ^4H)_{13/2}$				-	43504	-	0	0.0002	~0
$(^4G, ^2H, ^4H)_{11/2}$				43800	43845	-45	0	0.0008	0.0006
$(^2G, ^4H)_{7/2}$				-	44237	-	0.0002	~0	~0
$^2G_{9/2}$				-	44832	-	~0	~0	0.0002
$(^4G, ^4H, ^2G)_{7/2}$				-	45269	-	~0	0.0006	~0
$^4G_{9/2}$				-	45615	-	~0	0.0006	0
$^2I_{13/2}$				-	45801	-	0	~0	~0
$^4G_{11/2}$				-	46123	-	0	0.0001	0.0002
$^2L_{17/2}$				-	46370	-	0	0	~0
$^4H_{13/2}$				46500	46500	0	0	0.0004	0.0002
$^2H_{11/2}$				46500	46554	-54	0	0.0005	~0
$(^4P, ^2D)_{3/2}$				46500	46669	-169	0.0002	0.0010	0
$^2D_{5/2}$				-	47127	-	~0	~0	0
$^2H_{11/2}$				47400	47307	93	0	0.0010	0.0001
$^2L_{15/2}$				-	47843	-	0	0	~0
$(^2F, ^4P, ^2D)_{5/2}$				-	47940	-	0	0.0003	0
$^2H_{9/2}$				-	48288	-	~0	~0	~0
	RMS Deviation		119			80			

[a] The parameters used to generate this set of levels are given in Table XXX.

[b] $U(\lambda) = \left[\psi J \| U^{(\lambda)} \| \psi' J'\right]^2$.

[c] Assumed based on data for Sm^{3+} in $LaCl_3$[49].

5. Eu^{3+} (f^6)

Europium is the only trivalent lanthanide in which the ground term has J = 0. This factor imposes special restrictions on the allowed transitions. The triangular conditions[73] on the 6-j symbol of Eq. 4 for J = 0 require that the symbol vanish if J' is odd or zero. In addition, for even values of J', the symbol vanishes except for $\lambda = \Delta J$. Thus, only a few transitions arising from the ground state are expected to have any intensity via the forced electric-dipole mechanism. For example, the only matrix elements of $\mathbf{U}^{(\lambda)}$ that are nonzero for the $^7F_0 \rightarrow {}^7F_2$ transition are those of U(2) (as can be seen in Table XIII).

The observed spectrum, shown in Fig. 7, is actually much more complex than the preceding discussion implies, since it includes bands due to transitions arising from the $^7F_1$ and $^7F_2$ levels, which lie near 350 and 1000 cm^{-1}, respectively. These levels are partially occupied at room temperature.

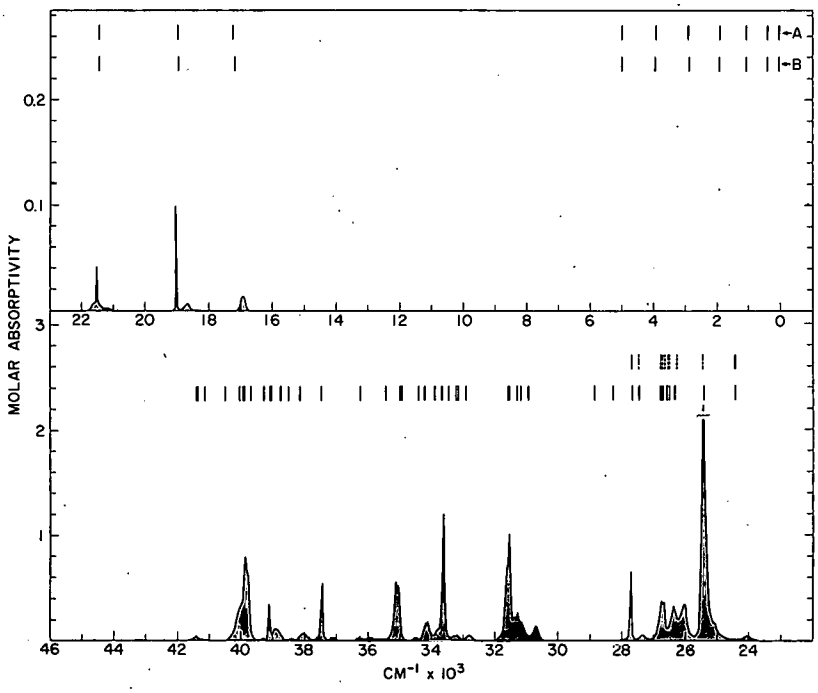

121-2518 Rev. 3

Fig. 7. Comparison of Experimental and Calculated Energy Levels with Observed Absorption Spectrum of Eu^{3+} (AQ)

A. Average energies of Stark components of Eu^{3+} in $LaCl_3$ (Ref. 18).

B. Calculated free-ion levels for Eu^{3+} (AQ).

In aqueous solution, we could only measure spectra at >6000 cm^{-1}. Thus transitions from ^7F to components of the ^5D multiplet gave rise to the lowest-energy bands within the experimental range. An

TABLE XIII. Energy Level Assignments and Matrix Elements of $U^{(\lambda)}$ for Eu^{3+} (AQ)

	Eu^{3+} in $LaCl_3$[18]			Eu^{3+} (AQ)					
S'L'J'	E_{expt} (cm^{-1})	E_{calc}[a] (cm^{-1})	ΔE (cm^{-1})	E_{expt} (cm^{-1})	E_{calc}[a] (cm^{-1})	ΔE (cm^{-1})	U(2)[b]	U(4)[b]	U(6)[b]
$^7F_0$	0	30	-30	0	-31	31	-	-	-
$^7F_1$	380.16	398	-18	360	350	10	0	0	0
$^7F_2$	1044.8	1046	-1	1020	1018	2	0.1375	0	0
$^7F_3$	1882.0	1887	-5	1882.0[c]	1880	7	0	0	0
$^7F_4$	2877.2	2851	26	2877.2[c]	2866	-1	0	0.1402	0
$^7F_5$	3909.0	3891	18	3909.0[c]	3927	-18	0	0	0
$^7F_6$	4978	4973	5	4980	5029	-49	0	0	0.1450
$^5D_0$	17267.4	17393	-126	17277	17286	-9	0	0	0
$^5D_1$	19030	19077	-47	19028	19026	-2	0	0	0
$^5D_2$	21504	21491	13	21519	21499	-20	0.0008	0	0
$^5D_3$	24390	24328	62	24408	24389	19	0	0	0
$^5L_6$	-	25317	-	25400	25375	25	0	0	0.0155
$^5G_2$	-	26260	-	26300	26296	4	0.0006	0	0
$^5L_7$	-	26375	-	-	26469	-	0	0	0
$^5G_3$	-	26487	-	-	26535	-	0	0	0
$^5G_4$	-	26614	-	26620	26672	-52	0	0.0007	0
$^5G_5$	-	26672	-	-	26733	-	0	0	0
$^5G_6$	-	26702	-	26700	26762	-62	0	0	0.0038
$^5L_8$	-	27315	-	-	27435	-	0	0	0
$^5D_4$	27632	27529	103	27670	27641	29	0	0.0011	0
$^5L_9$				-	28244	-	0	0	0
$^5L_{10}$				-	28813	-	0	0	0
$^5H_3$				-	30863	-	0	0	0
$^5H_7$				-	31145	-	0	0	0
$^5H_4$				31250	31281	-31	0	0.0013	0
$^5H_5$				-	31512	-	0	0	0
$^5H_6$				31520	31539	-19	0	0	0.0056
$^3P_0$				-	32862	-	0	0	0
$^5F_2$				33190	33126	64	0.0004	0	0
$^5F_3$				-	33188	-	0	0	0
$^5F_1$				-	33429	-	0	0	0
$^5F_4$				33590	33641	-51	0	0.0034	0
$^5I_4$				-	33862	-	0	0.0006	0
$^5F_5$				-	34171	-	0	0	0
$(^5I, ^5H)_5$				-	34366	-	0	0	0
$^5I_8$				-	34879	-	0	0	0
$(^5I, ^5H)_6$				35030	34941	89	0	0	0.0017
$^5I_7$				-	35382	-	0	0	0
$^5K_5$				36205	36235	-30	0	0	0
$^5K_6$				37440	37448	-8	0	0	0.0011
$^3P_1$				-	38103	-	0	0	0
$^5K_7$				-	38452	-	0	0	0
$^5G_2$				-	38701	-	0.0004	0	0
$^5K_8$				-	38991	-	0	0	0
$(^3K, ^3I)_6$				39060	39063	-3	0	0	0.0005
$^5G_3$				-	39243	-	0	0	0
$(^5D, ^5P)_2$				-	39664	-	0.0008	0	0
$^5K_9$				-	39867	-	0	0	0
$^5G_4$				39890	39897	-7	0	0.0050	0
$(^5D, ^5P)_3$				-	40041	-	0	0	0
$^5G_5$				-	40465	-	0	0	0
$^5D_1$				-	41113	-	0	0	0
$^3O_{10}$				-	41329	-	0	0	0
$^5G_6$				41370	41353	17	0	0	0.0002
	RMS Deviation		59	-		40			

[a]The parameters used to generate this set of energies are given in Table XXX.

[b]$U(\lambda) = \left[\psi_J \| U^{(\lambda)} \| \psi_{J'}\right]^2$.

[c]Assumed energy based on data in Ref. 18.

extremely weak band was detected near 17,300 cm^{-1} and attributed to $^7F_0 \rightarrow {}^5D_0$ (Refs. 1, 18, 31). Since this transition is forbidden by both electric- and magnetic-dipole selection rules, the slight observed intensity may be the result of a very weak J-mixing by the crystal field. The band at 19,028 cm^{-1} was attributed to $^7F_0 \rightarrow {}^5D_1$. In this case, the selection rules forbid an electric dipole but allow a magnetic-dipole transition. As shown in Table XIV, the experimental and calculated results are in excellent agreement. The magnitude of the band centered at 21,519 cm^{-1}, together with the calculated matrix element of $\mathbf{U}^{(2)}$ for $^7F_0 \rightarrow {}^5D_2$, determine a value of $\mathcal{T}_2$ that is consistent with that for other lanthanides. The extremely weak absorption at 24,408 cm^{-1} is identified with the forbidden $^7F_0 \rightarrow {}^5D_3$ transition.

In addition to the foregoing, several bands at higher energies were identified with transitions from $^7F_0$. All the oscillator strengths given in Table XIV are for transitions that originate in $^7F_0$ and were relatively well resolved from identifiable components arising from $^7F_1$ and $^7F_2$. In fitting the data, note that although $\mathcal{T}_6$ was well determined, the values of $\mathcal{T}_2$ and $\mathcal{T}_4$ were determined from single transitions.

For comparison with the results for other lanthanides, it was necessary to correct the values of $\mathcal{T}_\lambda$ calculated from the experimental data for Eu^{3+}. This correction arises since at 25° the observed oscillator strengths are a function of C_0, the concentration of Eu^{3+} ions in the ground state $^7F_0$, and this is only a fraction of the total Eu^{3+} ion concentration, C_T. Thus,

$$\frac{C_J}{C_0} = \frac{g_J}{g_0} \exp\left[\frac{-(E_J - E_0)}{kT}\right],$$

where $C_T = \sum C_J$, C_J is the concentration of atoms in the initial ^7F_J level with energy E_J, and $g_J = 2J + 1$. We neglect terms for $J > 2$. From Table XIII, $E_1 - E_0 = 360$ cm^{-1}, $E_2 - E_0 = 1020$ cm^{-1}, and we can calculate $C_T/C_0 = (C_0 + C_1 + C_2)/C_0 = 1.546$. Instead of applying the foregoing to the experimental oscillator strengths in Table XIV, we can make an equivalent correction directly to the values of $\mathcal{T}_\lambda$. Thus, the values of $\mathcal{T}_\lambda$ given in Table VI are a factor of 1.546 greater than those used to calculate oscillator strengths for comparison with experiment in Table XIV.

6. Gd^{3+} (f^7)

The f^7 configuration of Gd^{3+} represents a half-filled shell of equivalent electrons. Thus, to a first-order approximation, neither the ground state nor the excited states should be split by a crystal field.[74] Indeed, the absorption spectrum as observed in solution, shown in Fig. 8, comprises for the most part extremely sharp bands, all of which occur in the ultraviolet region of the spectrum. Transitions from the ground state

TABLE XIV. Oscillator Strengths for Eu^{3+} (AQ)

Spectral Range[a] (cm^{-1})	S'L'J'	P x 10^8 $HClO_4$ Expt	$HClO_4$ Calc[b]	$EuCl_3$[32] Expt	$Eu(ClO_4)_3$[62] Expt	$Eu(NO_3)_3$[1] Expt[e]
17000-17400	$^5D_0$	0	0	-	-	~0.01
18900-19100	$^5D_1$	1.4	1.4[c] / 0[d]	1.5	10	~1.3
21400-21600	$^5D_2$	2.1	2.1	0.9	90	~1.3
	$^5D_3$	-	-			
25100-25600	$^5L_6$	177	178	158	190	
	$^5G_2$	-	-			
	$^5L_7$	-	-			
	$^5G_3$	-	-			
26400-27000	$^5G_4$	-	-			
	$^5G_5$	43	56			
	$^5G_6$	-	-			
	$^5L_8$	-	-			
27500-27800	$^5D_4$	17	17			
	$^5L_9$	-	-			
	$^5L_{10}$	-	-			
	$^5H_3$	-	-			
	$^5H_7$	-	-			
	$^5H_4$	-	-			
	$^5H_5$	-	-			
31400-32350	$^5H_6$	73	80			
	$^3P_0$	-	-			
	$^5F_2$	-	-			
	$^5F_3$	-	-			
	$^5F_1$	-	-			
	$^5F_4$	-	-			
	$^5I_4$	-	-			
	$^5F_5$	-	-			
	$(^5I, ^5H)_5$	-	-			
	$^5I_8$	-	-			
	$(^5I, ^5H)_6$	-	-			
	$^5I_7$	-	-			
	$^5K_5$	-	-			

TABLE XIV. (Contd.)

Spectral Range[a] (cm^{-1})	S'L'J'	P x 10^8 $HClO_4$ Expt	$HClO_4$ Calc[b]	$EuCl_3$[32] Expt	$Eu(ClO_4)_3$[62] Expt	$Eu(NO_3)_3$[1] Expt[e]
37300-37600	$^5K_6$	22	19			
	$^3P_1$	-	-			
	$^5K_7$	-	-			
	$^5G_2$	-	-			
	$^5K_8$	-	-			
38900-39100	$(^3K, ^3I)_6$	8.2	8.8			
	RMS Deviation		2.3×10^{-8}			

[a]Range encompassing observed band(s).
[b]The parameters used to obtain these values are a factor of 1.546 smaller than those recorded in Table VI.
[c]Calculated magnetic dipole oscillator strength (Table III), corrected to the experimental conditions $C_0/C_T = 0.647$ where C_0/C_T is the fraction of transitions arising from the $^7F_0$ level.
[d]Calculated electric dipole oscillator strength (see b).
[e]Corrected to the present experimental conditions (25°).

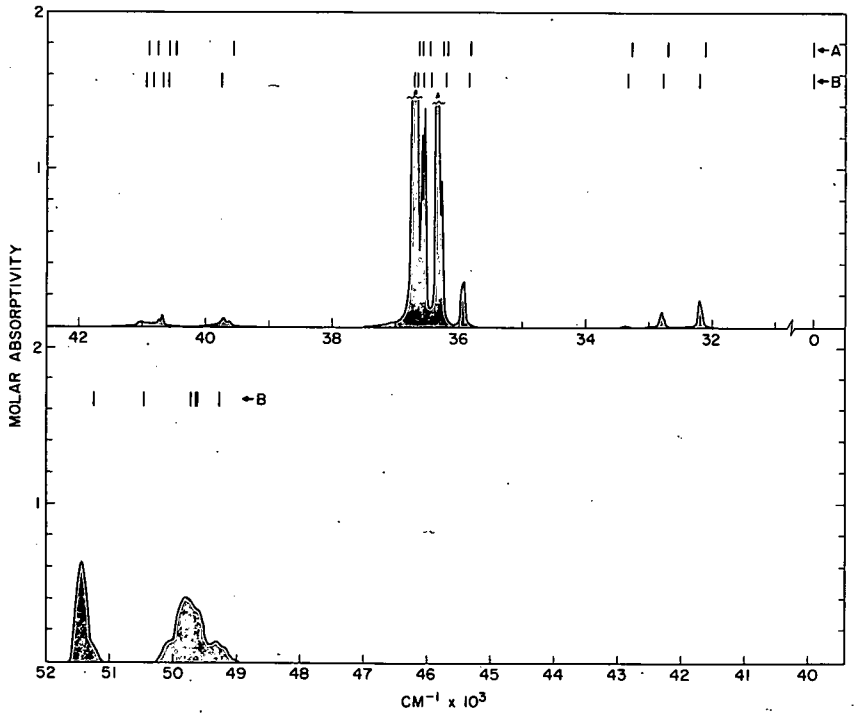

121-3078 Rev. 1

Fig. 8. Comparison of Experimental and Calculated Energy Levels with Observed Absorption Spectrum of Gd^{3+} (AQ)

A. Centers of gravity of Stark components for $GdCl_3 \cdot 6H_2O$ (Ref. 29).
B. Calculated free-ion levels for Gd^{3+} (AQ).

to three different multiplet groups ^6P, ^6I, and ^6D are normally observed, but those to ^6P, and particularly to ^6D, result in very weak absorption bands. In addition, we have discerned bands arising from transitions to components of the ^6G multiplet near 50,000 cm^{-1}. Since the transition to $^6G_{13/2}$ is superimposed on the tail of a more intense absorption centered at >>50,000 cm^{-1}, the intensity of the band arising from this transition is particularly difficult to measure accurately and reproducibly.

For parameter fitting, the situation in Gd^{3+} is somewhat similar to that in Eu^{3+}. The distribution of the nonzero matrix elements of $\mathbf{U}^{(\lambda)}$ (given in Table XV) indicates that bands arising from transitions to ^6P and ^6D determine the value of $\mathcal{T}_2$, whereas $\mathcal{T}_4$ and $\mathcal{T}_6$ are independently determined by transitions to ^6G and ^6I, respectively.

TABLE XV. Energy Level Assignments and Matrix Elements of $\mathbf{U}^{(\lambda)}$ for Gd^{3+} (AQ)

	$GdCl_3 \cdot 6H_2O$[29]			Gd^{3+} (AQ)					
S'L'J'	E_{expt} (cm^{-1})	E_{calc}[a] (cm^{-1})	ΔE (cm^{-1})	E_{expt} (cm^{-1})	E_{calc}[a] (cm^{-1})	ΔE (cm^{-1})	U(2)[b]	U(4)[b]	U(6)[b]
$^8S_{7/2}$	0	0	0	0	14	-14	-	-	-
$^6P_{7/2}$	32105	32153	-48	32200	32224	-24	0.0010	~0	~0
$^6P_{5/2}$	32700	32697	3	32780	32766	14	0.0004	~0	~0
$^6P_{3/2}$	33272	33237	35	33350	33302	48	~0	~0	0
$^6I_{7/2}$	35832	35772	60	35930	35878	52	~0	~0	0.0041
$^6I_{9/2}$	36176	36126	50	36270	36231	39	~0	~0	0.0104
$^6I_{17/2}$	36242	36358	-116	36340	36461	-121	0	0	0.0214
$^6I_{11/2}$	36458	36421	37	36560	36526	34	~0	~0	0.0177
$^6I_{13/2}$	36571	36606	-35	36660	36711	-51	0	~0	0.0242
$^6I_{15/2}$	36631	36621	10	36710	36725	-15	0	~0	0.0269
$^6D_{9/2}$	39562	39637	-75	39720	39779	-59	0.0057	0.0001	~0
$^6D_{1/2}$	40468	40478	-10	40560	40621	-61	0	~0	0
$^6D_{7/2}$	40574	40579	-5	40700	40712	-12	0.0044	~0	~0
$^6D_{3/2}$	40754	40714	40	40850	40851	-1	0.0008	~0	0
$^6D_{5/2}$	40901	40845	56	41000	40977	23	0.0025	~0	~0
$(^6G, ^6F)_{7/2}$				49270	49288	-18	0.0001	0.0040	~0
$^6G_{9/2}$				49680	49620	60	0.0001	0.0083	~0
$^6G_{11/2}$				49680	49667	13	~0	0.0103	~0
$^6G_{5/2}$				49680	49730	-50	~0	0.0019	~0
$^6G_{3/2}$				-	50457	-	~0	0.0005	0
$^6G_{13/2}$				51413	51259	154	0	0.0117	~0
	RMS Deviation		58			63			

[a] The parameters used to generate this set of energies are given in Table XXX.

[b] $U(\lambda) = \left[\psi J \| U^{(\lambda)} \| \psi' J'\right]^2$.

The correlation between (1) the observed intensities of the bands arising from transitions to $^6P_{7/2}$ and $^6P_{5/2}$ and (2) their calculated magnetic-dipole oscillator strengths is of particular interest. As shown in Table XVI, $P_{M.D.}$ accounts for essentially all the observed intensity. This is consistent with the very weak electric-dipole intensity calculated for these

TABLE XVI. Oscillator Strengths for Gd^{3+} (AQ)

Spectral Region[a] (cm^{-1})	S'L'J'	P x 10^6 $HClO_4$ Expt	P x 10^6 $HClO_4$ Calc[b]
32100-32300	$^6P_{7/2}$	0.073	0.055[c] 0.013[d]
32700-32900	$^6P_{5/2}$	0.041	0.031[c] 0.005[d]
33300-33500	$^6P_{3/2}$	0.0014	~0
35800-36100	$^6I_{7/2}$	0.121	0.112
36100-36450	$^6I_{9/2}$, $^6I_{17/2}$	0.845	0.877
36450-37400	$^6I_{11/2}$, $^6I_{13/2}$, $^6I_{15/2}$	1.914	1.918
39400-40400	$^6D_{9/2}$	0.078	0.093
40500-41200	$^6D_{1/2}$, $^6D_{7/2}$, $^6D_{3/2}$, $^6D_{5/2}$	0.082	0.008[c] 0.130[d]
49000-49400	$(^6G, ^6F)_{7/2}$	0.121	0.149
49400-50400	$^6G_{9/2}$, $^6G_{11/2}$, $^6G_{5/2}$	0.903	0.765
	$^6G_{3/2}$	-	-
51100-51700	$^6G_{13/2}$	0.639	0.459
	RMS Deviation		2.5×10^{-8}

[a]Range encompassing observed band(s).
[b]The parameters used to obtain these values are given in Table VI.
[c]Calculated magnetic dipole oscillator strength (Table III).
[d]Calculated electric dipole oscillator strength.

transitions. Wybourne[74] obtained the same results for the electric-dipole oscillator strength, assuming $\mathcal{T}_2 = 1.6 \times 10^{-9}$, but using somewhat different intermediate coupling eigenvectors.

The values of $\mathcal{T}_\lambda$ obtained in the fitting process are given in Table VI.

7. Tb^{3+} (f^8)

The assigned and calculated energy levels, together with the matrix elements of $U^{(\lambda)}$ based upon the present study, are shown in Table XVII. Intensities could only be measured reproducibly at <36,000 cm^{-1} since at higher energies the f → f transitions were superimposed on more intense absorption bands which arise from 4f → $4f^{N-1}5d$ transitions, as shown in Fig. 9. Loh[48] suggests that the lowest 4f → 5d transition for Tb^{3+} in CaF_2 occurs near 46,500 cm^{-1}, which is in agreement with the calculation of Crozier.[17] The intense absorption band observed in solution at 45,800 cm^{-1} has already been identified as an f → d transition, but some doubt has been expressed about the nature of the weaker band at 38,000 cm^{-1} (Ref. 38). As

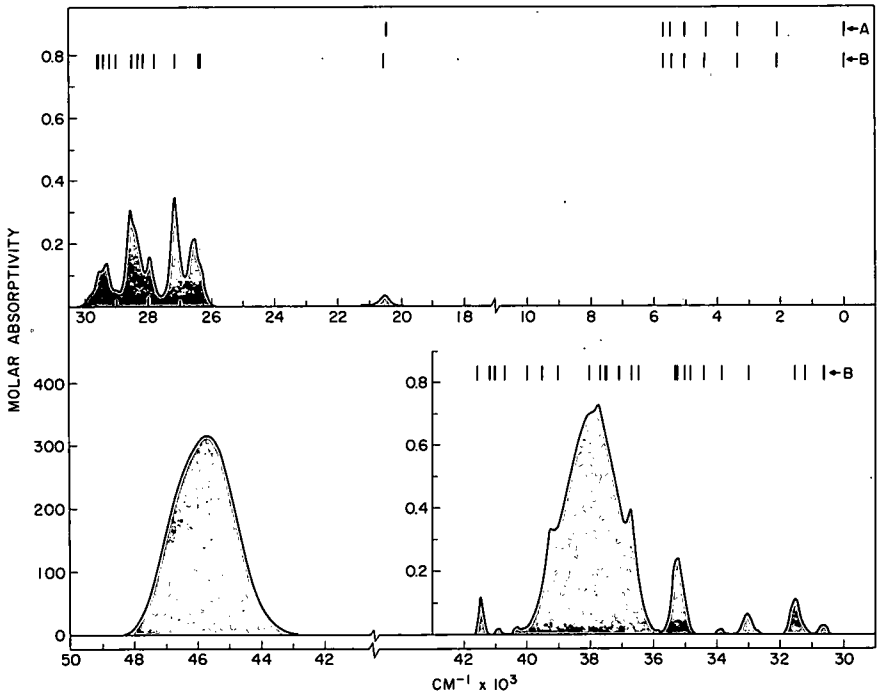

121-2521 Rev. 2

Fig. 9. Comparison of Experimental and Calculated Energy Levels with Observed Absorption Spectrum of Tb^{3+} (AQ)

A. Centers of gravity of Stark components for Tb^{3+} in $LaCl_3$ (Ref. 65).
B. Calculated free-ion levels for Tb^{3+} (AQ).

TABLE XVII. Energy Level Assignments and Matrix Elements of $U^{(\lambda)}$ for Tb^{3+} (AQ)

	Tb^{3+} in $LaCl_3$[65]			Tb^{3+} (AQ)					
S'L'J'	E_{expt} (cm^{-1})	E_{calc}[a] (cm^{-1})	ΔE (cm^{-1})	E_{expt} (cm^{-1})	E_{calc}[a] (cm^{-1})	ΔE (cm^{-1})	U(2)[b]	U(4)[b]	U(6)[b]
$^7F_6$	85	84	1	85[c]	74	11	-	-	-
$^7F_5$	2103.79	2111	-7	2100[c]	2112	-12	0.5376	0.6418	0.1175
$^7F_4$	3355.63	3366	-10	3356[c]	3370	-14	0.0889	0.5159	0.2654
$^7F_3$	4348.27	4340	8	4400	4344	56	0	0.2324	0.4126
$^7F_2$	5024.24	5023	1	5038	5028	10	0	0.0482	0.4695
$^7F_1$	5471.90	5476	-4	5440	5481	-41	0	0	0.3763
$^7F_0$	5700.93	5697	4	5700	5703	-3	0	0	0.1442
$^5D_4$	20453.9	20470	-16	20500	20545	-45	0.0010	0.0008	0.0013
$^5D_3$	26273.0	26256	17	-	26336	-	0	0.0002	0.0014
$^5G_6$				26500	26425	75	0.0017	0.0045	0.0118
$^5L_{10}$				27100	27146	-46	0	0.0004	0.0592
$^5G_5$				27800	27795	5	0.0012	0.0018	0.0135
$^5D_2$				-	28150	-	0	~0	0.0008
$^5G_4$				-	28319	-	0.0001	0.0003	0.0091
$^5L_9$				28400	28503	-103	0	0.0021	0.0466
$^5G_3$				-	29007	-	0	0.0001	0.0031
$^5L_8$				29300	29202	98	~0	0.0001	0.0235
$^5L_7$				29450	29406	44	0.0005	0.0001	0.0119
$^5L_6$				-	29550	-	0.0001	0.0001	0.0003
$^5G_2$				-	29577	-	0	~0	0.0005
$^5D_1$				30650	30658	-8	0	0	0.0003
$^5D_0$				-	31228	-	0	0	0.0001
$^5H_7$				31600	31557	43	0.0060	0.0019	0.0131
$^5H_6$				33000	33027	-27	0.0027	~0	0.0126
$^5H_5$				33900	33879	21	0.0004	0.0002	0.0037
$^5H_4$				-	34442	-	~0	0.0002	0.0004
$^5F_5$				34900	34927	-27	0.0030	0.0038	0.0026
$^5H_3$				-	35040	-	0	~0	~0
$^5I_8$				35200	35262	-62	0.0004	0.0067	0.0193
$^5F_4$				-	35380	-	0.0014	0.0014	0.0022
$^5F_3$				-	36559	-	0	0.0001	0.0018
$^5I_7$				36700	36723	-23	0.0001	0.0045	0.0113
$^5F_2$				-	37188	-	0	~0	0.0012
$^5F_1$				-	37575	-	0	0	0.0003
$^5I_4$				-	37578	-	~0	0.0001	~0
$^5I_6$				37760	37714	46	~0	0.0021	0.0020
$^5I_5$				-	38081	-	~0	0.0005	0.0002
$^5K_9$				39100	39094	6	0	0.0150	0.0117
$(^3P, ^5D)_2$				-	39548	-	0	0.0006	~0
$(^3I, ^5G)_6$				-	40114	-	0.0027	0.0010	0.0022
$^5K_8$				-	40749	-	~0	0.0074	0.0043
$^5G_6$				-	41082	-	0.0067	0.0082	0.0025
$(^5K, ^3I)_5$				-	41236	-	0.0007	0.0003	0.0007
$^5K_7$				-	41614	-	~0	0.0012	0.0002
	RMS Deviation		11			56			

[a]The parameters used to generate this set of energies are given in Table XXX.

[b]$U^{(\lambda)} = \left[\psi_J \| U^{(\lambda)} \| \psi_{J'}\right]^2$.

[c]Assumed energy based on data in Ref. 65.

can be seen from the consistently small values of the matrix elements of $\mathbf{U}^{(\lambda)}$ for transitions near 38,000 cm^{-1} (listed in Table XVII), the intensity of the principal band could not be accounted for as an f → f transition, but those bands superimposed upon it do qualitatively appear to have the intensities predicted for f → f transitions.

It was necessary to treat most of the bands observed at <36,000 cm^{-1} as composites involving several transitions, as shown in Table XVIII. Normally, this procedure would make it possible to calculate all three parameters, $\mathcal{T}_\lambda$, since a sufficient number of independent groups were resolved. However, in the case of Tb^{3+}, none of the observed transitions were strongly dependent upon the matrix elements of $\mathbf{U}^{(2)}$. As a consequence, $\mathcal{T}_2$ was poorly defined (as may be seen in Table VI), but nonetheless was shown to be very small.

TABLE XVIII. Oscillator Strengths for Tb^{3+} (AQ)

Spectral Region[a] (cm^{-1})	S'L'J'	P x 10^7 $HClO_4$ Expt	P x 10^7 $HClO_4$ Calc[b]	$TbCl_3$[32] Expt.
20000-21200	$^5D_4$	0.52	0.21	~0.04
25900-27600	$^5D_3$, $^5G_6$, $^5L_{10}$	8.46	0.07[c] / 7.61[d]	5.7
27600-28950	$^5G_5$, $^5D_2$, $^5G_4$, $^5L_9$	7.46	7.61	
28950-30200	$^5G_3$, $^5L_8$, $^5L_7$, $^5L_6$, $^5G_2$	3.04	4.03	
30400-30900	$^5D_1$	0.37	0.32	
30950-32000	$^5D_0$, $^5H_7$	2.02	1.85	
32500-33500	$^5H_6$	1.20	1.41	
33600-34100	$^5H_5$	0.18	0.47	
34400-35800	$^5H_4$, $^5F_5$, $^5H_3$, $^5I_8$, $^5F_4$	5.05	5.32	
	RMS Deviation		6.4×10^{-8}	

[a]Range encompassing observed band(s).
[b]The parameters used to obtain these values are given in Table VI.
[c]Calculated magnetic dipole oscillator strength (Table III).
[d]Calculated electric dipole oscillator strength.

8. Dy^{3+} (f^9)

Many of the more intense transitions in Dy^{3+}, shown in Fig. 10, are well identified, and their intensities could be measured with a high degree of reproducibility. The calculated matrix elements of $\mathbf{U}^{(\lambda)}$ are given in Table XIX. Calculated and experimentally determined oscillator strengths are compared in Table XX, based on the parameters $\mathcal{T}_\lambda$ given in Table VI. There is appreciable general absorption in the ultraviolet region of the Dy^{3+} spectrum. This results in a considerable error in the areas determined for bands at >35,000 cm^{-1}, and no measurements were possible beyond ~43,000 cm^{-1}.

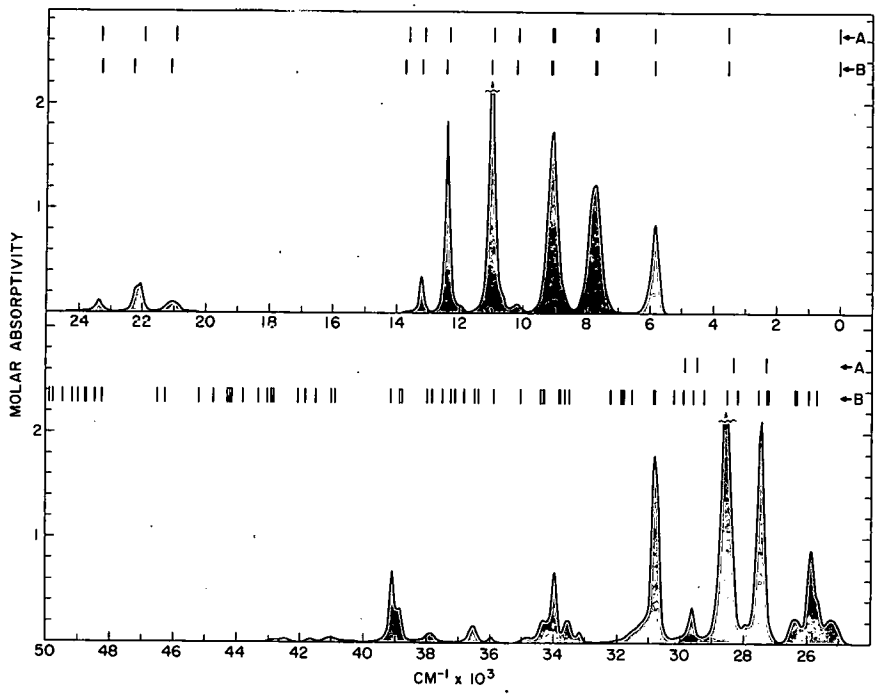

121-2515

Fig. 10. Comparison of Experimental and Calculated Energy Levels with Observed Absorption Spectrum of Dy^{3+} (AQ)

A. Centers of gravity of Stark components for Dy^{3+} in $LaCl_3$ (Ref. 16).

B. Calculated free-ion levels for Dy^{3+} (AQ).

TABLE XIX. Energy Level Assignments and Matrix Elements of $U^{(\lambda)}$ for Dy^{3+} (AQ)

	Dy^{3+} in $LaCl_3$ [16]			Dy^{3+} (AQ)					
S'L'J'	E_{expt} (cm^{-1})	E_{calc}[a] (cm^{-1})	ΔE (cm^{-1})	E_{expt} (cm^{-1})	E_{calc}[a] (cm^{-1})	ΔE (cm^{-1})	$U^{(2)}$[b]	$U^{(4)}$[b]	$U^{(6)}$[b]
$^6H_{15/2}$	52	35	17	52[c]	40	12	-	-	-
$^6H_{13/2}$	3517	3480	37	3517[c]	3506	11	0.2457	0.4139	0.6824
$^6H_{11/2}$	5835	5804	31	5850	5833	17	0.0923	0.0366	0.6410
$^6H_{9/2}$	7667	7637	30	7700	7692	8	0	0.0176	0.1985
$^6F_{11/2}$	7667	7663	4	7700	7730	-30	0.9387	0.8292	0.2048
$^6F_{9/2}$	9014	9011	3	9100	9087	13	0	0.5736	0.7213
$^6H_{7/2}$	9014	9099	-85	9100	9115	-15	0	0.0007	0.0392
$^6H_{5/2}$	10140	10146	-6	10200	10169	31	0	0	0.0026
$^6F_{7/2}$	10926	10945	-19	11000	11025	-25	0	0.1360	0.7146
$^6F_{5/2}$	12323	12341	-18	12400	12432	-32	0	0	0.3452

TABLE XIX. (Contd.)

S'L'J'	Dy^{3+} in $LaCl_3$[16] E_{expt} (cm^{-1})	E_{calc}[a] (cm^{-1})	ΔE (cm^{-1})	Dy^{3+} (AQ) E_{expt} (cm^{-1})	E_{calc}[a] (cm^{-1})	ΔE (cm^{-1})	U(2)[b]	U(4)[b]	U(6)[b]
$^6F_{3/2}$	13116	13109	7	13250	13212	38	0	0	0.0610
$^6F_{1/2}$	-	13650	-	-	13760	-	0	0	0
$^4F_{9/2}$	20963	21056	-93	21100	21144	-44	0	0.0047	0.0295
$^4I_{15/2}$	21954	21956	-2	22100	22293	-193	0.0073	0.0003	0.0654
$^4G_{11/2}$	23303	23288	15	23400	23321	79	0.0004	0.0145	0.0003
$^4F_{7/2}$	-	25640	-	25800	25754	46	0	0.0768	0.0263
$^4I_{13/2}$	-	25539	-	25800	25919	-119	0.0041	0.0013	0.0248
$^4M_{21/2}$	-	25562	-	-	26341	-	0	0.0102	0.0822
$^4K_{17/2}$	-	25627	-	26400	26365	35	0.0109	0.0048	0.0935
$^4M_{19/2}$	-	26374	-	27400	27219	181	0.0004	0.0166	0.1020
$(^4P, ^4D)_{3/2}$	-	26832	-	27400	27254	146	0	0	0.0448
$^6P_{5/2}$	-	27038	-	27400	27503	-103	0	0	0.0697
$^4I_{11/2}$	-	27728	-	-	28152	-	0.0001	~0	0.0074
$^6P_{7/2}$	28326	28346	-20	28550	28551	-1	0	0.5222	0.0125
$(^4M, ^4I)_{15/2}$	-	28575	-	-	29244	-	0.0023	0.0005	0.0009
$(^4F, ^4D)_{5/2}$	29480	29383	97	29600	29593	7	0	0	0.0249
$^4I_{9/2}$				-	29885	-	0	0.0003	0.0003
$^4G_{9/2}$				-	30200	-	0	0.0014	0.0005
$^6P_{3/2}$				30800	30803	-3	0	0	0.1095
$^4M_{17/2}$				-	30892	-	0.0032	~0	0.0012
$(^4G, ^2F)_{7/2}$				-	31560	-	0	0.0066	0.0002
$^4K_{15/2}$				-	31795	-	0.0028	0.0001	0.0093
$^4D_{1/2}$				-	31842	-	0	0	0
$(^4D, ^4G)_{5/2}$				-	31857	-	0	0	~0
$^4L_{19/2}$				-	32187	-	0.0004	0.0203	0.0056
$^4H_{13/2}$				33500	33471	29	0.0099	0.0100	0.0016
$^4F_{3/2}$				-	33642	-	0	0	0.0045
$(^4K, ^4L)_{13/2}$				-	33776	-	0.0060	0.0024	~0
$^4D_{7/2}$				33900	33834	66	0	0.0661	0.0016
$^4H_{11/2}$				-	34307	-	0.0029	0.0018	0.0022
$^4G_{9/2}$				-	34311	-	0	0.0007	0.0041
$^4F_{5/2}$				-	34398	-	0	0	0.0004
$^4G_{11/2}$				34900	34954	-54	0.0016	0.0054	0.0075
$^4L_{17/2}$				34900	35047	-147	0.0003	0.0088	0.0018
$(^4G, ^4H)_{7/2}$				35900	35891	9	0	0.0042	0.0001
$^4K_{11/2}$				-	36432	-	0.0001	~0	0.0001
$(^4G, ^4P)_{5/2}$				36550	36524	26	0	0	0.0040
$^4G_{9/2}$				-	36794	-	0	0.0013	0.0014
$(^4L, ^4K)_{13/2}$				-	37103	-	0.0003	0.0001	0.0006
$^4L_{15/2}$				-	37230	-	0.0001	0.0016	0.0002
$^4P_{1/2}$				-	37435	-	0	0	0
$^4H_{7/2}$				-	37807	-	0	~0	0.0002
$^4F_{3/2}$				37900	38031	-131	0	0	0.0043
$(^2K, ^2L)_{15/2}$				-	38811	-	0.0003	0.0001	0.0007
$(^4G, ^4P)_{5/2}$				38900	38860	40	0	0	0.0061
$(^4P, ^4F)_{3/2}$				39100	39127	-27	0	0	0.0091
$^4F_{5/2}$				-	40922	-	0	0	~0
$(^4F, ^2G)_{9/2}$				41050	41035	15	0	0.0015	0.0002
$^4I_{15/2}$				41700	41596	104	0.0030	0.0043	0.0001
$^2L_{17/2}$				-	41848	-	0.0001	~0	0.0002
$^4F_{7/2}$				-	42127	-	0	0.0021	0.0002
$^2P_{3/2}$				-	42807	-	0	0	0.0005
	RMS Deviation		56			86			

[a]The parameters used to generate this set of energies are given in Table XXX.

[b]$U(\lambda) = \left[\langle \psi J \| U^{(\lambda)} \| \psi' J' \rangle\right]^2$.

[c]Assumed energy based on data in Ref. 16.

TABLE XX. Oscillator Strengths for Dy^{3+} (AQ)

Spectral Range[a] (cm^{-1})	S'L'J'	P x 10^6 $HClO_4$-$DClO_4$ Expt	P x 10^6 $HClO_4$-$DClO_4$ Calc[b]	P x 10^6 $Dy(NO_3)_3$ [32] Expt
5500-6400	$^6H_{11/2}$	1.14	1.17	
7000-8400	$^6F_{11/2}$, $^6H_{9/2}$	1.10	3.55	
8400-9800	$^6F_{9/2}$, $^6H_{7/2}$	2.97	3.38	2.76
9800-10400	$^6H_{5/2}$	0.11	2.62	3.04
10400-11700	$^6F_{7/2}$	2.74		
11700-12900	$^6F_{5/2}$	1.55	1.19	1.61
12900-13600	$^6F_{3/2}$	0.33	0.23	0.38
20400-21600	$^4F_{9/2}$	0.21	0.20	0.19
21700-22600	$^4I_{15/2}$	0.44	0.08[c] / 0.42[d]	0.34
23000-24000	$^4G_{11/2}$	0.16	0.10	0.11
24600-26800	$^4F_{7/2}$, $^4I_{13/2}$, $^4M_{21/2}$, $^4K_{17/2}$	2.38	2.34	2.54
27000-28200	$^4M_{19/2}$, $(^4P, ^4D)_{3/2}$, $^6P_{5/2}$, $^4I_{11/2}$	2.85	1.84	2.67
28200-29200	$^6P_{7/2}$	4.36	4.24	
29200-30100	$(^4M, ^4I)_{15/2}$, $(^4F, ^4D)_{5/2}$, $^4I_{9/2}$	0.39	0.01[c] / 0.23[d]	

TABLE XX. (Contd.)

Spectral Range[a] (cm^{-1})	S'L'J'	P x 10^6 $HClO_4$-$DClO_4$ Expt	P x 10^6 $HClO_4$-$DClO_4$ Calc[b]	P x 10^6 $Dy(NO_3)_3$[32] Expt
30100-32400	$^4G_{9/2}$, $^6P_{3/2}$, $^4M_{17/2}$, $(^4G, ^2F)_{7/2}$, $^4K_{15/2}$, $(^4D, ^4G)_{5/2}$, $^4D_{1/2}$, $^4L_{19/2}$	2.59	1.36	
32800-35200	$^4H_{13/2}$, $^4F_{3/2}$, $(^4K, ^4L)_{13/2}$, $^4D_{7/2}$, $^4H_{11/2}$, $^4G_{9/2}$, $^4F_{5/2}$, $^4G_{11/2}$, $^4L_{17/2}$	1.43	1.23	
35800-36200	$(^4G, ^4H)_{7/2}$	0.05	0.04	
	RMS Deviation		2.05×10^{-7}	

[a]Range encompassing observed band(s).
[b]The parameters used to obtain these values are given in Table VI.
[c]Calculated magnetic dipole oscillator strength (Table III).
[d]Calculated electric dipole oscillator strength.

The value of $\mathcal{T}_2$ given in Table VI was determined after excluding the intensity data for $^6F_{9/2}$ and $^6H_{11/2}$ at 7700 cm^{-1} from the averaging process. As can be seen from Tables XIX and XX, the matrix elements of $\mathbf{U}^{(4)}$ and $\mathbf{U}^{(6)}$ for these two transitions, taken together with the values of $\mathcal{T}_4$ and $\mathcal{T}_6$ (which were determined by averaging results for a number of transitions) establish a calculated oscillator strength that is much larger than that observed. Including the data for $^6F_{9/2}$ and $^6H_{11/2}$ in the fit forced $\mathcal{T}_2$ to assume a negative value.

In this case, the magnitude and sign of $\mathcal{T}_2$ were effectively determined by the very large value of the matrix element of $\mathbf{U}^{(2)}$ for the transition to $^6H_{11/2}$. Thus the best overall "fit" resulted from making $\mathcal{T}_2$ negative to correct for the excess oscillator strength calculated from the matrix elements of $\mathbf{U}^{(4)}$ and $\mathbf{U}^{(6)}$ for the transitions $^6H_{15/2} \rightarrow {}^6F_{9/2}$, $^6H_{11/2}$.

9. Ho^{3+} (f^{10})

It was possible to obtain at least a reasonable estimate of band intensities in Ho^{3+} to ~45,000 cm^{-1} (as indicated in Fig. 11). The matrix elements of $\mathbf{U}^{(\lambda)}$, as shown in Table XXI, indicate that in many complex bands, the intensity is due almost entirely to one transition. Experimental and calculated oscillator strengths are shown in Table XXII; the latter are based on the parameters summarized in Table VI. In general, the correlation is good. The big discrepancy in the broad band at 31,000 cm^{-1}, may be partly experimental since the subtraction of an arbitrary background in the case of such a broad absorption is subject to considerable error.

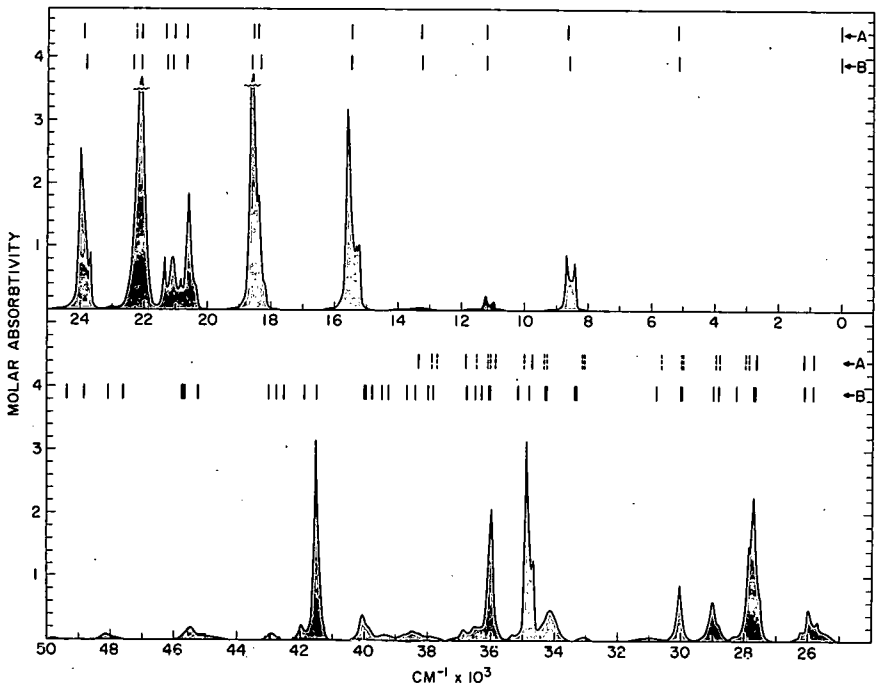

121-2516

Fig. 11. Comparison of Experimental and Calculated Energy Levels with Observed Absorption Spectrum of Ho^{3+} (AQ)

A. Centers of gravity of Stark components for Ho^{3+} in $LaCl_3$ (Refs. 20, 25).
B. Calculated free-ion levels for Dy^{3+} (AQ).

TABLE XXI. Energy Level Assignments and Matrix Elements of $U^{(\lambda)}$ for Ho^{3+} (AQ)

	Ho^{3+} in $LaCl_3$[20,55]			Ho^{3+} (AQ)					
S'L'J'	E_{expt} (cm^{-1})	E_{calc}[a] (cm^{-1})	ΔE (cm^{-1})	E_{expt} (cm^{-1})	E_{calc}[a] (cm^{-1})	ΔE (cm^{-1})	U(2)[b]	U(4)[b]	U(6)[b]
$^5I_8$	107.7	140	-32	108[c]	80	28	-	-	-
$^5I_7$	5154.8	5169	-13	5130[d]	5116	14	0.0250	0.1344	1.5216
$^5I_6$	8656.9	8668	-11	8580	8614	-34	0.0084	0.0386	0.6921
$^5I_5$	11218.9	11216	3	11120	11165	-45	0	0.0100	0.0936
$^5I_4$	13284.1	13272	12	13300	13219	81	0	~0	0.0077
$^5F_5$	15482.0	15508	-26	15500	15519	-19	0	0.4250	0.5687
$^5S_2$	18430.3	18284	146	18500	18354	146	0	0	0.2268
$^5F_4$	18553.9	18619	-65	18500	18612	-112	0	0.2392	0.7071
$^5F_3$	20614.0	20644	-30	20600	20673	-73	0	0	0.3460
$^5F_2$	21069.2	21058	11	21100	21130	-30	0	0	0.1921
$^3K_8$	21350.7	21310	41	21370	21308	62	0.0208	0.0334	0.1578
$^5G_6$	22100.6	22118	-17	22100	22094	6	1.5201	0.8410	0.1411
$^5F_1$	-	22304	-	-	22375	-	0	0	0
$(^5G, ^3G)_5$	23936.4	23782	154	23950	23887	63	0	0.5338	0.0002
$^5G_4$	25820.4	25798	22	25800	25826	-26	0	0.0315	0.0359
$^3K_7$	26139.7	26114	26	26200	26117	83	0.0058	0.0046	0.0338
$(^5G, ^3H)_5$	27648.8	27640	9	27700	27653	47	0	0.0790	0.1610
$^3H_6$	-	27703	-	27700	27675	25	0.2155	0.1179	0.0028
$(^5F, ^3F, ^5G)_2$	27968.8	28136	-167	28250	28301	-51	0	0	0.0041
$^5G_3$	28810.6	28786	24	28800	28816	-16	0	0	0.0133
$^3L_9$	28911.4	28988	-77	29000	29020	-20	0.0185	0.0052	0.1536
$(^3F, ^3H, ^3G)_4$	-	29915	-	30000	30017	-17	0	0.1260	0.0047
$^3K_6$	-	29994	-	30000	30036	-36	0.0026	0.0002	0.0026
$^5G_2$	-	30687	-	30900	30813	87	0	0	0.0010
$^3D_3$	33066.5	33130	-64	33200	33339	-139	0	0	0.0030
$^3P_1$	-	33152	-	-	33398	-	0	0	0
$^3M_{10}$	-	34375	-	34200	34264	-64	0.0003	0.0696	0.0808
$^3L_8$	-	34273	-	34200	34306	-106	0.0017	0.0005	0.0108
$(^5G, ^5D, ^3G)_4$	34728.3	34761	-33	34800	34794	6	0	0.3040	0.0492
$(^3F, ^3G)_3$	-	34977	-	35200	35224	-24	0	0	0.0036
$^3P_0$	-	35852	-	-	36050	-	0	0	0
$(^3H, ^5D, ^1G)_4$	-	35980	-	36000	36046	-46	0	0.2635	0.0041
$^3F_2$	-	36006	-	-	36364	-	0	0	0.0035
$^1L_8$	-	36488	-	36500	36516	-16	0.0002	0.0056	0.0016
$(^3H, ^3G)_5$	36722.2	36684	38	36800	36773	27	0	0.0024	0.0032
$(^3P, ^1D)_2$	-	37686	-	-	37845	-	0	0	~0
$^3L_7$	-	37924	-	38000	38022	-22	0.0020	~0	0.0036
$^3I_7$	38314.2	38268	46	38500	38470	30	0.0157	0.0003	0.0080
$^3F_4$				38500	38509	-9	0	0.0084	0.0023
$^3I_5$				-	39271	-	0	0.0008	0.0008
$^3M_9$				39500	39435	65	0.0005	0.0057	0.0029
$^3I_6$				-	39830	-	0.0065	~0	0.0043
$(^3D, ^5D, ^3P)_1$				-	39982	-	0	0	0
$^5D_3$				40000	39992	8	0	0	0.0293
$(^3F, ^5D)_4$				41550	41532	18	0	0.2577	0.0144

TABLE XXI. (Contd.)

	Ho^{3+} in $LaCl_3$[20, 55]			Ho^{3+} (AQ)					
$S'L'J'$	E_{expt} (cm^{-1})	E_{calc}[a] (cm^{-1})	ΔE (cm^{-1})	E_{expt} (cm^{-1})	E_{calc}[a] (cm^{-1})	ΔE (cm^{-1})	U(2)[b]	U(4)[b]	U(6)[b]
$^5D_2$				41900	41922	-22	0	0	0.0128
$^5D_0$				-	42582	-	0	0	0
$(^3F, ^5D)_3$				42850	42811	39	0	0	0.0079
$^5D_1$				-	43066	-	0	0	0
$(^1D, ^3D)_2$				-	45286	-	0	0	0.0004
$^3M_8$				-	45691	-	~0	~0	0.0001
$^3H_4$				-	45705	-	0	0.0068	0.0003
$(^3H, ^1I)_6$				45700	45724	-24	0.0001	0.0118	0.0005
$^3F_3$				-	47448	-	0	0	0.0008
$(^3H, ^3G, ^3I)_5$				48200	48102	98	0	0.0034	~0
$(^1D, ^3F)_2$				-	48736	-	0	0	~0
$^1H_5$				-	49335	-	0	0.0016	~0
	RMS Deviation		82			62			

[a]The parameters used to generate this set of energies are given in Table XXX.

[b]$U(\lambda) = \left[\psi J \| U^{(\lambda)} \| \psi' J'\right]^2$.

[c]Assumed energy based on data in Ref. 20.

10. Er^{3+} (f^{11})

The present data for Er^{3+}, given in Tables XXIII and XXIV and shown in Fig. 12, represent a considerable extension of the results previously

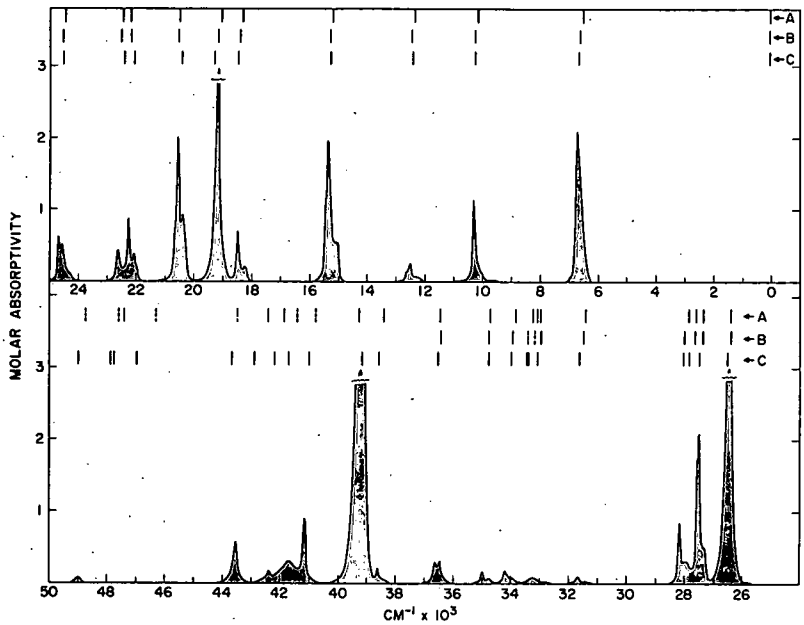

121-2519 Rev. 2

Fig. 12. Comparison of Experimental and Calculated Energy Levels with Observed Absorption Spectrum of Er^{3+} (AQ)

A. Experimentally determined free-ion levels of Er^{3+} (Ref. 12).
B. Centers of gravity of Stark components for Er^{3+} in $LaCl_3$ (Refs. 56, 68).
C. Calculated free-ion levels for Er^{3+} (AQ).

TABLE XXII. Oscillator Strengths for Ho^{3+} (AQ)

Spectral Range[a] (cm^{-1})	S'L'J'	P x 10^6 $HClO_4$-$DClO_4$ Expt	P x 10^6 $HClO_4$-$DClO_4$ Calc[b]	P x 10^6 $HoCl_3$[32] Expt
8000-9000	$^5I_6$	1.07	1.46	-
10800-11400	$^5I_5$	0.22	0.27	~0.05
13000-13500	$^5I_4$	0.02	0.02	
15000-16000	$^5F_5$	3.76	3.62	4.77
18000-19200	$^5S_2$, $^5F_4$	5.23	5.07	4.81
20100-20900	$^5F_3$	1.78	1.66	
20900-21600	$^5F_2$, $^3K_8$	1.43	0.08[c], 1.92[d]	3.09
21600-23200	$^5G_6$, $^5F_1$	6.00	6.11	7.66
23400-24600	$(^5G, ^3G)_5$	3.14	3.05	4.0
25000-26400	$^5G_4$, $^3K_7$	1.03	0.65	~1.8
27200-28500	$(^5G, ^3H)_5$, $^3H_6$, $(^5F, ^3F, ^5G)_2$	3.24	2.53	~2.3
28500-29600	$^5G_3$, $^3L_9$	0.83	1.09	
29600-30500	$(^3F, ^3H, ^3G)_4$, $^3K_6$	0.80	0.95	
30500-31600	$^5G_2$	0.13	0.01	
32900-33200	$^3D_3$, $^3P_1$	~0.02	0.02	
33600-34600	$^3M_{10}$, $^3L_8$	1.01	1.30	
34600-35500	$(^5G, ^5D, ^3G)_4$, $(^3F, ^3G)_3$	2.72	3.01	

TABLE XXII. (Contd.)

Spectral Range[a] (cm^{-1})	S'L'J'	P x 10^6 $HClO_4$-$DClO_4$ Expt	P x 10^6 $HClO_4$-$DClO_4$ Calc[b]	P x 10^6 $HoCl_3$[20] Expt
35500-37400	$^3P_0$, $(^3H, ^5D, ^1G)_4$, $^3F_2$, $^1L_8$, $(^3H, ^3G)_5$	2.59	2.41	
37500-39700	$(^3P, ^1D)_2$, $^3L_7$, $^3I_7$, $^3F_4$, $^3I_5$, $^3M_9$			
39700-40500	$^3I_6$, $(^3D, ^5D, ^3P)_1$, $^5D_3$	0.54	0.32	
41100-41800	$(^3F, ^5D)_4$	2.54	2.70	
41800-42200	$^5D_2$	0.20	0.13	
42700-43200	$(^3F, ^5D)_3$, $^5D_1$	0.10	0.08	
44400-45900	$(^1D, ^3D)_2$, $^3H_4$, $^3M_8$, $(^3H, ^1I)_6$	0.37	0.21	
	RMS Deviation		2.87×10^{-7}	

[a]Range encompassing observed band(s).
[b]The parameters used to obtain these values are given in Table VI.
[c]Calculated magnetic dipole oscillator strength (Table III).
[d]Calculated electric dipole oscillator strength.

TABLE XXIII. Energy Level Assignments and Matrix Elements of $U^{(\lambda)}$ for Er^{3+} (AQ)

$S'L'J'$	E_{expt} (cm^{-1})	E_{calc}[a] (cm^{-1})	ΔE (cm^{-1})	U(2)[b]	U(4)[b]	U(6)[b]
$^4I_{15/2}$	108[c]	109	-1	-	-	-
$^4I_{13/2}$	6600	6610	-10	0.0195	0.1173	1.4316
$^4I_{11/2}$	10250	10219	31	0.0282	0.0003	0.3953
$^4I_{9/2}$	12400	12378	22	0	0.1733	0.0099
$^4F_{9/2}$	15250	15245	5	0	0.5354	0.4618
$^4S_{3/2}$	18350	18462	-112	0	0	0.2211
$^2H_{11/2}$	19150	19256	-106	0.7125	0.4125	0.0925
$^4F_{7/2}$	20450	20422	28	0	0.1469	0.6266
$^4F_{5/2}$	22100	22074	26	0	0	0.2232
$^4F_{3/2}$	22500	22422	78	0	0	0.1272
$(^2G, ^4F, ^2H)_{9/2}$	24550	24505	45	0	0.0189	0.2256
$^4G_{11/2}$	26400	26496	-96	0.9183	0.5262	0.1172
$^4G_{9/2}$	27400	27478	-78	0	0.2416	0.1235
$^2K_{15/2}$	-	27801	-	0.0219	0.0041	0.0758
$^2G_{7/2}$	28000	27979	21	0	0.0174	0.1163
$(^2P, ^2D, ^4F)_{3/2}$	31600	31653	-53	0	0	0.0172
$^2K_{13/2}$	33200	33085	115	0.0032	0.0029	0.0152
$^4G_{5/2}$	33400	33389	11	0	0	0.0026
$^2P_{1/2}$	-	33453	-	0	0	0
$^4G_{7/2}$	34050	34022	28	0	0.0334	0.0029
$^2D_{5/2}$	34850	34800	50	0	0	0.0228
$(^2H, ^2G)_{9/2}$	36550	36566	-16	0	0.0501	0.0001
$^2D_{5/2}$	38600	38576	24	0	0	0.0267
$^4D_{7/2}$	39200	39158	42	0	0.8921	0.0291
$^2I_{11/2}$	41150	41009	141	0.0002	0.0284	0.0034
$^2L_{17/2}$	41650	41686	-36	0.0047	0.0664	0.0327
$^4D_{3/2}$	42300	42257	43	0	0	0.0126
$(^2D, ^2P)_{3/2}$	-	42966	-	0	0	0.0002
$^2I_{13/2}$	43550	43717	167	0.0050	0.0170	0.0050
$^4D_{1/2}$	-	47040	-	0	0	0
$^2H_{9/2}$	-	47822	-	0	0.0038	0.0001
$^2L_{15/2}$	-	47916	-	0.0002	0.0026	0.0021
$(^2D, ^4D)_{5/2}$	49000	49033	-33	0	0	0.0096
$^2H_{11/2}$	-	51000	-	0.0001	0.0082	~0
	RMS Deviation		81			

[a] The parameters used to generate this set of energies are given in Table XXX.

[b] $U(\lambda) = \left[\psi J \| U^{(\lambda)} \| \psi' J'\right]^2$.

[c] Assumed energy based on data in Ref. 68.

TABLE XXIV. Oscillator Strengths for Er^{3+} (AQ)

Spectral Range[a] (cm^{-1})	S'L'J'	P x 10^6 $HClO_4$-$DClO_4$ Expt	P x 10^6 $HClO_4$-$DClO_4$ Calc[b]	P x 10^6 $ErCl_3$[32] Expt
6200-7000	$^4I_{13/2}$	2.19	0.41[c] 1.98[d]	-
9400-10800	$^4I_{11/2}$	0.84	0.66	0.50
12000-12900	$^4I_{9/2}$	0.29	0.35	0.34
14800-15800	$^4F_{9/2}$	2.25	2.36	2.37
18000-18700	$^4S_{3/2}$	0.66	0.62	0.83
18700-19800	$^2H_{11/2}$	2.89	3.26	2.91
20000-21100	$^4F_{7/2}$	2.27	2.43	2.22
21800-23000	$^4F_{5/2}$, $^4F_{3/2}$	1.25	1.20	1.31
24100-25100	$(^2G, ^4F, ^2H)_{9/2}$	0.80	0.92	0.74
25800-27100	$^4G_{11/2}$	5.92	5.76	
27100-27700	$^4G_{9/2}$	1.75	1.56	
27700-28400	$^2K_{15/2}$, $^2G_{7/2}$	0.91	0.05[c] 0.99[d]	
31300-31900	$(^2P, ^2D, ^4F)_{3/2}$	0.091	0.083	
32700-33600	$^2K_{13/2}$, $^4G_{5/2}$, $^2P_{1/2}$	0.12	0.12	
33600-34500	$^4G_{7/2}$	0.21	0.19	
34500-35200	$^2D_{5/2}$	0.14	0.12	
36100-36900	$(^2H, ^2G)_{9/2}$	0.44	0.29	
38300-38700	$^2D_{5/2}$	0.14	0.16	
38700-40200	$^4D_{7/2}$	10.2	5.68	
	RMS Deviation		1.43×10^{-7}	

[a]Range encompassing observed band(s).
[b]The parameters used to obtain these values are given in Table VI.
[c]Calculated magnetic dipole oscillator strength (Table III).
[d]Calculated electric dipole oscillator strength.

reported.[6] The re-evaluation of band intensities has modified only a few of those given earlier. The new values for $\mathcal{T}_\lambda$ (Table VI) are all slightly larger than those originally computed, and are also better determined. In the ultraviolet range, the poor fit to the intense band near 40,000 cm^{-1} may be in part experimental. However, since the whole of the intensity can be unequivocally attributed to one transition ($^4D_{7/2}$), the indication is that the calculated matrix elements of $\mathbf{U}^{(4)}$ or $\mathbf{U}^{(6)}$ or both are too small. We note that the matrix elements for the corresponding transition in Nd^{3+} were also apparently too small. Except in this case, the agreement shown in Table XXIV is good.

11. Tm^{3+} (f^{12})

It was not possible to significantly extend the results reported earlier for Tm^{3+}, since accurately reproducible experimental data in the ultraviolet region of the spectrum could not be obtained (as is evident from Fig. 13). An improved energy-level fit, upon which the calculation of the matrix elements of $\mathbf{U}^{(\lambda)}$ (shown in Table XXV) was based, and the experimental observation of one additional absorption band, were the principal factors responsible for the differences between the calculated oscillator strengths given in Table XXVI and those computed earlier.[6] The parameters $\mathcal{T}_\lambda$ are given in Table VI.

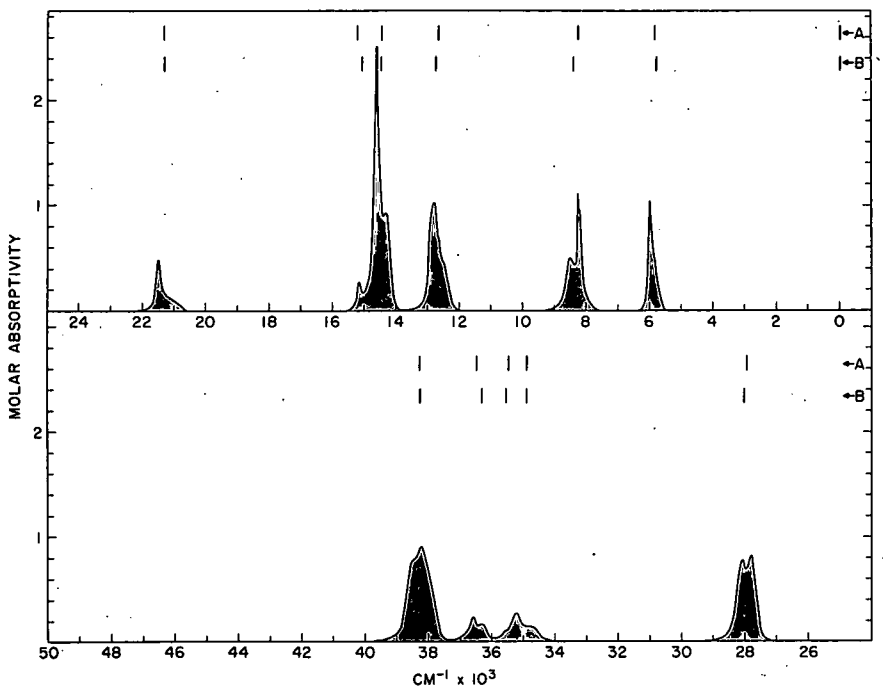

121-2514 Rev. 2

Fig. 13. Comparison of Experimental and Calculated Energy Levels with Observed Absorption Spectrum of Tm^{3+} (AQ)

A. Average energies of Stark components of $Tm(C_2H_5SO_4)_3 \cdot 9H_2O$ (Refs. 22, 24, 26, 36, 45, 71).
B. Calculated free-ion levels for Tm^{3+} (AQ).

TABLE XXV. Energy Level Assignments and Matrix Elements of $U^{(\lambda)}$ for Tm^{3+} (AQ)

	$Tm(C_2H_5SO_4)_3 \cdot 9H_2O$ [22,24,26,36,45,71]			Tm^{3+} (AQ)					
S'L'J'	E_{expt} (cm^{-1})	E_{calc}[a] (cm^{-1})	ΔE (cm^{-1})	E_{expt} (cm^{-1})	E_{calc}[a] (cm^{-1})	ΔE (cm^{-1})	U(2)[b]	U(4)[b]	U(6)[b]
$^3H_6$	170	141	29	170[c]	202	-32	-	-	-
$^3F_4$	5846	5787	59	5900	5811	89	0.5375	0.7261	0.2382
$^3H_5$	8250	8326	-76	8400	8390	10	0.1074	0.2314	0.6383
$^3H_4$	12665	12673	-8	12700	12720	-20	0.2373	0.1090	0.5947
$^3F_3$	14464	14514	-50	14500	14510	-10	0	0.3164	0.8411
$^3F_2$	15192	15112	80	15100	15116	-16	0	~0	0.2581
$^1G_4$	21300	21306	-6	21350	21374	-24	0.0483	0.0748	0.0125
$^1D_2$	27916	28014	-98	28000	28032	-32	0	0.3156	0.0928
$^1I_6$	34870	34851	19	34900	34886	14	0.0106	0.0388	0.0134
$^3P_0$	35444	35641	-197	35500	35637	-137	0	0	0.0756
$^3P_1$	36461	36295	166	36400	36298	102	0	0	0.1239
$^3P_2$	38257	38175	82	38250	38193	57	0	0.2645	0.0223
$^1S_0$	-	79720	-	-	79592	-	0	0	0.0002
	RMS Deviation		143			94			

[a]The parameters used to generate this set of energies are given in Table XXX.

[b]$U(\lambda) = \left[\psi J \| U^{(\lambda)} \| \psi' J'\right]^2$

[c]Assumed energy based upon data in Refs. 22 and 71.

TABLE XXVI. Oscillator Strengths for Tm^{3+} (AQ)

Spectral Region[a] (cm^{-1})	S'L'J'	P x 10^6		
		$HClO_4$-$DClO_4$		$TmCl_3$[32]
		Expt	Calc[b]	Expt
5600-6300	$^3F_4$	1.08	1.40	
7700-9200	$^3H_5$	1.67	0.37[c] / 1.46[d]	
12000-13600	$^3H_4$	2.12	1.92	1.98
13800-15500	$^3F_3$, $^3F_2$	3.91	3.97	3.18
20600-22100	$^1G_4$	0.71	0.45	~0.45
27300-29100	$^1D_2$	2.38	2.30	
34100-35900	$^1I_6$, $^3P_0$	0.84	0.89	
35900-37400	$^3P_1$	0.56	0.83	
37400-39700	$^3P_2$	3.28[e]	2.25	
	RMS Deviation		2.59×10^{-7}	

[a]Range encompassing observed band(s).

[b]The parameters used to obtain these values are given in Table VI.

[c]Calculated magnetic dipole oscillator strength (Table III).

[d]Calculated electric dipole oscillator strength.

[e]This value was not included in the parameter fitting process since a large error was associated with determining background absorption in this region.

12. Yb^{3+} (f^{13})

The single f → f transition for Yb^{3+} which results in a band observed near 10,000 cm^{-1} (shown in Fig. 14), does not provide sufficient information for the determination of the three parameters $\mathcal{T}_\lambda$. Thus, in this case, several further assumptions must be made.

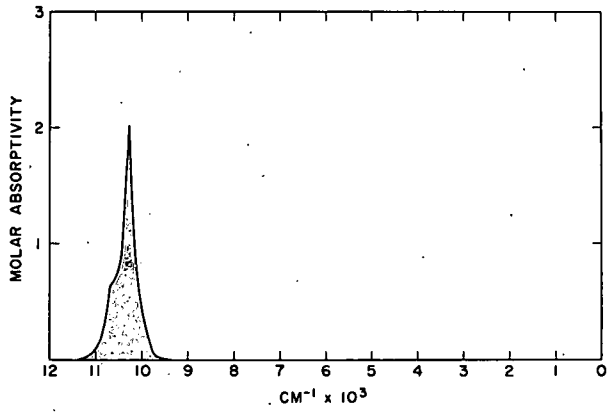

121-2507

Fig. 14. Observed Absorption Spectrum of Yb^{3+} (AQ)

For the transition involved, Judd's expression reduces to

$$P = \frac{\sigma}{196}(3\mathcal{T}_2 + 10\mathcal{T}_4 + 21\mathcal{T}_6). \qquad (13)$$

Note, from Table VI, that for each of the heavy lanthanides the values of $\mathcal{T}_4$ and $\mathcal{T}_6$ are nearly identical and $\mathcal{T}_2 < \mathcal{T}_4$. Equation 13 indicates that neglecting $\mathcal{T}_2$ under the above circumstances should not lead to a large error since the first term would be expected to contribute $<1/11$ of the total due to $\mathcal{T}_2$, $\mathcal{T}_4$, and $\mathcal{T}_6$. Before calculating $\mathcal{T}_4$ (= $\mathcal{T}_6$), we corrected the total observed oscillator strength of the $^2F_{7/2}$ band, as tabulated in Table XXVII, for the contribution due to magnetic-dipole absorption. Thus we obtain the estimate

$$\mathcal{T}_4 = \mathcal{T}_6 = 2.13 \times 10^{-9}.$$

TABLE XXVII. Oscillator Strengths for Yb^{3+} (AQ)

Spectral Region[a] (cm^{-1})	S'L'J'	P x 10^6		
		$DClO_4$		$YbCl_3$[32]
		Expt	Calc[b]	Expt
9400-11300	$^2F_{5/2}$	3.74	0.24[c] 3.47[d]	3.86

[a]Range encompassing observed band.
[b]The parameters used to obtain this value are given in Table VI.
[c]Calculated magnetic dipole oscillator strength (Table III).
[d]Calculated electric dipole oscillator strength.

B. Conclusions

For the tripositive lanthanides, the Judd-Ofelt theory has been shown to be applicable even in the near-ultraviolet region of the spectrum. In this range, one might have expected it to break down, since the approximation

made in the derivation, that the energy difference between configurations is much greater than the transition energy, becomes less valid. Actually, the approximation is probably more valid than it first appears. In the absence of large deviations from LS coupling, interaction only occurs between levels of the same spin in two interacting configurations. Since the levels of both f^N and $f^{N-1}d$ tend to be ordered by spin, with the highest spin multiplicity lying lowest, the approximation of a constant energy difference between interacting levels may be justified even when levels near 40,000 cm^{-1} in the f^N-configuration are considered.

The theory appears to be unable to fully account for the observed intensities in the case of Pr^{3+}, and other discrepancies have been noted for isolated bands in other lanthanides. In the case of Pr^{3+}, perturbing states in the $f^{N-1}d$ configuration are only ~50,000 cm^{-1} above the ground level;[17,48] therefore the assumption relative to energy differences is admittedly weak at this point. Indeed, one might expect an even more pronounced recurrence of this effect at Tb^{3+}, where the lowest term of $4f^{N-1}d$ is found near 38,000 cm^{-1}. An examination of the structures of the f^8 and f^7d configurations reveals that this is not the case, however. The two lowest multiplets of f^7d are expected to be ^9D and ^7D, which result from the coupling of a d electron to the ^8S ground state of f^7. For Gd^{2+}, these are spread by approximately 1500 cm^{-1} each and their centers are 8000-9000 cm^{-1} apart.[4] The structure is expected to be similar for Tb^{3+}. The band at 38,000 cm^{-1} must arise from transitions from $f^8(^7F_6)$ to $f^7d(^9D)$. One would then expect, by analogy with Gd^{2+}, that the transition to $f^7d(^7D)$ would appear at 46,000-47,000 cm^{-1}, which agrees well with the observed band at 45,800 cm^{-1}.

The crystal-field interaction that mixes f^8 with f^7d is independent of spin. Thus, since there are no nonet states in f^8, it cannot be affected by $f^7d(^9D)$. The only septet in f^8 is the ground multiplet, ^7F; consequently, this is the only multiplet that can be affected by $f^7d(^7D)$. The higher states of f^7 are ~30,000 cm^{-1} above the ^8S. The next higher states of f^7d are expected to lie at least 25,000 cm^{-1} above ^9D and ^7D, or at about 65,000 cm^{-1}. These are then the first states that could interact with the quintets of f^8. Thus, even though the lowest states of f^7d are very low in Tb^{3+}, they can affect only the ^7F multiplet. This multiplet lies in the infrared region and was not considered in the intensity calculation. We conclude that while the proximity of $f^{N-1}d$ states could contribute to the poor intensity correlation obtained for Pr^{3+}, similar arguments could not apply for Tb^{3+}. Consequently, it is not surprising that the theory accounts as well for the Tb^{3+} results as it does for the other cases.

C. Interpretation of $\mathcal{T}_\lambda$

In examining the intensity correlations, we should recall some of the restrictions that were built into the calculations. In particular, the triangular conditions on the 6-j symbol of Eq. 4 imply the selection rule

$\Delta J \leq \lambda$, where $\lambda = 2, 4, 6$. For $\lambda = 2$, $\Delta J \leq 2$; i.e., for transitions in which $\Delta J > 2$, the matrix elements of $\mathbf{U}^{(2)}$ will vanish. Clearly, $\mathcal{T}_2$ will in general be the most poorly determined parameter, since most transitions will involve $\Delta J > 2$. $\mathcal{T}_4$ will be determined by $\Delta J \leq 4$, and $\mathcal{T}_6$ by $\Delta J \leq 6$. Thus the latter will be the best determined parameter. The 6-j symbol vanishes for $\Delta J > 6$. No induced electric-dipole intensity is expected for such transitions.

Examination of the parameters in Table VI and reference to the tables of matrix elements of $\mathbf{U}^{(\lambda)}$ reveal that only a limited number of transitions in aqueous solution are at all influenced by the value of $\mathcal{T}_2$. Most of the data fitting involved only two parameters, $\mathcal{T}_4$ and $\mathcal{T}_6$. The magnitude of each of the three parameters does not appear to change appreciably, although there is some decrease with increasing Z. These results for $\mathcal{T}_4$ and $\mathcal{T}_6$ are consistent with the trend calculated by Krupke[44] using free-ion radial-wave functions. The parameters $\mathcal{T}_2$ and $\mathcal{T}_6$ for Pr^{3+} are essentially an order of magnitude larger than the average for the series.

The fact that $\mathcal{T}_4 \cong \mathcal{T}_6$ for most of the lanthanides has already been mentioned. From the point of view of a purely electrostatic model, we might have expected $\mathcal{T}_6 > \mathcal{T}_4$ since

$$\mathcal{T}_\lambda \sim \frac{\langle r^{t+1} \rangle^2}{(R^{t+1})^2} \qquad (14)$$

where r refers to the distance of the f-electron from the nucleus, and R is the distance from the central ion to the centers of charge in the ligands that comprise the first coordination sphere. For $\lambda = 4$, $t = 3,5$; for $\lambda = 6$, $t = 5,7$. The assumption $r < R$ was made in arriving at Eq. 14. By neglecting perturbing configurations except those of the type $4f^{N-1}5d$, Judd[40] calculated T_4/T_6 $(=\mathcal{T}_4/\mathcal{T}_6) \cong 0.5$ for Nd^{3+} and Er^{3+}. Although the computation does give $\mathcal{T}_6 > \mathcal{T}_4$, the small ratio and the approximate nature of the calculations suggest that the present experimental results for $\mathcal{T}_\lambda$ are not inconsistent with the theory.

We conclude then that the intensity aspects of lanthanide absorption spectra in aqueous solution can be predicted, to a good approximation, on the basis of two parameters, $\mathcal{T}_4$ and $\mathcal{T}_6$. The additional parameter $\mathcal{T}_2$ becomes important for only one or two bands in each ion. These bands are, however, identically those that show a hypersensitivity to medium effects.[6]

The parameters comparable to $\mathcal{T}_\lambda$, reported by Krupke[44] for spectra observed in crystals at room temperature, appear to be of the same order of magnitude as the present values of $\mathcal{T}_\lambda$. The intensities for Pr^{3+} and for Nd^{3+} in LaF_3 are approximately one-third to one-half of those observed for the same transitions in solution, but the intensity patterns are quite similar. Comparison of the spectra of lanthanides in a Y_2O_3 matrix

with the results in solution is not straightforward because of the large crystal-field splitting reported for the oxide crystal. However, the oscillator strengths are clearly comparable in magnitude. The fact that the lanthanide ions occupy sites of approximate C_2 symmetry in Y_2O_3 (Ref. 44) is consistent with the observation of very large values of P at energies corresponding to hypersensitive transitions. These transitions show their "normal" intensity in the LaF_3 matrix, where it has been suggested that the site symmetry is D_{3h},[44] and in the aqueous solutions studied here.

D. Symmetries That Allow Nonzero A_0^1 Terms

The hypersensitive transitions are accommodated in Judd's theory by correlating their existence in a given host lattice with the presence of lanthanide ions at site symmetries which give nonzero A_0^1 terms in the crystal-field potential.[37] The symmetries that would allow such terms are

$$C_s,\ C_p\ (p = 1,2,3,4,6),\ \text{and}\ C_{pV}\ (p = 2,3,4,6).$$

The suggestion[42] of possible ninefold coordination and C_{3v} site symmetry for lanthanide ions in dilute acid solutions, such as studied in the present investigation, would allow an increased intensity at the energies corresponding to hypersensitive transitions, but no such increase is apparent. The limited evidence correlating structure and spectra at present appears to be consistent with the theory.

V. USE OF INTENSITY CORRELATIONS TO REFINE ENERGY-LEVEL PARAMETERS

A. Introduction

We have deferred discussing the refinement of the energy-level fitting process until after the intensity calculations were summarized, since the intensity data provided the basis for this refinement. The initial parameters for the energy-level calculations were obtained from fits based upon assignments to levels observed in crystal matrices. The eigenvectors computed from these parameters were then used in preliminary intensity calculations. We were able to show the following:

1. The theory can provide a good correlation between calculated intensities and those observed for solutions of the trivalent lanthanides in the near-infrared and visible regions of the spectrum.

2. The values of the calculated matrix elements of $\mathbf{U}^{(\lambda)}$ for most of the transitions for a given lanthanide were rather insensitive to small variations in the electrostatic and spin-orbit parameters. Thus the changes in these parameters occasioned by progressively improving the fit to experimental data produced only minor variations in the magnitudes of the calculated matrix elements of $\mathbf{U}^{(\lambda)}$ from the initial to the final stages of the fitting process.

Throughout the visible and ultraviolet regions of the spectrum (to 50,000 cm^{-1}), a pattern of single transitions with large matrix elements of $\mathbf{U}^{(4)}$ and/or $\mathbf{U}^{(6)}$ occurred near the same energy as a number of transitions with very small matrix elements of $\mathbf{U}^{(\lambda)}$. In many cases, the theory could represent the experimental data only if a given transition which had large matrix elements of $\mathbf{U}^{(4)}$ or $\mathbf{U}^{(6)}$ was assumed to occur within a given relatively intense absorption band. For example, an absorption band in Ho^{3+} (shown in Fig. 11), is observed near 41,500 cm^{-1}. Table XXI reveals that the only large matrix elements of $\mathbf{U}^{(\lambda)}$ within ± 1000 cm^{-1} are calculated for the transition $^5I_8 \rightarrow (^3F, ^5D)_4$. On the basis of this criterion, we assigned this transition an energy corresponding to the center of gravity of the observed band. Similarly, four transitions are expected to occur in the region 47,000-50,000 cm^{-1} in Ho^{3+}, where only two weak absorption bands could be discerned. Table XXI shows that the only matrix elements of $\mathbf{U}^{(\lambda)}$ in this range large enough to account for the experimental results are for transitions to $(^3H, ^3G, ^3I)_5$ and $^1I_5$. The observed band intensities, although they cannot be measured accurately, do conform to the predicted intensity relationship. Therefore, the energies corresponding to the centers of the observed bands were assigned to the indicated transitions.

Because of the complexity of the systems, relatively few assignments based on crystal data have been made in the ultraviolet region. The results in solution, then, appeared to offer a means of extending the crystal data.

The fitting procedure adopted here consisted of assigning several new levels, in addition to those that could be related to levels established in crystal systems, and carrying out a least-squares fitting process to define the corresponding new parameters. In each case, the identified transition was assigned an energy corresponding to the center of a band observed in solution, so that the parameters as they were refined were characteristic of the solution spectrum. The new parameters were used to calculate matrix elements of $\mathbf{U}^{(\lambda)}$, which could be compared with the experimental results to be certain that no inconsistencies developed. On the basis of these new calculations, additional assignments were made, and the procedure was repeated.

Assignments for the various lanthanides have already been reported for many of the bands observed in solution in the visible-near-infrared region of the spectrum.[7-9,39] However, to assemble as many of the pertinent facts as possible in one report, we will mention the basis for all the assignments made here.

In aqueous solutions, there is an infrared cutoff at ~7000 cm^{-1} due to overtones of OH vibration frequencies. This can be extended to ~5500 cm^{-1} using D_2O solutions,[11] but observations at lower energies must be made in other media. The spectra of the lanthanides in fused $LiNO_3$-KNO_3 at ~150° may be conveniently measured to ~4000 cm^{-1} (Ref. 10), and diffuse reflectance spectra of lanthanide chlorides or oxides have also been studied in the infrared region.[35,69]

Lanthanide absorption bands observed in the $LiNO_3$-KNO_3 melt[10] occur at very nearly the same frequencies as in H_2O (D_2O) solutions. Thus, in the following sections, the energies of the centers of gravity of a number of bands observed in the nitrate melt at <5500 cm^{-1} have also been taken as characteristic of the lanthanide in aqueous solution. The reflection spectra results have not been sufficiently extended into the infrared region to provide any additional information over that obtained in fused nitrates.

B. Discussion of Experimental Results

1. Ce^{3+} (f^1)

The single f → f transition ($^2F_{5/2} \rightarrow {}^2F_{7/2}$) in Ce^{3+} occurs in the infrared region beyond the range measured experimentally in the present investigation. From the literature, values of ζ_{4f} can be calculated as follows: 644 cm^{-1} (free ion),[46] 647 cm^{-1} (Ce^{3+} in $LaCl_3$),[30] and 706 cm^{-1} (Ce^{3+} in LaF_3 and in CeF_3).[3] Since only one multiplet is involved, the energy levels are independent of E^k.

2. Pr^{3+} (f^2)

The literature contains numerous reports of investigations of the energy-level structure of Pr^{3+}, but for comparison with the data obtained in solution, the free-ion levels,[64] and those obtained for Pr^{3+} in $LaCl_3$ (Ref. 59) and in LaF_3,[13] are particularly relevant. These experimental results are shown in Fig. 3 and in Table XXVIII from which it was concluded that, of the results given, the centers of the absorption bands observed in aqueous solution correspond most closely to the centers of gravity of the levels for Pr^{3+} in LaF_3.

TABLE XXVIII. Energy Level Assignments for Pr^{3+}

	Pr^{3+} Free Ion[64]			Pr^{3+} in $LaCl_3$[59]			Pr^{3+} in LaF_3[13]		
S'L'J'	E_{expt} (cm^{-1})	E_{calc}[a] (cm^{-1})	ΔE (cm^{-1})	E_{expt} (cm^{-1})	E_{calc}[a] (cm^{-1})	ΔE (cm^{-1})	E_{expt} (cm^{-1})	E_{calc}[a] (cm^{-1})	ΔE (cm^{-1})
$^3H_4$	0	20	-20	99.3	118	-9	200	228	-28
$^3H_5$	2152.2	2147	5	2209	2200	9	2363	2309	54
$^3H_6$	4389.1	4375	14	4390	4380	10	4464	4490	-26
$^3F_2$	4996.7	4989	8	4906	4911	-5	5215	5182	33
$^3F_3$	6415.4	6406	9	6322	6305	17	6555	6581	-26
$^3F_4$	6854.9	6888	-33	6766	6790	-24	7031	7044	-13
$^1G_4$	9921.4	9903	18	9766	9753	13	9997	9989	8
$^1D_2$	17334.5	17329	5	16714	16709	5	16846	16850	-4
$^3P_0$	21390.1	21362	28	20475	20450	25	20925	20899	26
$^3P_1$	22007.6	21984	24	21081	21057	24	(21473)[b]	21528	-55
$^1I_6$	22211.6	22211	1	21410	21410	0	21519	21519	0
$^3P_2$	23160.9	23214	-53	22227	22279	-52	22754	22722	32
$^1S_0$	50090.3	50090	0	48800	48800	0	46900	46900	0
RMS Deviation			36			33			47

[a]The parameters used to generate this set of energies are given in Table XXX.
[b]Based on the lowest three Stark levels in the $^3P_1$-$^1I_6$ manifold.

Experimental data for aqueous solution, together with calculated levels obtained by fitting procedures applied in the present work, are given in Table V.

a. ^3H and ^3F Levels. In general, the energies of the centers of the bands observed in solution corresponded closely to those reported in LaF_3.[13] For purposes of parameter fitting, it was assumed, therefore, that splitting of the ground term $^3H_4$ and the energy of the $^3H_5$ level, which could not be observed in the present study, would be similar in the two media. The energies corresponding to the transitions to $^3H_6$ and $^3F_2$ were assigned on the basis of bands observed for Pr^{3+} in a molten nitrate salt.[7]

A complex band, which could be resolved into four components, extends from 6000 to 7200 cm^{-1}. The four components appeared

to form two groups. The two bands within each group were separated by ~160 cm^{-1}. The centers of gravity of the two sets correspond closely to the centers for $^3F_3$ and $^3F_4$ observed in LaF_3.

b. $^1G_4$ and $^1D_2$ Levels. Transitions to these two levels give rise to well-isolated, rather broad absorption bands.

c. ^3P and ^1I Levels. Three sharp, relatively intense bands, the first of which is noticeably sharper than the others, are centered at 20,750, 21,320, and 22, 500 cm^{-1}. These energies correspond to the ^3P levels established for Pr^{3+} in LaF_3. Preliminary calculations revealed that the intensity of the $^1I_6$ level, which was found near 21,500 cm^{-1} in LaF_3, would be considerably less than that of the ^3P levels. Thus, an asymmetry in the absorption curve, which was resolved into a band centered at 21,500 cm^{-1}, was attributed to the $^1I_6$ transition in solution.

d. $^1S_0$ Level. The relatively intense absorption in Pr^{3+} at >43,500 cm^{-1} is known to be caused by 4f → 5d transitions.[17,38,48] The maximum absorbance of the resolved shoulder at 46,700 cm^{-1}, as may be seen from Fig. 3, also corresponds closely to the energy at which the $^1S_0$ level would be expected.[47] However, the intensity of the $^1S_0$ level, as shown in Table V, depends only on a relatively small matrix element of $\mathbf{U}^{(4)}$. It follows that the corresponding absorption band should be very weak as well as extremely narrow since it would not be split by a crystal field. Thus we would expect it to be lost in the very strong f → d band. To determine the value of γ, we therefore assumed that the transition to $^1S_0$ occurs in the solution spectrum at the same energy (46,900 cm^{-1}) as in the LaF_3 matrix.

The results of fitting the free-ion spectra of Pr^{3+} with four, six, and seven parameters are shown in Table XXIX. Two levels, $^1D_2$ and $^1I_6$, are particularly poorly fit with four parameters, but are brought into good agreement with experiment by including α and β. The energy of the $^1S_0$ level was not assigned in either the four- or six-parameter fits because its inclusion completely distorted the fit to all the levels. This was to be expected since $^1S_0$ is the only level in the f^2 scheme with a seniority number different from that of the ground state. The energy parameters for Pr^{3+} are given in Table XXX.

3. Nd^{3+} (f^3)

A comparison of the energies for Nd^{3+} transitions in $LaCl_3$ (Ref. 5) and LaF_3 (Ref. 14) with the centers of band systems in aqueous solution (as shown in Tables II and VIII and Fig. 4) revealed a rather close correlation between

the aqueous solution and the $LaCl_3$ data. Thus, it was assumed that the center of gravity of the $^4I_{9/2}$ and $^4I_{11/2}$ levels in solution would be identical to those reported for Nd^{3+} in $LaCl_3$. The $^4I_{13/2}$ and $^4I_{15/2}$ levels have been assigned to bands observed in fused nitrates.[7]

TABLE XXIX. Energy Level Fits to Pr^{3+} (Free-ion) Data

		4 Parameter	6 Parameter	7 Parameter
S'L'J'	νcm^{-1} Expt	νcm^{-1} Calc	νcm^{-1} Calc	νcm^{-1} Calc
$^3H_4$	0	12	17	20
$^3H_5$	2152.2	2061	2146	2147
$^3H_6$	4389.1	4228	4377	4375
$^3F_2$	4996.7	4977	4988	4989
$^3F_3$	6415.4	6339	6407	6406
$^3F_4$	6854.9	6983	6887	6888
$^1G_4$	9921.4	10152	9903	9903
$^1D_2$	17334.5	17668	17330	17329
$^3P_0$	21390.1	21442	21371	21362
$^3P_1$	22007.6	22025	21978	21984
$^1I_6$	22211.6	21703	22211	22211
$^3P_2$	23160.9	23236	23210	23214
$^1S_0$	50090.3	52233[a]	52122[a]	50090
E^1		5034.6 ± 121	5010.7 ± 17	4864.6 ± 5.5
E^2		22.159 ± .89	23.147 ± .14	23.138 ± .10
E^3		475.32 ± 5.0	488.02 ± .92	488.11 ± .70
ζ		737.74 ± 50	759.69 ± 6.5	758.82 ± 4.9
α			23.753 ± 1.2	23.684 ± .88
$\beta/12$			-49.374 ± 5.7	-48.784 ± 4.3
γ			-	727.78 ± 45
RMS Deviation		265 cm^{-1}	34 cm^{-1}	36 cm^{-1}

[a]This level was not included in the fitting process.

TABLE XXX. Energy Level Parameter Values Calculated for the Trivalent Lanthanides in Various Media (in cm^{-1})

	Matrix	E^1	E^2	E^3	ζ_{4f}	α	β	γ	No. of Levels Fit
Pr^{3+}	Free ion[64]	4864.6 ± 5.5	23.138 ± 0.10	488.11 ± 0.70	758.82 ± 4.9	23.684 ± 0.88	- 585.40 ± 52	727.78 ± 45	13
	$LaCl_3$[59]	4713.8 ± 5.0	21.890 ± 0.10	464.23 ± 0.64	742.68 ± 4.4	22.898 ± 0.81	- 676.94 ± 47	599.51 ± 42	13
	LaF_3[13]	4548.1 ± 7.2	21.659 ± 0.14	470.02 ± 0.90	743.25 ± 6.4	18.648 ± 1.2	- 754.47 ± 67	1396.2 ± 60	13
	AQ	4548.2 ± 7.5	21.937 ± 0.14	466.73 ± 0.94	740.75 ± 6.5	21.255 ± 1.2	- 799.93 ± 70	1342.9 ± 62	13
Nd^{3+}	$LaCl_3$[5]	4974.6 ± 13	23.734 ± 0.22	478.03 ± 1.1	879.42 ± 5.7	-0.8174 ± 1.2	- 163.94 ± 53	-	22
	AQ	4739.3 ± 16	23.999 ± 0.16	485.96 ± 1.0	884.58 ± 6.3	0.5611 ± 1.4	- 117.15 ± 56	1321.3 ± 84	32
Pm^{3+}	AQ	4921.6 ± 62	24.522 ± 0.74	525.53 ± 1.6	1000.8 ± 7.4	10.991 ± 2.5	- 244.88 ± 70	789.74 ± 370	22
Sm^{3+}	$LaCl_3$[49]	5594.9 ± 28	27.365 ± 0.57	545.50 ± 3.4	1162.5 ± 15	16.192 ± 2.8	- 540.36 ± 176	-	20
	AQ	5496.9 ± 42	25.809 ± 0.14	556.40 ± 1.7	1157.3 ± 5.8	22.250 ± 1.3	- 742.55 ± 53	796.64 ± 216	48
Eu^{3+}	$LaCl_3$[18]	5566.8	27.073	562.34	1298.0	22.0	- 235.78 ± 25	1000	12
	AQ	5573.0 ± 40	26.708 ± 0.90	557.39 ± 2.4	1326.0 ± 3.9	25.336 ± 1.6	- 580.25 ± 88	1155.7 ± 230	26
Gd^{3+}	$GdCl_3 \cdot 6H_2O$[29]	5761.0	28.020	582.00	1450.0	23.567 ± 0.70	190.00 ± 200	655.61 ± 170	15
	AQ	5761.0	28.020	582.00	1450.0	22.552 ± 0.73	- 103.7 ± 170	996.98 ± 145	20
Tb^{3+}	$LaCl_3$[65]	5955.9	28.965	601.60	1707.0	20.0	- 210.73 ± 6.7	1300	9
	AQ	6021.5 ± 70	29.030 ± 0.14	608.54 ± 4.0	1709.5 ± 7.7	20.131 ± 2.6	- 370.21 ± 104	1255.9 ± 360	23
Dy^{3+}	$LaCl_3$[16]	6411.2 ± 19	28.544 ± 0.25	603.84 ± 2.0	1923.4 ± 8.0	38.661 ± 2.3	-1184.7 ± 89	-	16
	AQ	6119.6 ± 58	30.012 ± 0.20	610.14 ± 2.2	1932.0 ± 7.8	37.062 ± 1.9	-1139.1 ± 74	2395.3 ± 300	34
Ho^{3+}	$LaCl_3$[20, 55]	6520.2 ± 104	31.438 ± 0.52	620.76 ± 2.1	2138.3 ± 9.2	23.490 ± 1.6	- 803.30 ± 63	887.56 ± 516	23
	AQ	6440.6 ± 35	30.220 ± 0.18	624.39 ± 0.95	2141.3 ± 4.9	23.635 ± 0.88	- 807.20 ± 36	1278.4 ± 190	41
Er^{3+}	Free ion[12]	6855.3 ± 17	32.126 ± 0.22	645.57 ± 2.4	2369.4 ± 11	20.385 ± 2.6	- 666.60 ± 107	-	27
	LaF_3[43]	6884.4 ± 25	32.586 ± 0.21	649.64 ± 2.0	2380.0 ± 9.7	17.044 ± 2.4	- 527.03 ± 83	-	21
	$LaCl_3$[56, 68]	6885.3 ± 22	32.272 ± 0.24	641.14 ± 2.6	2379.5 ± 11	17.431 ± 2.2	- 655.28 ± 86	-	20
	AQ	6769.9 ± 130	32.388 ± 0.14	646.62 ± 1.2	2380.7 ± 8.3	18.347 ± 1.2	- 509.28 ± 58	649.71 ± 640	27
Tm^{3+}	Ethyl Sulfate[a]	7150.8 ± 92	33.886 ± 0.62	675.73 ± 5.2	2628.1 ± 28	14.688 ± 6.4	- 741.59 ± 333	-	12
	AQ	7142.4 ± 60	33.795 ± 0.41	674.27 ± 3.4	2628.7 ± 18	14.677 ± 4.2	- 631.79 ± 216	-	12

[a]Ref. 22, 24, 26, 36, 45, 71.

a. ^4F, ^2H, and ^4S Levels. The transitions to ^4F, ^2H, and ^4S were assigned as indicated in Table VIII to well-characterized absorption bands, five of which were isolated.

b. ^4G, ^2G, ^2K, ^2P, and ^2D Levels. The $^4G_{5/2}$ transition is hypersenitive[6,37] and thus can be identified with the complex band observed in solution at ~17,300 cm^{-1}. This band could be resolved into two components centered at 17,300 and 17,460 cm^{-1}; the latter energy was assigned to the $^2G_{7/2}$ level. Of the transitions to $^2K_{13/2}$, $^4G_{7/2}$, and $^4G_{9/2}$, the only one with matrix elements of $U^{(\lambda)}$ (listed in Table VIII) large enough to account for the intensity of the principal component of the system was $^4G_{7/2}$, and it was thus assigned an energy of 19,160 cm^{-1}. The $^4G_{9/2}$ level was placed at the center of the next resolved band, which was consistent with the pattern of these three levels in $LaCl_3$ and with the preliminary intensity calculations. The next four transitions, $^2K_{15/2}$, $^2G_{9/2}$, $^2D_{3/2}$, and $^4G_{11/2}$, were also assigned energies corresponding to absorption maxima in a complex band system extending from 20,200 to 22,400 cm^{-1} on the basis of the correlation between calculated and observed intensities. The energy of the $^2P_{1/2}$ level in Nd^{3+} is well defined, as are the bands identified with $^2D_{5/2}$ and $^2P_{3/2}$. These transitions are unequivocally assigned by comparison with the levels found in $LaCl_3$.

c. ^4D and ^2D Levels. Three ^4D levels ($^4D_{3/2}$, $^4D_{5/2}$, and $^4D_{1/2}$) were assigned energies corresponding to the centers of resolved components of the complex band extending from 27,800 to 29,200 cm^{-1}. This was done on the basis of preliminary intensity calculations and the experimental verification of the occurrence of two of these levels near the same energies in $LaCl_3$. The isolated band at 26,300 cm^{-1} was clearly identified as $(^2P, ^2D)_{3/2}$. The intensity relationships shown in Table VIII indicate that the $^4D_{7/2}$ level should be assigned an energy of 30,500 cm^{-1}, which coincides with the center of an isolated band. The same criterion led to the assignment of $^2D_{3/2}$ at 33,400 cm^{-1} and $^2D_{5/2}$ at 34,450 cm^{-1}.

d. ^2F and ^2G Levels. The determination of a set of six parameters providing the best fit to the foregoing assignments, and subsequent use of these parameters to calculate the expected positions of bands in the range 35,000-50,000 cm^{-1}, revealed that only four transitions should be observed. In agreement with experimental results, it was predicted that these transitions should give rise to relatively weak and well-isolated bands. Examination of the eigenvectors for the $^2F_{5/2}$ and $^2F_{7/2}$ levels revealed that both contained large percentages of components differing in seniority number from that of the ground state. The magnitude of the parameter γ obtained in a seven-parameter fit to the data was therefore primarily determined by the assignment of energies to these two levels. The final parameters arrived at are summarized in Table XXX.

4. Pm^{3+} (f^4)

A center for the Stark components of the ground term $^5I_4$ was assumed to be 150 cm^{-1}, since no spectroscopic investigations of Pm^{3+} in a crystal lattice have been reported. The energies of the $^5I_5$ and $^5I_6$ levels are unknown, but isolated bands corresponding to the transitions to the $^5I_7$ and $^5I_8$ levels have been observed in a molten nitrate medium.[8]

a. ^5F, ^5S, and ^3K Levels. Preliminary intensity calculations indicated that it would be reasonable to assign the five transitions, $^5F_1$, $^5F_2$, $^5F_3$, $^5S_2$, and $^5F_4$, energies coincident with the centers of gravity of the five resolved absorption bands in the 12,000-15,000 cm^{-1} range, as indicated in Fig. 5. Both $^5F_5$ and $^3K_6$ were assigned an energy corresponding to the center of the isolated band at 15,900 cm^{-1}. This accounted satisfactorily for the observed intensity (as shown in Table IX).

b. ^5G, ^3D, ^3H, and ^3L Levels. The transitions to both $^5G_2$ and $^5G_3$ have been identified as hypersensitive.[8] They have correspondingly large matrix elements of $\mathbf{U}^{(2)}$. Thus, of the several levels with energies near 18,000 cm^{-1}, the indicated transitions were assigned to the known hypersensitive bands centered at 17,700 and 18,300 cm^{-1}, respectively,[8] and $^3H_4$ was placed at the center of a resolved component at 17,300 cm^{-1}.

Three transitions were shown by preliminary calculations to occur near 20,000 cm^{-1}. The one with the largest matrix elements of $U^{(\lambda)}$, $^5G_4$, was assigned an energy corresponding to the center of the band observed at 20,250 cm^{-1}. Of the next five transitions, $^5G_5$ and $^5G_6 + {}^3L_7$ were identified with two distinct absorption bands at 21,900 and 22,300 cm^{-1}, respectively.

The $^3L_8$ level was placed at 23,500 cm^{-1}. A transition of similar intensity to $^3G_4$, which should have been observed nearer 24,000 cm^{-1}, could not be discerned. The transition with the largest matrix elements of $U^{(\lambda)}$ calculated to occur near 25,000 cm^{-1}, $^3D_3$, was assigned to the center of the band at 24,800 cm^{-1}.

The spectrum at $>25,000$ cm^{-1} was not measured in the present investigation. However, Gruber and Conway[23] reported finding three relatively intense bands centered at 30,039, 30,478, and 31,250 cm^{-1}. Using the assignments at $<30,000$ cm^{-1} as the basis for parameter fitting and subsequently for an intensity calculation showed that among numerous transitions predicted to occur near 30,000 cm^{-1}, only three had large matrix elements of $U^{(\lambda)}$: $^5D_0$, $^5D_1$, and $^5D_2$. The calculated intensity pattern correlated quite well with the bands reported by Gruber and Conway; therefore the assignments were made as indicated in Table IX.

Several of the assigned levels had some dependence on states with seniority number different from that of the ground state. Thus it was possible to adequately determine seven parameters in the energy-level fitting process. The parameters arrived at are summarized in Table XXX.

5. Sm^{3+} (f^5)

The center of gravity of the ground term and the energies of the first three excited levels in solution were assumed to be the same as those reported for Sm^{3+} in $LaCl_3$,[49] since at higher energies the correlation between levels in the two media appeared to be very good, as is shown in Fig. 6. The $^6H_{13/2}$ level is isolated and was identified with an absorption band observed at 5000 cm^{-1} in a molten nitrate salt.[7] The energies of the $^6F_{1/2}$ and $^6F_{3/2}$ levels were assigned after comparing results in aqueous solution with those in a fused nitrate salt. Preliminary intensity calculations showed that the intensity of the band centered at 6630 cm^{-1} could only be accounted for on the basis of a transition from the ground state to $^6F_{3/2}$. Since a large matrix element of $U^{(2)}$ was calculated for the $^6F_{1/2}$ level (as may be seen from Table XII), the corresponding absorption band could be identified with a hypersensitive transition.[6] In aqueous solution, only a tailing to the infrared region of the band associated with the $^6F_{3/2}$ level could be observed, but in the nitrate melt, an intense absorption was found centered at 6400 cm^{-1}. The latter energy was therefore assigned to

the transition to the $^6F_{1/2}$ level in aqueous solution. Aside from Eu^{3+}, this is the only lanthanide transition observed in solution where the intensity is solely dependent on the matrix element of $\mathbf{U}^{(2)}$. Since calculations indicated that the transition to $^6H_{15/2}$ should give rise to a very weak band near 6500 cm^{-1}, no assignment was made in this case. The remaining terms in the ^6H and ^6F multiplets were assigned energies corresponding to the centers of distinct bands, as shown in Table XII.

a. ^4G, ^4F, and ^4I Levels. Extremely weak, isolated bands are found at 17,900 and 18,900 cm^{-1}. By comparison with the results in $LaCl_3$, these bands were unequivocally identified with the $^4G_{5/2}$ and $^4F_{3/2}$ levels, respectively. A distinct weak band at 20,050 cm^{-1} correlated well with the energy of $^4G_{7/2}$ in $LaCl_3$ and its calculated low intensity. The next relatively intense transition was calculated to be to the $^4M_{15/2}$ level, and it was assigned to the center of the band at 20,800 cm^{-1}. The latter band could be resolved into two principal components. To account for the intensity of the complex group extending from 20,300 to 22,000 cm^{-1}, the second component of the 20,800 cm^{-1} band was associated with the $^4I_{11/2}$ level at 21,100 cm^{-1}, and the next resolved band, centered at 21,600 cm^{-1}, with $^4I_{13/2}$. Similarly, on the basis of preliminary intensity calculations, and in agreement with levels assigned in $LaCl_3$, $^4F_{5/2}$ was assigned at 22,200 cm^{-1}, and $^4G_{9/2}$ was placed at the center of the band at 22,700 cm^{-1}.

b. ^6P, ^4L, and ^4D Levels. The transition to $^6P_{5/2}$ was identified with the band centered at 24,050 cm^{-1}, a somewhat higher energy than the assignment in $LaCl_3$, but consistent with it in terms of intensity. The $^4L_{13/2}$ level has the requisite intensity associated with it to account for a resolved component at 24,570 cm^{-1}. The matrix elements of $\mathbf{U}^{(\lambda)}$ for the transition to $^6P_{3/2}$ are of sufficient magnitude to be unequivocally correlated with the large band centered at 24,950 cm^{-1}. Similarly, the only transition that can account for the band centered at 25,650 cm^{-1} is $^4L_{15/2}$, and the intensity of the band at 26,750 cm^{-1} required the assignment to $^6P_{7/2}$. Energy-level calculations based on a fit to assigned levels at $<26{,}000$ cm^{-1} predicted that transitions to $^4D_{3/2}$ and $^4D_{5/2}$ would occur at nearly the same energy. Since both have relatively large matrix elements of $\mathbf{U}^{(4)}$, they are assigned energies corresponding to the center of the band at 27,700 cm^{-1}. A weak, well-resolved band at 28,250 cm^{-1} can reasonably be identified with the transition to $^4H_{7/2}$ since the nearest higher level, $^4K_{15/2}$, should exhibit no intensity.

The assignments at $>29{,}000$ cm^{-1} were all made on the basis of intensity since none of these levels has been identified in crystals. Although a great many transitions occur between 29,000 and 50,000 cm^{-1}, Table XII shows that only very few have calculated matrix elements of $\mathbf{U}^{(\lambda)}$ that could account for the magnitude of the observed absorption bands.

A number of the assigned levels in the Sm^{3+} spectrum contained large components with a seniority number different from that of the ground state, and thus it was possible to define a value of the parameter γ (as listed in Table XXX).

6. Eu^{3+} (f^6), Gd^{3+} (f^7), and Tb^{3+} (f^8)

A discussion of the energy-level systematics for these three ions will be deferred until Section V.D after the heavy lanthanides have been discussed.

7. Dy^{3+} (f^8)

Assignments to a number of the levels of Dy^{3+} in $LaCl_3$ have been made,[16] and there is a close correlation between the energies of transitions in the latter medium and in aqueous solution, as may be seen in Fig. 10 and Table XIX.

a. ^6H and ^6F Levels. The splitting of the ground term and the energy of the $^6H_{13/2}$ level in solution were assumed to be the same as those reported for Dy^{3+} in $LaCl_3$. The remaining transitions in the ^6H and ^6F multiplets give rise to solution absorption bands that are sharp, without structure, and centered near levels reported for $LaCl_3$. Confirmation of the existence of a hypersensitive band at 7750 cm^{-1} in the nitrate melt gives an additional basis for assigning $^6F_{11/2}$ at 7700 cm^{-1}. Since we expect no intensity for $\Delta J > 6$, $^6F_{1/2}$ is missing.

b. ^4F, ^4I, and ^4G Levels. Three transitions within this group, $^4F_{9/2}$, $^4I_{15/2}$, and $^4G_{11/2}$, were readily identified with the three weak isolated bands found in the interval 20,500-24,000 cm^{-1}, and the centers correspond well with those found in $LaCl_3$. The eigenvectors of the levels involved include appreciable contributions from states of seniority different from that of the ground state.

c. ^4F, ^4I, ^4M, ^4K, and ^6P Levels. The group of transitions from the ground state to $^4F_{7/2}$, $^4I_{13/2}$, $^4M_{21/2}$, and $^4K_{17/2}$ have the requisite calculated intensity to account for the band system that extends from 24,600 to 26,800 cm^{-1}. Of the latter two levels, only the higher-energy transition was assigned since it can account primarily for the intensity centered near 26,400 cm^{-1}. Preliminary intensity calculations placed $^4M_{19/2}$, $^4P_{3/2}$, and $^6P_{5/2}$ near the center of the rather intense band at 27,400 cm^{-1}. This is consistent with the energy of $^6P_{5/2}$ as identified in $LaCl_3$.

The very large matrix element of $\mathbf{U}^{(4)}$ for $^6P_{7/2}$ (listed in Table XIX) indicates that it should be assigned to the center of the principal band at 28,550 cm^{-1}. Similarly, $^4F_{5/2}$ and $^6P_{3/2}$ are assigned to account for distinct bands at 29,600 and 30,800 cm^{-1}, respectively.

Intensity calculations made it possible to assign several additional bands in the ultraviolet, as noted in Table XIX. Because of the strong general absorption in the ultraviolet region, no distinct bands were observed beyond 43,000 cm^{-1}.

The results of a six-parameter fit to the assigned levels were particularly revealing in this case since it was impossible to correlate the observed and calculated band energies on such a basis. When levels such as $^4F_{9/2}$, $^4I_{15/2}$, and $^6G_{11/2}$, which are strongly dependent on γ, were excluded from the six-parameter fit, their calculated energies varied by 300-400 cm^{-1} from the centers of the bands observed experimentally. For Dy^{3+}, the experimental data could only be correlated with a calculated energy level and intensity scheme based upon the seven-parameter fit.

8. Ho^{3+} (f^{10})

The good correlation between the energy levels established in a $LaCl_3$ matrix and the centers of bands observed in solution, which is found for most of the lanthanide series, was also observed for Ho^{3+} (Refs. 20 and 55). In this and in subsequent heavier lanthanides, all terms in the ground-state multiplet are observed either in the nitrate melt[9] or directly in aqueous solution.

a. ^5I, ^5F, and ^5G Levels. Since the lower terms of Ho^{3+} are well isolated, the assignments can be made unambiguously, as shown in Fig. 11 and Table XXI. For the complex band corresponding to the energies observed for transitions to $^5F_3$, $^5F_2$, and $^3K_8$, in $LaCl_3$, individual components could be resolved with intensities corresponding closely to those predicted from preliminary intensity calculations. The next large band centered at 22,100 cm^{-1} is hypersensitive[9] and thus is consistent with the calculated large matrix element of $\mathbf{U}^{(2)}$ for the transition to $^5G_6$ (as indicated in Table XXI). No intensity is expected to be associated with the transition to $^5F_1$ ($\Delta J > 6$). The isolated band at 23,950 cm^{-1} was identified as $^5G_5$, and the next group near 26,000 cm^{-1} could be resolved into two components centered at 25,800 and 26,200 cm^{-1}. These energies correspond closely with those identified with transitions to $^5G_4$ and $^3K_7$, respectively, in $LaCl_3$.

b. ^3H, ^3L, ^3K, ^5G, and ^3P Levels. The relatively intense band at 27,700 cm^{-1} shows hypersensitivity in the nitrate melt,[9] where the center is also at 27,700 cm^{-1}, and thus is identified with the transition to $^3H_6$, for which a large matrix element of $\mathbf{U}^{(2)}$ is calculated. Intensity considerations required, in addition, the assignment of $(^5G, ^3H)_5$ at this energy, and indicated that a weak but distinct band at 28,250 cm^{-1} could reasonably be assigned to transitions to $^5F_2$. The group centered at 29,000 cm^{-1} was resolved into two components at 28,800 and 29,000 cm^{-1}. The intensity pattern agreed with that expected for $^5G_3$ and $^3L_9$, respectively.

A sharp band at 30,000 cm^{-1} was correlated with two transitions, $^3F_4$ and $^3K_6$, while the weak rather broad band at 30,900 cm^{-1} could unambiguously be assigned to $^5G_2$. The isolated weak band at 33,200 cm^{-1} was also clearly identified as $^3D_3$ since the only alternative assignment, $^3P_1$, could be predicted to have no intensity ($\Delta J > 6$).

The complex band extending from 33,600 to 35,500 cm^{-1} was resolved into three components. Based on the results in $LaCl_3$, a transition to $^5G_4$ was expected near 34,700 cm^{-1}. Intensity calculations predicted that this transition should give rise to an intense band, and indeed a large absorption was found in solution centered at 34,800 cm^{-1}. Both $^3L_8$ and $^3M_{10}$ were then identified with the component of the system centered at 34,200 cm^{-1}, and $^3F_3$ was placed at 35,200 cm^{-1} where, according to calculations, it could account for the weak transition observed at this energy.

The transition to the $^3H_4$ level was assigned an energy corresponding to the center of an intense band at 36,000 cm^{-1}, on the basis of the intensity calculations. No other neighboring transition could account for the magnitude of the observed absorption. The remaining intensity of the system (36,200-37,000 cm^{-1}) was attributed, on the basis of results in $LaCl_3$, to transitions to $^1L_8$ and $^3H_5$.

c. ^3L, ^3I, ^3M, ^5D, and ^3H Levels. Several isolated bands were observed in the region ~38,000-50,000 cm^{-1}. A preliminary fit to the levels assigned at $<40{,}000$ cm^{-1} made it possible to predict which transitions would occur in the higher-energy range. The resulting assignments are shown in Table XXI. Even though in some cases several transitions were expected to occur near a given energy, only one could account for the observed intensity. The results of the seven-parameter fit to the experimental data are given in Table XXX.

9. Er^{3+} (f^{11})

A considerable amount of experimental work on the energy-level scheme of Er^{3+} in different media has been reported, including a study of the free-ion spectrum.[12] Table XXXI summarizes the latter results, together with those for Er^{3+} in $LaCl_3$,[56,68] and LaF_3.[43] Figure 12 compares the experimentally determined levels for Er^{3+} (free ion) and Er^{3+} in $LaCl_3$ to the solution absorption spectrum. On the basis of the foregoing, it was concluded that the levels observed in $LaCl_3$ were most closely related to those observed in aqueous solution, and a center for the ground term in solution was taken as 108 cm^{-1}.

a. ^4I, ^4S, ^2H, and ^4F Levels. The sharp isolated bands resulting from transitions between the ground state and the first few multiplet levels are well characterized by comparison with the energies of the levels in crystalline media. Below 25,000 cm^{-1}, the only assignments requiring reference to preliminary intensity calculations were those that involved the complex group extending from 21,800 to 23,100 cm^{-1}. This latter system was resolved into

two principal bands centered at 22,100 and 22,500 cm^{-1}. Reference both to intensity requirements (shown in Table XXIII) and to the levels identified in $LaCl_3$ indicated the assignments to $^4F_{5/2}$ and $^4F_{3/2}$, respectively.

TABLE XXXI. Energy Level Assignments for Er^{3+}

	Er^{3+} (Free ion)[12]			Er^{3+} in LaF_3[43]			Er^{3+} in $LaCl_3$[56, 68]		
S'L'J'	E_{expt} (cm^{-1})	E_{calc}[a] (cm^{-1})	ΔE (cm^{-1})	E_{expt} (cm^{-1})	E_{calc}[a] (cm^{-1})	ΔE (cm^{-1})	E_{expt} (cm^{-1})	E_{calc}[a] (cm^{-1})	ΔE (cm^{-1})
$^4I_{15/2}$	0	96	-96	217	232	-15	108	130	-22
$^4I_{13/2}$	6485.9	6567	-81	6697	6732	-35	6589	6630	-41
$^4I_{11/2}$	10123.6	10140	-16	10340	10335	5	10219	10226	-7
$^4I_{9/2}$	12345.5	12294	61	12567	12504	63	12438	12377	61
$^4F_{9/2}$	15182.9	15202	-19	15452	15432	20	15283	15260	23
$^4S_{3/2}$	18299.6	18445	-145	18570	18696	-126	18398	18536	-138
$(^2H, ^4G)_{11/2}$	19010.8	19096	-85	19334	19398	-64	19144	19181	-37
$^4F_{7/2}$	20494.1	20391	103	20709	20652	57	20515	20449	66
$^4F_{5/2}$	22181.8	22014	168	22378	22305	73	22174	22097	77
$^4F_{3/2}$	22453.9	22368	86	22711	22645	66	22516	22449	67
$(^2G, ^4F)_{9/2}$	24475.2	24367	108	24744	24644	100	24565	24471	94
$^4G_{11/2}$	26376.9	26348	29	26585	26680	-95	26367	26397	-30
$^4G_{9/2}$	27319.2	27333	-14	27629	27693	-64	27327	27358	-31
$^2K_{15/2}$	27584.9	27597	-12	-	27857	-	27605	27643	-38
$^2G_{7/2}$	27825.0	27843	-18	28298	28176	122	27987	27909	78
$(^2P, ^2D)_{3/2}$	31414.4	31496	-82	31718	31844	-126	31497	31625	-128
$^2K_{13/2}$	32972.2	32862	110	33139[b]	33145	-6	32963	32927	36
$^4G_{5/2}$	33088.4	33266	-178	-	33666	-	-	33284	-
$^2P_{1/2}$	33240.2	33218	12	-	33629	-	-	33418	-
$^4G_{7/2}$	33849.1	33840	9	34211	34209	2	33944	33921	23
$^2D_{5/2}$	34733.3	34534	199	35055	35010	45	34755	34743	12
$(^2H, ^2G)_{9/2}$	36479.5	36326	144	36641	36676	-35	36440	36501	-61
$^2D_{5/2}$	38406.1	38375	31	38827[c]	38816	11			
$^4D_{7/2}$	39268.5	39026	242	39530	39519	11			
$^2I_{11/2}$	-	40808	-						
$^2L_{17/2}$	-	41438	-						
$^4D_{3/2}$	41854.7	42028	-173						
$(^2D, ^2P)_{3/2}$	42426.2	42710	-284						
$^4I_{13/2}$	-	43507	-						
$^4D_{1/2}$	-	46829	-						
$^2H_{9/2}$	47420.0	47532	-112						
	RMS Deviation		141			84			84

[a]The parameters used to generate this set of energies are given in Table XXX.
[b]This energy was assigned to the transition to $^4G_{5/2}$ in Ref. 43, but intensity considerations suggest the indicated assignment.
[c]Not all of the Stark components of this level were observed.

b. ^4G, ^2K, and ^2G Levels. The group of bands in the range 27,000-28,400 cm^{-1} was resolved into three components centered at 27,400, 27,850, and 28,000 cm^{-1}. The first and third were of sufficient magnitude to clearly indicate, based on the intensity calculations, that they should be ascribed to transitions from the ground level to $^4G_{9/2}$ and $^2G_{7/2}$, respectively. Since the transition to the $^2K_{15/2}$ level was expected to be relatively weak, the criteria available were not deemed sufficient to warrant an assignment.

c. ^2P, ^2K, ^2D, ^2I, and ^2L Levels. The isolated band at 31,600 cm^{-1} was clearly attributable to the transition to $^2P_{3/2}$. Intensity calculations showed that the band at 33,200 cm^{-1} should be assigned to $^2K_{13/2}$ since transitions to both the neighboring levels $^4G_{5/2}$ and $^2P_{1/2}$ were predicted to give rise to bands of much lower intensity. Resolved bands with centers at 34,050, 34,850, and 36,550 cm^{-1} were identified with transitions to the $^4G_{7/2}$, $^2D_{5/2}$, and $^2H_{9/2}$ levels, respectively, at nearly the same energies as those reported for Er^{3+} in $LaCl_3$.

The very large matrix element for $U^{(4)}$ calculated for the transition to $^4D_{7/2}$ and its known energy of approximately 39,000 cm^{-1}, clearly identifies it with the intense band centered at 39,200 cm^{-1}. Since $^2D_{5/2}$ was found at a somewhat lower energy than $^4D_{7/2}$ in $LaCl_3$, it was assumed that the weak band observed at 38,600 cm^{-1} could be attributed to the $^2D_{5/2}$ transition in solution.

Assignments involving $^2I_{11/2}$, $^2L_{17/2}$, and $^4D_{3/2}$ were made resolved components of a group of bands extending from 40,700 to 43,000 cm^{-1} on the basis of apparent correlation between observed intensities and the magnitude of calculated matrix elements. Most of the intensity was identified with the transition to $^2L_{17/2}$ at 41,650 cm^{-1}. The isolated band at 43,550 cm^{-1} could be unambiguously associated with the $^2I_{13/2}$ level. It was assumed that the transitions predicted to occur in the 47,000-48,000-cm^{-1} range gave rise to broad absorption bands because they could not be clearly discerned over the background absorption in solution. Calculations predicted that they would be weak. A weak isolated band centered at 49,000 cm^{-1} could clearly be correlated with the transition to the $^2D_{5/2}$ level.

In Er^{3+}, almost all states that contain appreciable components with seniority number different than the ground state, lie at >50,000 cm^{-1}. Thus, even though many levels could be assigned to the solution spectrum, the parameter γ was rather poorly determined (as may be seen in Table XXX). The results of six-parameter fits to experimental data for Er^{3+} free ion and for Er^{3+} in $LaCl_3$ and LaF_3 are included in Table XXX.

10. Tm^{3+} (f^{12})

All the transitions to excited multiplet levels in Tm^{3+}, except to $^1S_0$, occur within the energy range that can be examined in aqueous

solution. The energy-level schemes for Tm^{3+} in several crystal media have been reported. However, the most complete data are available only in oxide media where the Stark splitting of the levels and the nephelauxetic effect are both known to be much larger than for most crystals.[25,44] We have taken the data reported by several different authors for $Tm(C_2H_5SO_4)_3 \cdot 9H_2O$ crystals as the primary basis for making assignments to the present results in aqueous solution.[22,24,26,36,45,71] The crystal-field splitting in the ethylsulfate is comparable to that in $LaCl_3$ and the centers of gravity of the levels appear to correspond quite well to those in solution, as shown in Fig. 13 and Table XXV. Although not all the Stark components of the ground level have been identified experimentally, the work of Wong and Richman,[71] as confirmed by thermodynamic studies,[22] indicates a center of gravity of ~170 cm^{-1} for Tm^{3+} in the ethylsulfate matrix.

The assignments in most cases were unambiguous because the bands are well isolated. The relatively weak component resolved at 15,100 cm^{-1} was consistent with the results of the preliminary intensity calculation, which could correlate this with the transition to the $^3F_2$ level. Two transitions in the group ^3P and ^1I gave rise to isolated identifiable bands--$^3P_2$ at 38,250 cm^{-1} and $^3P_1$ at 36,400 cm^{-1}--whereas the assignments of $^1I_6$ at 34,900 cm^{-1} and $^3P_0$ to 35,500 cm^{-1} were made on the basis of intensity calculations for resolved bands, and levels observed in the ethylsulfate.

The results of six-parameter fits to both the solution and crystal data are given in Table XXX.

11. Yb^{3+} (f^{13})

The single $f \rightarrow f$ transition in Yb^{3+}, $^2F_{7/2} \rightarrow {}^2F_{5/2}$, gives in solution, an absorption band centered near 10,300 cm^{-1} (as shown in Fig. 14). From this we calculate $\zeta_{4f} = (2/7)(10,300) = 2943$ cm^{-1}.

C. Systematic Behavior of Energy-level Parameters for All Lanthanides Except Eu^{3+}, Gd^{3+}, and Tb^{3+}

1. Introduction

Intensity considerations have been a useful tool in the assignment of energy levels in lanthanide spectra. Since the resolution possible in solution is much less than in crystal media, analysis of solution spectra has previously been limited to assignment of those transitions for which unambiguous correlation with crystal data was possible. By using intensity correlations as well as fitting of the energy parameters, we have extended the range of assignments well into the ultraviolet region, frequently much further than previous crystal analyses. Thus we have been able to obtain

a good set of parameter values derived from the same media for all of the 3+ lanthanides, except Eu, Gd, and Tb. It now becomes possible to examine the behavior of these parameters across the lanthanide series.

2. Slater Parameters (F_k)

A plot of F_2 versus atomic number, Z, for all the lanthanides except Eu^{3+}, Gd^{3+}, and Tb^{3+}, can be fit by the linear function shown in Fig. 15. Using an equation of the same form as that given by Elliott et al.,[21] where an empirical screening constant is introduced, but fitting the present experimental values for F_2, we obtain

$$F_2 = 12.820(Z - 34). \quad (15)$$

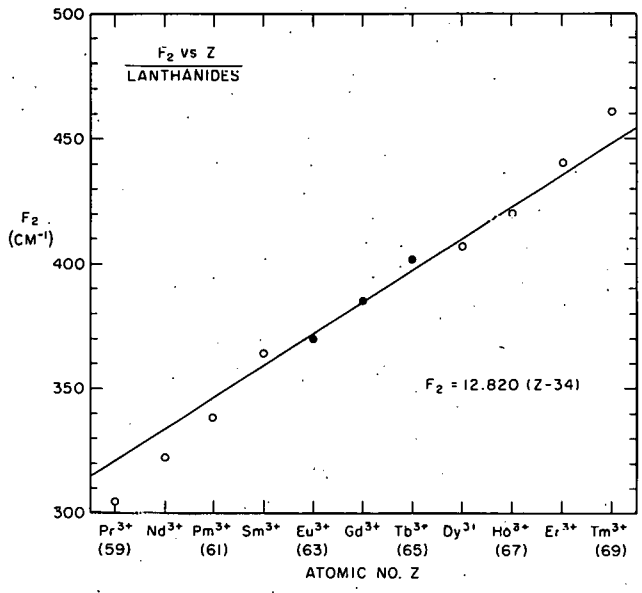

121-2508 Rev. 9

Fig. 15. Variation across Lanthanide Series of Parameter F_2 Obtained from a Fit to Lanthanide Aquo Ion Data

Approximate values for F_2 derived from four-parameter fits to the few levels that have been assigned in the crystal spectra of Eu^{3+}, Gd^{3+}, and Tb^{3+}, are well above the line determined by Eq. 15, as can be seen from the results in Table I. This deviation is much greater than expected since the parameters obtained give excellent fits to the observed levels. We would not, however, expect these parameters to give a good prediction of the positions of higher-energy levels. Several of the observed levels for each of these three ions have large contributions from states of different seniority from that of the ground state. Experience leads us to believe that any fitting process that does not include the parameter γ will be meaningless in such cases. All the observed levels in these ions are identified with very pure LS states. Thus the E^k parameters can change drastically without appreciably altering the percent composition of the principal state. The deviation from the line in Fig. 15, of F_2 values based upon four-parameter fits to the data for Eu^{3+}, Gd^{3+}, and Tb^{3+}, is therefore not physically significant. As will be shown later in this section, and as is indicated in Fig. 15, when sufficient data are available to adequately define complete sets of electrostatic, spin-orbit, and configuration interaction parameters for Eu^{3+}, Gd^{3+}, and Tb^{3+}, the corresponding values of F_2 are near the line defined by Eq. 15.

Values of the ratio F_4/F_2 as a function of Z are quite regular. As shown in Fig. 16, the average is near 0.15, which is somewhat larger than the ratio calculated assuming that the 4f-wave functions are hydrogenic.

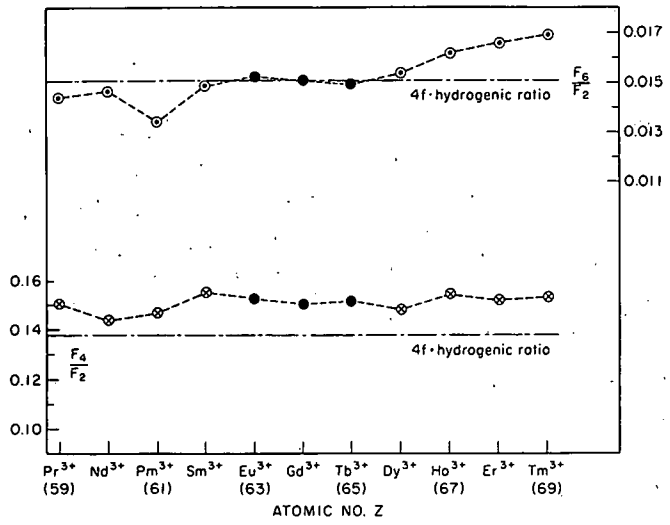

121-2509 Rev. 7

Fig. 16. Variation across Lanthanide Series of Ratios F_4/F_2 and F_6/F_2 Calculated from a Fit to Lanthanide Aquo Ion Data

There is an apparent change in the ratio F_6/F_2 from somewhat less than the hydrogenic ratio for the light lanthanides to greater than this ratio for the heavy lanthanides, as shown in Fig. 16. There is no obvious explanation for this behavior. Of course, the usefulness of the hydrogenic approximation in obtaining initial values of the Slater integrals does not imply that the actual radial wave functions are at all similar to hydrogenic wave functions.[73] The final results for Eu^{3+}, Gd^{3+}, and Tb^{3+} are included in Fig. 16, but the discussion appears later in this section.

3. Spin-orbit Coupling Constant (ζ_{4f})

The variation of ζ_{4f} across the lanthanide series is shown in Fig. 17, which also includes values for Ce^{3+} and Yb^{3+}. This parameter can be defined for Eu^{3+}, Gd^{3+}, and Tb^{3+}, even when the experimental data are limited to the components of only two or three different multiplets.

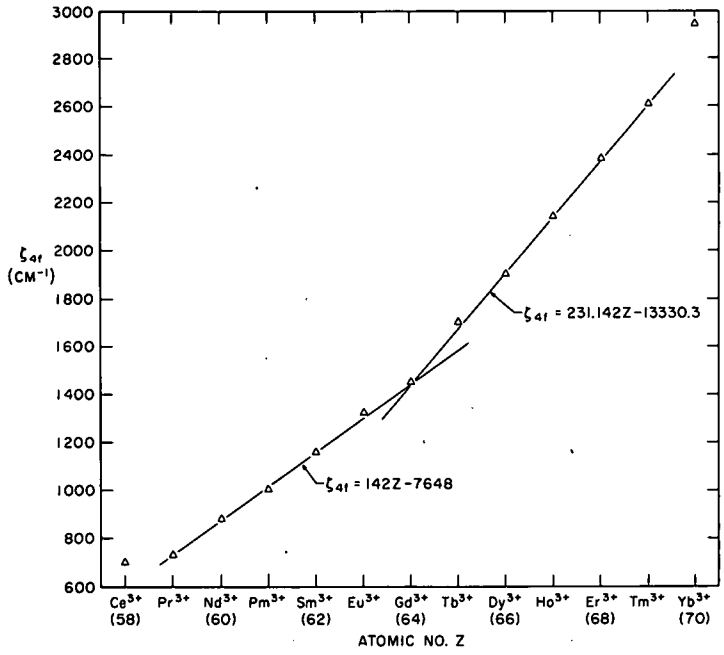

121-2506 Rev. 6

Fig. 17. Variation across Lanthanide Series of Spin-orbit Coupling Constant, ζ_{4f}, Calculated from a Fit to Lanthanide Aquo Ion Data

Attempts were made to express ζ_{4f}, both as a linear and as a quadratic function of Z. At the outset, it became clear that the average deviation from the experimental value was appreciably increased if the values of ζ_{4f} for Ce^{3+} and Yb^{3+} were included in the fit, regardless of whether the expression was quadratic or linear. Results excluding Ce^{3+} and Yb^{3+} showed that the average deviation was appreciably less when two linear functions with a common value at Gd^{3+} were used as compared to a single quadratic function. The functions were:

(1) $\zeta_{4f} = -79.5522\ Z^2 + 2539.45\ Z - 325360.$
Average deviation from experiment = 16.2.

(2) $\zeta_{4f} = 142\ Z - 7648$ (Pr^{3+} through Gd^{3+}).
Average deviation from experiment = 11.3.

$\zeta_{4f} = 231.142\ Z - 13330.3$ (GD^{3+} through Tm^{3+}).
Average deviation from experiment = 9.5.

4. Configuration Interaction Parameters (α, β, and γ)

The systematic behavior of the configuration interaction parameters has been studied previously only in the $3d^N$ and $4d^N$ configurations. By assuming that each of the parameters follows an equation of the form

$$A = A_0 + A_1 x + A_2 y,$$

where

$$x = N - 6$$

and

$$y = x^2 - 10,$$

Shadmi[60,61] has been able to simultaneously fit the energy levels of an entire series by the determination of only the "general parameters," A_i. In doing this, he assumed that α and β vary linearly with N; i.e., $A_2 = 0$. However, if we compare the values of α obtained on the basis of this assumption with those obtained as a result of individual fits to the levels of a single ion, there are frequent large differences well outside the rms deviation of the parameters.[61] Thus a linear variation of α with N is not apparent for the single-ion fits.

For the lanthanides, the absolute magnitudes of α and β increase in the first half of the series after Pr^{3+} (as shown in Fig. 18), and decrease again in the second half after Dy^{3+}. The behavior in the center of the series for Eu^{3+}, Gd^{3+}, and Tb^{3+} will be discussed in Section V.C. However,

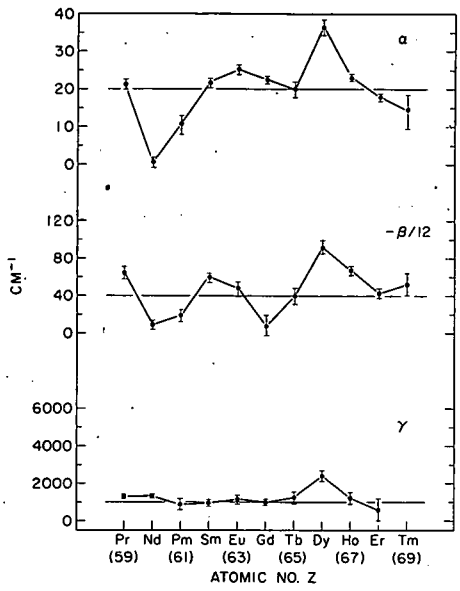

121-2853 Rev. 6

Fig. 18. Variation across Lanthanide Series of Configuration Interaction Parameters α, β, and γ Calculated from a Fit to Lanthanide Aquo Ion Data

it is clear that the magnitude of the variation in these parameters across the $4f^N$ series is much greater than that observed in the d^N series. The parameters for Pr^{3+}, where α and β are well determined, are large in comparison to those for Nd^{3+} and Pm^{3+}.

In all cases except for Tm^{3+}, a positive value could be adequately defined for γ. The results for Dy^{3+} were larger than the average of approximately 1100 cm^{-1}. The only previous determination of γ was from the free-ion spectrum of Pr^{2+}, and in this case a negative value for the parameter was obtained.[58] The latter result depended upon only one level, which was somewhat doubtful. In view of the present results, a negative value for γ in Pr^{2+} seems unlikely. It is highly probable that the $^2F_{5/2}$ level from which the value of γ was determined is spurious. This view is further supported by the calculation of Trees,[66] which indicated that γ should be positive. Recent Hartree-Fock calculations for Pr^{2+} indicate that the major contribution to γ comes from interaction with $4d^8 4f^5$ (Ref. 70). Although negative terms arise from interaction with configurations such as $4f^2 6p$ and $4p^5 4f^4$, these are not sufficient to overcome the large positive contributions from $4d^8 4f^5$.

D. Energy-level Calculations for Eu^{3+}, Gd^{3+}, and Tb^{3+}

It was pointed out earlier in this section that, because of the paucity of assignments made to the spectra of the ions Eu^{3+}, Gd^{3+}, and Tb^{3+} ions in crystals, and the general complexity of their level structure, it was not immediately possible to determine all the electrostatic, spin-orbit, and configuration interaction parameters on the basis of solution spectra. We also noted that predictions of the positions of higher-energy levels based upon four-parameter fits to the few levels that had been characterized were not expected to be useful. The values of the parameter F_2 resulting from these four-parameter fits were wholly inconsistent with those obtained for all the other lanthanides.[11] The foregoing is well illustrated by the results obtained for Gd^{3+}.

1. Gd^{3+} (f^7)

All the terms in the ^6P, ^6I, and ^6D multiplets of Gd^{3+} in crystals of $GdCl_3 \cdot 6H_2O$ were recently assigned,[29] and, as can be seen from Table XV and Fig. 8, there is a close correlation between the levels observed in the crystal and the maxima of bands observed in solution. The levels assigned

to the experimental data are all relatively pure L-S states, and there are insufficient data to determine more than four parameters. These are given in Table I and provide an excellent fit to the levels observed, both in $GdCl_3 \cdot 6H_2O$ and in solution. However, the fact that the ^6P group has a seniority number different from that of the ground state, indicates that γ should be included in the calculation.

During the present investigation we were able to identify several absorption bands near 50,000 cm^{-1} characteristic of Gd^{3+}. These bands have not previously been reported. As shown in Fig. 19, based upon the four-parameters for Gd^{3+} given in Table I, the next-higher-lying multiplet after ^6D is predicted to be ^4D. Intensity calculations revealed that only very weak bands should be observed, in contrast to those obtained experimentally.

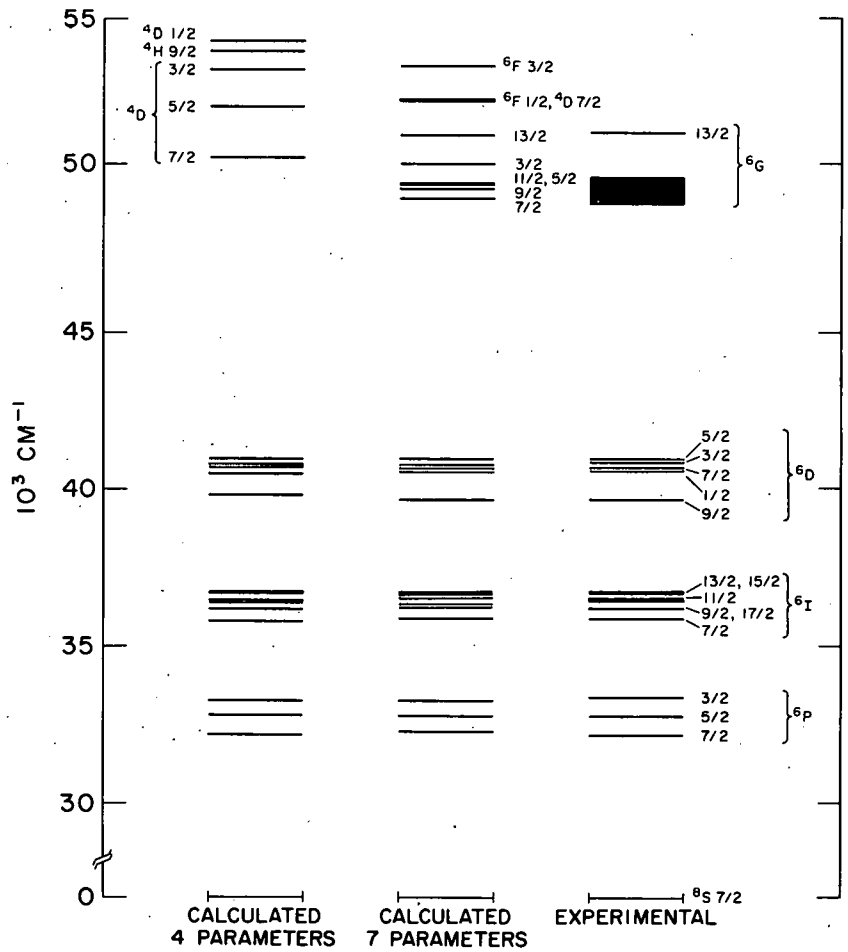

121-2854 Rev. 2

Fig. 19. Comparison between Calculated and Experimentally Determined Energy Levels for Gd^{3+} (AQ)

At this point, we assumed that the values of F_2 and the ratios of F_4/F_2 and F_6/F_2 for Gd^{3+} should be consistent with those for the other lanthanides. From Eq. 15, we obtained $F_2 = 385$; and from the results shown in Fig. 16, we assumed $F_4/F_2 = 0.15$ and $F_6/F_2 = 0.015$. Using values

of E^k calculated from the foregoing, together with ζ_{4f} obtained from the four-parameter fit, we obtained a seven-parameter fit to the known ^6P, ^6I, and ^6D levels by varying only the three configuration interaction parameters α, β, and γ. The results are also shown in Fig. 19. As we had predicted, with an entirely different set of electrostatic parameters than had been obtained from the four-parameter fit, the agreement between calculated and observed energies for the ^6P, ^6I, and ^6D multiplets was good, and the ordering of the higher-lying multiplets was completely changed. Indeed the new fit placed several ^6G levels near 49,000 cm^{-1}, and an isolated $^6G_{13/2}$ level near 51,000 cm^{-1}, in excellent agreement with the experimental results. A preliminary intensity calculation showed that the ^6G levels near 49,000 cm^{-1} had large matrix elements of $\mathbf{U}^{(4)}$, as did the $^6G_{13/2}$ level. Thus, additional assignments were made as shown in Table XV, and a final set of parameters was obtained. Since all the additional assignments involved only a single multiplet, ^6G, there were still insufficient data to directly determine the electrostatic as well as the configuration interaction parameters, so only the latter were varied. The results are given in Table XXX, together with a fit to the $GdCl_3 \cdot 6H_2O$ data computed using the same assumptions. The values of α and γ obtained are obviously consistent with those for other lanthanides (as shown in Fig. 18), while the value of β suggests a break in the variation of this parameter as a function of Z at the center of the series.

The present results are confirmed in the experimental investigation of the levels of Cm^{3+} in $LaCl_3$ reported by Gruber et al.[27] Since the multiplets in Cm^{3+} are all shifted toward lower energies with respect to Gd^{3+}, the presence of ^6G levels directly above the ^6P multiplet was confirmed experimentally.

Wybourne[74] has considered in detail some of the mechanisms that could account for the reported ground-state splitting in Gd^{3+}. He pointed out that experimental g-factors for the ground state require much larger values of ζ_{4f} than are consistent with the observed multiplet splittings. The value of ζ_{4f} obtained in the present study is lower than that adopted by Wybourne and gives a good representation of the experimental data. Use of a larger value (1480 cm^{-1}) for ζ_{4f}, while assuming the fixed value of α = 20 cm^{-1} and E^k as before, gave $\beta/12$ = -20.58 and γ = 1177.23. However, the overall fit to the data was not as good as with the lower value of ζ_{4f}.

2. Tb^{3+} (f^8)

Only the ground-term multiplet and two components of the first excited multiplet of Tb^{3+} have been identified.[65] The very complex spectrum found in the ultraviolet region has not been elucidated.

In aqueous solution, only the $^5D_4$ level is readily assigned. Distinct bands observed near 5000 cm^{-1} in the nitrate melt[9] identify the

centers of gravity of the $^7F_3$, $^7F_2$, and $^7F_1$ levels, both in that medium and in aqueous solution. The $^7F_0$ level is revealed in the shoulder of the absorption due primarily to $^7F_1$ in the melt.

Preliminary intensity calculations based upon fitting α, β, and γ to the levels assigned to Tb^{3+} in $LaCl_3$,[65] assuming a value of F_2 computed using Eq. 15, $F_4/F_2 = 0.15$, $F_6/F_2 = 0.015$, and $\zeta_{4f} = 1707\ cm^{-1}$, suggested that a number of further assignments could be made to the solution absorption spectrum. Those transitions with large matrix elements of $\mathbf{U}^{(\lambda)}$ were assigned to the centers of the more intense bands found in the range 26,000-30,000 cm^{-1} as shown in Table XVII.

The relatively isolated bands at 30,650, 31,600, 33,000, and 33,900 cm^{-1} could be ascribed to transitions from the ground term to $^5D_1$, $^5H_7$, $^5H_6$, and $^5H_5$, respectively. The large matrix element of $\mathbf{U}^{(6)}$ for the transition to $^5I_8$, and its predicted energy near 35,000 cm^{-1}, was in good agreement with the absorption band observed in this range. This band was resolved into two components. The more intense component, centered at 35,200 cm^{-1}, was attributed to the transition to $^5I_8$, while the weaker, at 34,900 cm^{-1}, was identified with that to the $^5F_5$ level.

The identification of the relatively intense broad band centered near 38,000 cm^{-1} in terms of a $4f \rightarrow 4f^{N-1}5d$ transition was discussed in Section IV.A above. Three additional assignments were made to the centers of bands superimposed upon the f → d absorption. The weaker resolved bands had intensities that were qualitatively in keeping with the magnitude of the matrix elements of $\mathbf{U}^{(\lambda)}$ for f → f transitions, as indicated in Table XVII. A much more intense component of the $4f^N \rightarrow 4f^{N-1}5d$ system is observed near 46,000 cm^{-1}. Any f → f transitions in this region would be too weak to observe over such a large background.

A seven-parameter fit to the 23 levels assigned, where all seven parameters were varied, gave the results shown in Table XXX. All the parameters were well determined and in good agreement with those determined originally by extrapolation.

3. Eu^{3+} (f^6)

The levels of Eu^{3+} that occur in the visible region of the spectrum are of interest in connection with laser studies and thus have been the subject of numerous investigations. However, the levels above 25,000 cm^{-1}, with the exception of $^5D_4$, have not been clearly defined by investigations in an appropriate crystalline medium. The assignments for Eu^{3+} in a $LaCl_3$ matrix [18] are recorded in Table XIII. Thus, with respect to determining electrostatic and configuration interaction parameters, the situation is similar to that with Tb^{3+}.

In solution, the first excited component in the ground-term multiplet is only ~360 cm^{-1} above the ground level; the second excited component is near 1000 cm^{-1}. Thus, at room temperature, transitions originating in both of these levels are observed. Such transitions give rise to satellites, in many cases well resolved, to the low-energy side of bands due to transitions originating in $^7F_0$. They contribute to a complex spectrum in the ultraviolet region. It is this displacement of the satellites as observed in the visible region of the spectrum that makes it possible to clearly define the energy of the $^7F_1$ and $^7F_2$ levels with respect to the $^7F_0$ ground state in the solution spectra. In addition, Bayer-Helms placed $^7F_3$ at 1900 cm^{-1} in nitrate solutions.[1] The energy corresponding to $^7F_6$ was taken from results obtained in the nitrate melt.[7]

The extremely weak band at 17,277 cm^{-1} is clearly identified with the $^7F_0 \rightarrow {}^5D_0$ transition.[1,18,31] It occurs at ~360 cm^{-1} above the much more intense, normally observed band near 16,920 cm^{-1} due to $^7F_1 \rightarrow {}^5D_0$. Sharp bands identified by their close correlation with transitions observed for Eu^{3+} in $LaCl_3$ were assigned for $^7F_0 \rightarrow {}^5D_1$ and $^5D_2$, as shown in Table XIV. As mentioned in Section IV.A, the intensity of the band at 19,028 cm^{-1} arises entirely via a magnetic-dipole mechanism. The broader band at 18,691 cm^{-1} is attributed to $^7F_1 \rightarrow {}^5D_1$, and very weak absorptions at 18,018 and 20,500 cm^{-1} correspond to the transitions $^7F_2 \rightarrow {}^7D_1$ and $^7F_2 \rightarrow {}^7D_2$, respectively. The $^7F_0 \rightarrow {}^5D_3$ transition was placed at 24,408 cm^{-1}, where a small absorption was found, in agreement with the results in $LaCl_3$.

On the basis of the foregoing assignments to ^7F and ^5D, following the procedure used with Tb^{3+}, an attempt was made to obtain an energy-level fit to the data. The values $F_2 = 372$, $F_4/F_2 = 0.15$, $F_6/F_2 = 0.015$, and $\zeta_{4f} = 1298$ cm^{-1} were taken from Figs. 15, 16, and 17. Only the three configuration interaction parameters, α, β, and γ, were varied. The results gave $\alpha = \sim 20$ cm^{-1}, but both β and γ were extremely large and poorly determined. The energies and intensities predicted for higher-lying levels bore no apparent relation to the experimental data. Since the values of α and γ for other lanthanides appeared to be sufficiently constant over the center of the series to warrant an assumption of their magnitude for Eu^{3+} (as may be seen from Fig. 18), a further attempt was made to fit the assigned ^7F and ^5D levels. The parameter values already cited, together with $\alpha = 20$ cm^{-1} and $\gamma = 1200$ cm^{-1}, were used as constants. Thus only <u>one</u> parameter was varied. The results defined $\beta/12 = -23$ cm^{-1} and made it possible to obtain an excellent correlation between the assigned and calculated levels. This set of parameters also predicted higher energy levels and intensity relationships than could immediately be correlated with the experimental results. As expected, the sharpness of the bands arising from $^7F_0$ in the visible region was characteristic of the corresponding bands in the ultraviolet.

The intense band at 25,400 cm^{-1} and the weaker sharp band at 27,670 cm^{-1} (shown in Fig. 7) could immediately be assigned to transitions to $^5L_7$ and $^5D_4$, respectively, on the basis of an intensity correlation. The latter assignment also agreed with results obtained for Eu^{3+} in $LaCl_3$.[18] Similarly, $^5H_6$, $^5F_4$, $(^5I, ^5H)_6$, $^5K_6$, $(^3K, ^3I)_6$, $^5G_4$, and $^5G_6$ were assigned as shown in Table XIII. In each case, satellites ~360 cm^{-1} to the low-energy side of the assigned bands were observed as predicted.

Several further assignments were made after carrying out an intensity calculation based upon transitions from $^7F_1$ as the ground level. This showed, for example, that of the group of bands observed in the range 25,800-27,000 cm^{-1}, the component centered near 26,000 cm^{-1} could be accounted for as arising from the transition $^7F_1 \rightarrow {}^5L_7$. A comparable intensity was predicted to occur near 26,400 cm^{-1} due to $^7F_1 \rightarrow {}^5G_5$ and $^5G_6$, but no intensity was calculated for $^7F_1 \rightarrow {}^5L_8$, which was the only transition originating in $^7F_1$ and terminating in the 26,500-27,100-cm^{-1} range. Thus, sharp bands detected at 26,300 and 26,620 cm^{-1}, superimposed on larger absorptions, were assigned to transitions from $^7F_0$ to $^5G_2$ and $^5G_4$, respectively. The larger absorption at 26,700 cm^{-1} could then be attributed primarily to $^7F_0 \rightarrow {}^5G_6$, which has a relatively large matrix element of $\mathbf{U}^{(6)}$ (as given in Table XIII). Similar considerations accounted for the assignment of $^5H_4$ at 31,250 cm^{-1}, superimposed on a band arising from the transition $^7F_1 \rightarrow {}^5H_5$ at 31,162 cm^{-1}, and $^5F_2$ at 33,190 cm^{-1} superimposed on $^7F_1 \rightarrow {}^5F_4 + {}^5I_4$ at ~33,400 cm^{-1}. On the basis of the calculations, and in good agreement with experiment, the transition $^7F_1 \rightarrow {}^5H_5$ was predicted to have a slightly greater intensity than the isolated absorption at 30,656 cm^{-1} arising from $^7F_1 \rightarrow {}^5H_7$.

At the highest concentrations examined, several extremely weak bands were observed at energies that could not be correlated with allowed transitions from $^7F_0$, $^7F_1$, or $^7F_2$. They were also not attributable to rare-earth impurities. The most intense of these absorptions was at 36,205 cm^{-1}. A transition from $^7F_0$ to $^5K_5$ is calculated to occur at 36,235 cm^{-1} (as may be seen from Table XIII), but would be forbidden by the selection rule $\Delta J \neq$ odd. Since the next higher allowed transition, corresponding to $^7F_0 \rightarrow {}^5K_6$, occurs at 37,440 cm^{-1}, no transition from $^7F_1$ could account for the band in question. Similarly, $^7F_2 \rightarrow {}^5K_5$ would give rise to a somewhat higher energy band (36,400 cm^{-1}), and from the results obtained at lower energies, $^7F_2$ is so weakly populated at 25°C, that transitions originating in it are only detected at very high concentrations. We conclude that this may be a case in which a slight breakdown of selection rules is revealed, and that the transition involved actually is $^7F_0 \rightarrow {}^5K_5$. An examination of the energies calculated for all possible transitions from $^7F_0$ to J = ODD (as given in Table XIII) as compared to the experimental results shown in Fig. 7, indicates that practically all these transitions occur in regions where they would be masked by the presence of bands due to other transitions.

On the basis of the 26 assignments made, a final fit to the data was carried out in which all of the electrostatic, spin-orbit, and configuration interaction parameters were varied. The results in Table XXX show that each parameter is well defined and varies only slightly from that originally predicted.

In connection with the experimental results shown in Fig. 7, we found no absorption bands beyond 42,000 cm^{-1} that could be resolved from the generally increasing absorption in the ultraviolet. We did not observe the relatively intense band that Stewart[62] and Stewart and Kato[63] reported near 46,700 cm^{-1}. For Eu^{3+}, the lowest $4f \rightarrow 4f^{N-1}5d$ band occurs at very high energies. Loh[48] placed it near 68,500 cm^{-1} for Eu^{3+} in CaF_2, and Crozier[17] calculated it near 90,000 cm^{-1}. The present results are in agreement with the foregoing and with those reported by Jørgensen and Brinen.[38]

VI. CONCLUDING REMARKS

At present it is possible to compare the solution parameters determined here with those of the free ion only for Pr^{3+} and Er^{3+} (Refs. 64 and 72). One would expect covalent bonding effects in solution to reduce the parameters slightly from those obtained for the free ion. The reduction is about 5% for the E^k and ζ_{4f} values of Pr^{3+}. The configuration interaction parameters are somewhat more sensitive. The E^k and ζ_{4f} values for Er^{3+} are slightly higher for the solution than for the free ion, while α and β are lower. Since the rms errors on the parameters are nearly the same as the differences, the effect may not be significant. We would expect the present results to provide a good starting point for further analyses of the $4f^N$ configurations in the free-ion spectra.

ACKNOWLEDGMENTS

We gratefully acknowledge the large contribution of B. G. Wybourne, University of Canterbury, Christchurch, New Zealand, which made much of this work possible. We would also like to thank F. L. Clark, C. Chamot, S. Katilavas, and J. Milsted for their assistance in programming and carrying out the computer calculations, and D. Kiple, G. E. Toogood, S. Neufeldt, A. Walker, and R. McBeth, for aid in performing the experimental measurements. We are indebted to J. G. Conway and T. Clements, Lawrence Radiation Laboratory, University of California, for providing us with a number of the computer programs and tapes used in this work.

REFERENCES

1. Bayer-Helms, F., Z. Naturforchg. *13a*, 161 (1958).

2. Broer, L. J. F., C. J. Gorter, and J. Hoogschagen, Physica *11*, 231 (1945).

3. Buchanan, R. A., H. E. Rast, and H. H. Caspers, J. Chem. Phys. *44*, 4063 (1966).

4. Callahan, W. R., J. Opt. Soc. Am. *53*, 695 (1963).

5. Carlson, E. H., and G. H. Dieke, J. Chem. Phys. *34*, 1602 (1961); F. Varsanyi and G. H. Dieke, J. Chem. Phys. *33*, 1616 (1960).

6. Carnall, W. T., P. R. Fields, and B. G. Wybourne, J. Chem. Phys. *42*, 3797 (1965).

7. Carnall, W. T., D. M. Gruen, and R. L. McBeth, J. Phys. Chem. *66*, 2159 (1962).

8. Carnall, W. T., P. R. Fields, and G. E. Toogood, J. Phys. Chem. *68*, 2351 (1964).

9. Carnall, W. T., J. Phys. Chem. *67*, 1206 (1963).

10. Carnall, W. T., Anal. Chem. *34*, 786 (1962).

11. Carnall, W. T., and P. R. Fields, *Developments in Applied Spectroscopy*, Plenum Press (1961); *Advances in Chemistry*, No. 71, Am. Chem. Society (1967).

12. Carter, W. J., and H. M. Crosswhite, J. Chem. Phys. (in press).

13. Caspers, H. H., H. E. Rast, and R. A. Buchanan, J. Chem. Phys. *43*, 2124 (1965).

14. Caspers, H. H., H. E. Rast, and R. A. Buchanan, J. Chem. Phys. *42*, 3214 (1965).

15. Choppin, G. R., D. E. Henrie, and K. Buijs, Inorg. Chem. *5*, 1743 (1966).

16. Crosswhite, H. M., and G. H. Dieke, J. Chem. Phys. *35*, 1535 (1961).

17. Crozier, M. H., Phys. Rev. *137*, A1781 (1965).

18. DeShazer, L. G., and G. H. Dieke, J. Chem. Phys. *38*, 2190 (1963).

19. Dieke, G. H., and H. M. Crosswhite, Applied Optics *2*, 675 (1963).

20. Dieke, G. H., and B. Pandy, J. Chem. Phys. *41*, 1952 (1964).

21. Elliott, J. P., B. R. Judd, and W. A. Runciman, Proc. Roy. Soc. London *A240*, 509 (1957).

22. Gerstein, B. C., L. D. Jennings, and F. H. Spedding, J. Chem. Phys. *37*, 1496 (1962).

23. Gruber, J. B., and J. G. Conway, J. Inorg. Nucl. Chem. *14*, 303 (1960).

24. Gruber, J. B., and J. G. Conway, J. Chem. Phys. *32*, 1531 (1960).

25. Gruber, J. B., W. F. Krupke, and J. M. Poindexter, J. Chem. Phys. *41*, 3363 (1964).

26. Gruber, J. B., and J. G. Conway, J. Chem. Phys. *32*, 1178 (1960).

27. Gruber, J. B., W., R. Cochran, J. G. Conway, and A. T. Nicol, J. Chem. Phys. *45*, 1423 (1966).

28. Gruen, D. M., *Fused Salts*, Ed., B. Sundheim, McGraw-Hill Book Co., New York (1964).

29. Hellwege, K. H., S. Hüfner, and H. Schmidt, Z. Physik *172*, 460 (1963).

30. Hellwege, K. H., E. Orlich, and G. Schaack, Phys. Kondens. Materie *4*, 196 (1965).

31. Hellwege, K. H., and H. G. Kahle, Z. Physik *129*, 62 (1951).

32. Hoogschagen, J., and C. J. Gorter, Physica *14*, 197 (1948).

33. Hoogschagen, J., Physica *11*, 513 (1946).

34. *International Critical Tables*, Vol. 7, p. 13, McGraw-Hill Publishing Co., New York (1930).

35. Jassie, L. B., Spectrochim. Acta *20*, 169 (1964).

36. Johnsen, U., Z. Physik *152*, 454 (1958).

37. Jorgensen, C. K., and B. R. Judd, Mol. Phys. *8*, 281 (1964); B. R. Judd, J. Chem. Phys. *44*, 839 (1966).

38. Jorgensen, C. K., and J. S. Brinen, Mol. Phys. *6*, 629 (1963).

39. Jorgensen, C. K., *Orbitals in Atoms and Molecules*, Academic Press, London (1962).

40. Judd, B. R., Phys. Rev. *127*, 750 (1962).

41. Judd, B. R., Proc. Roy. Soc. (London) *A250*, 562 (1959).

42. Katzin, L. I., and M. L. Barnett, J. Phys. Chem. *68*, 3779 (1964).

43. Krupke, W. F., and J. B. Gruber, J. Chem. Phys. *41*, 1225 (1964).

44. Krupke, W. F., Phys. Rev. *145*, 325 (1966).

45. Krupke, W. F., and J. B. Gruber, Phys. Rev. *139*, A2008 (1965).

46. Lang, R. J., Can. J. Res. *14*, 127 (1936).

47. Loh, E., Phys. Rev. *140*, A1463 (1965).

48. Loh, E., Phys. Rev. *147*, 332 (1966).

49. Magno, M. S., and G. H. Dieke, J. Chem. Phys. *37*, 2354 (1962).

50. Nielson, C. W., and G. F. Koster, *Spectroscopic Coefficients for p^n, d^n, and f^n Configurations*, The M.I.T. Press, Cambridge, Mass. (1963).

51. Ofelt, G. S., J. Chem. Phys. *37*, 511 (1962).

52. Prandtl, W., and K. Scheiner, Z. Anorg. Chem. *220*, 107 (1934).

53. Racah, G., Phys. Rev. *76*, 1352 (1949); *62*, 438 (1942).

54. Racah, G., Phys. Rev. *85*, 381 (1952).

55. Rajnak, K., and W. F. Krupke, J. Chem. Phys. *46*, 3532 (1967).

56. Rajnak, K., J. Chem. Phys. *43*, 847 (1965).

57. Rajnak, K., and B. G. Wybourne, Phys. Rev. *132*, 280 (1963).

58. Rajnak, K., J. Opt. Soc. Am. *55*, 126 (1965).

59. Sarup, R., and M. H. Crozier, J. Chem. Phys. *42*, 371 (1965); J. Makovsky, W. Low, and S. Yatsiv, Phys. Letters *2*, 186 (1962).

60. Shadmi, Y., Phys. Rev. *139*, A43 (1965).

61. Shadmi, Y., J. Res. Natl. Bureau Stds. *70A*, 435 (1966).

62. Stewart, D. C., *Absorption Spectra of Lanthanide and Actinide Rare Earths--II. Transition Probabilities for +3 Ions in the Two Series*, ANL-4812 (Feb 1952). These results are quoted in *Nouveau Traité de Chimie Minerale*, Ed. P. Pascal, Masson and Cie (1959), Vol 7, Part II.

63. Stewart, D. C., and K. Kato, Anal. Chem. *30*, 164 (1958).

64. Sugar, J., Phys. Rev. Letters *14*, 731 (1965); H. M. Crosswhite, G. H. Dieke, and W. J. Carter, J. Chem. Phys. *43*, 2047 (1965).

65. Thomas, K. S., S. Singh, and G. H. Dieke, J. Chem. Phys. *38*, 2180 (1963); H. F. Geisler, and K. H. Hellwege, Z. Physik *136*, 293 (1953).

66. Trees, R. E., J. Opt. Soc. Am. *54*, 651 (1964).

67. Van Vleck, J. H., J. Phys. Chem. *41*, 67 (1937).

68. Varsanyi, F., and G. H. Dieke, J. Chem. Phys. *36*, 2951 (1962); G. H. Dieke and S. Singh, Ibid *35*, 555 (1961).

69. White, W. B., Appl. Spectro. *21*, 167 (1967).

70. Wilson, M., and K. Rajnak, private communication (Nov 1967).

71. Wong, E. Y., and I. Richman, J. Chem. Phys. *34*, 1182 (1961).

72. Wong, E. Y., and I. Richman, J. Chem. Phys. *36*, 1889 (1962).

73. Wybourne, B. G., *Spectroscopic Properties of Rare Earths*, J. Wiley (1965).

74. Wybourne, B. G., Phys. Rev. *148*, 317 (1966).